

**Measurement and Validation of Rainstorm Parameters
with the VPI Radar**

by

Dennis Sweeney

Thesis submitted to the Faculty of the
Virginia Polytechnic Institute and State University
in partial fulfillment of the requirements for the degree of
Master of Science
in
Electrical Engineering

APPROVED:

T. Pratt, Chairman

C. W. Bostian

G. Brown

August 1986

Blacksburg, Virginia

**Measurement and Validation of Rainstorm Parameters
with the VPI Radar**

by

Dennis Sweeney

T. Pratt, Chairman

Electrical Engineering

(ABSTRACT)

This paper presents a broad overview of the equipment and rational of the experiment conducted by the VPI Satellite Communications Group under INTELSAT Contract 433. The object of this experiment is to assess the validity of meteorological radar as a predictor of satellite earth-space path fade statistics.

To validate the data collected by the VPI radar for this experiment, the differential reflectivity (ZDR) measured during the November 29-30, 1985 rainstorm is compared with calculated ZDR and ZDR from published plots.

The special hardware and calibration techniques required for this experiment are also described. An IBM-PC controlled antenna pointing system and a system to continuously monitor both the peak and average power of the radar transmitter are included. Also included is a calibration system for the radar receiver. A simple computer program is

developed which will give the radar cross section of a metal sphere. This sphere is used as a calibrated radar target.

TABLE OF CONTENTS

Chapter 1 Introduction	1
Chapter 2 Intelsat Experiment and Data Validation	5
2.1 INTELSAT EXPERIMENT	5
2.1.1 INTRODUCTION	5
2.1.2 EXPERIMENT OBJECTIVES	6
2.1.3 EXPERIMENTAL SETUP	8
2.1.4 DATA ANALYSIS	13
2.2 DATA VALIDATION	14
2.2.1 INTRODUCTION	14
2.2.2 Z-ZDR RELATIONS	16
2.2.3 ESTIMATING ZDR	17
2.2.4 ZDR FROM THE NOVEMBER 28, 1985 EVENT	19
2.2.5 ANTENNA CALIBRATION	23
Chapter 3 Radar Antenna Pointing System	27
3.1 INTRODUCTION	27
3.2 VERLORT ANTENNA POINTING SYSTEM	28
3.2.1 INTRODUCTION	28
3.2.2 SYNCRO OPERATION	31
3.2.3 SYNCRO ERROR DETECTOR	36

3.2.4	SYNCHRONOUS DETECTOR, THE VERLORT COMMUTATOR	37
3.2.5	DIFFERENTIAL AMPLIFIER AND AMPLIDYNE	40
3.3	RADAR POINTING SYSTEM TO PERSONAL COMPUTER INTERFACE	42
3.3.1	SYNCRO TO DIGITAL CONVERTERS	42
3.3.2	S/D MULTIPLEXER	43
3.3.3	PC OUTPUT TO VERLORT MECHANICAL INTERFACE	48
3.3.4	MOTOR DRIVER	49
3.4	ANTENNA CONTROL SOFTWARE	53
3.4.1	INPUT/OUTPUT CONSIDERATIONS	54
3.4.2	SYNCHRO READ PROCEDURE	55
3.5	SYSTEM PERFORMANCE	56
Chapter 4.	Radar Calibration	58
4.1	INTRODUCTION TO RADAR MEASUREMENT ERRORS	58
4.2	THE MEASUREMENT OF RADAR TRANSMITTER POWER	61
4.2.1	SYSTEM REQUIREMENTS	61
4.2.2	AVERAGE POWER MEASUREMENT	62
4.2.3	PEAK POWER MEASUREMENT	63
4.2.4	PEAK POWER DETECTOR AND SAMPLE/HOLD CIRCUIT	66
4.2.5	POWER MONITOR DAS INTERFACE	67
4.2.6	DAS INTERFACE CIRCUIT OPERATION	71
4.2.7	ADJUSTMENT PROCEDURE	73
4.3	RECEIVER CALIBRATOR	75
4.3.1	THE RADAR RECEIVER	75

4.3.2 RECEIVER CALIBRATOR	75
4.3.3 CALIBRATION AND USE	77
4.3.4 COMPUTER INTERFACE	78
Chapter 5. Conclusions	82
REFERENCES	84
APPENDIX 1 Electromagnetic Scattering From Conducting Spheres and Rain Drops	87
A.1 INTRODUCTION	87
A.2 THE SPHERICAL SCATTERING PROBLEM	88
A.2.1 THE SPHERICAL WAVE EQUATION	88
A.2.3 SOLUTIONS OF MAXWELL'S EQUATIONS IN SPHERICAL CO-ORDINATES	91
A.2.4 PLANE WAVE SCATTERING FROM SPHERES	92
A.2.5 RADAR CROSS SECTION OF SPHERES	96
A.2.6 SCATTERING FROM RAIN DROPS	99
A.3 DROP SIZE DISTRIBUTIONS	105
Appendix 2	108
ZDR versus Z Program: ZDRPLT	108
Appendix 3	114
Radar Antenna Channel Gain Difference Program: CHNGN	114

Appendix 4	121
Antenna Scan Program: ANTENNA	121
Appendix 5	141
Radar Cross Section Program: RCS	141
Vita	148

CHAPTER 1 INTRODUCTION

The VPI Satellite Communications Group operates an S-Band Band radar which is presently configured as a fast-switched differential reflectivity (ZDR) radar, Marshall et al. [1981], Andrews et al. [1983]. It can measure backscatter from rain in both horizontal and vertical polarizations within five milliseconds. This radar has been used as part of a effort to describe the nature of rain induced fading and depolarization on earth - space satellite paths.

In October 1985, the Group began the data collection phase of a year-long propagation experiment, funded by INTELSAT, using this radar. This work is being done to make ground based radar predictions of satellite slant path attenuation and depolarization more accurate and easier to perform.

This thesis describes the measurement of the rainstorm parameters which is the basis of the attenuation and depolarization predictions. The methods used to determine the validity of these parameters as measured with the VPI radar are also included.

The second chapter is an overview of the INTELSAT experiment. The main objective of the experiment is to improve the process of predicting satellite slant path attenuation and depolarization from ground based radar studies. To reach this objective, the radar observations must represent a valid data base.

The radar observations consist of rain reflectivity, Z, and ZDR. The ZDR measured by the VPI radar is compared against both theoretical predictions of ZDR made by several authors and measured ZDR from published reports of other observations. The results of these comparisons suggest that the VPI radar does measure ZDR in the expected range.

Chapters three and four describe special hardware constructed for the VPI radar for use with the INTELSAT experiment.

As a part of the experiment, it is necessary to have the radar antenna execute a scan pattern. The original radar antenna pointing system did not allow for the antenna to be pointed under computer command. An IBM PC is used to command the antenna position through a somewhat crude but quite effective electromechanical interface that leaves the original pointing system intact. Chapter three describes the original antenna pointing system and the system used to interface the IBM PC to it.

The INTELSAT experiment has several special calibration requirements. Chapter four contains a discussion of these requirements and the hardware developed to meet them.

It is necessary to monitor both the average and peak power output of the radar transmitter. The average power monitoring is done with a conventional microwave power measuring technique employing attenuators and a thermistor power meter. The peak power monitor required a more

sophisticated technique since the value of the peak power must be multiplexed with the receiver video. A square law detector and a high speed sample/hold are used to accomplish the task of peak power measurement.

Also in chapter four is a description of a computer controlled reference signal generator used for receiver calibration.

Included as an appendix is a review of the theoretical basis for rainstorm parameter measurement. Of particular interest is the scattering of electromagnetic radiation from rain drops. As a first order approximation the drops may be considered as small spheres. The scattering of electromagnetic radiation from spheres has been a subject of intense interest for many years. Lord Rayleigh first solved the problem in a rigorous way back in the 19th century and he used the results to explain the blueness of the sky. [Lord Rayleigh, 1881] The solution to this problem has a number of other applications as well. The use of radar for meteorological observations and propagation studies is based on the fact that rain drops act as dielectric spheres in the presence of radio waves and information about the rain drops themselves can be gleaned from the back scattered power.

Rain drops, at least the larger ones, are not perfect spheres however. They are slightly flattened as they fall and as a result they exhibit a horizontal bias. They will reflect more strongly in the horizontal plane. In order to develop a scattering model for a flattened rain drop, it is first helpful to understand the scattering

from the drop as if it were spherical. The spherical scattering model is presented in Appendix 1 and then it is modified to account for the drop shape distortion. This distortion gives rise to a radar reflectivity which depends on the polarization of the wave that is incident on the drop. This polarization is described by a differential reflectivity, ZDR, Seliga and Bringi [1976]. ZDR is usually defined as the ratio of the horizontal to vertical reflections. ZDR can also be defined for any set of orthogonal polarizations. The VPI radar is unique in that it can measure ZDR for any eight polarizations 22.5° apart.

The spherical scattering model is also used to calculate the echo area or radar cross section of a metallic sphere. Metal spheres are often used as calibration targets for radars. The size of these spheres is often such that the approximations for spheres that are either small or large with respect to wavelength will not produce accurate results. A simple computer program is presented that will calculate the radar cross section of any size sphere to a high degree of accuracy. This program is used to calculate the radar cross section of the sphere that is used to calibrate the VPI Radar.

CHAPTER 2 INTELSAT EXPERIMENT AND DATA VALIDATION

2.1 INTELSAT EXPERIMENT

2.1.1 INTRODUCTION

Since the Seliga and Bringi paper of 1976 was published, ZDR radars have been used for precipitation measurement and propagation research. Dual polarized radars have been used as well to predict slant path attenuation and depolarization on satellite links, Stapor and Pratt [1982].

The Satellite Communications Group at Virginia Tech is particularly interested in this latter application. The group has embarked on a year long study, under an INTELSAT contract, using its dual polarized radar along with its satellite beacon monitoring facilities and weather instrumentation in an effort to improve the accuracy of attenuation prediction techniques. Previously published predictions have been based on the observation of a relatively small number of storms. We are building a data base that will contain observations for 90% of the rainstorms in a one year period. The data base can then be used to test the accuracy of predictions on a statistical basis.

2.1.2 EXPERIMENT OBJECTIVES

While previous work has shown that dual polarized radars can be used to predict attenuation and depolarization on satellite paths for particular events, the use of radar as a survey and prediction tool has not been previously attempted. Its accuracy in predicting the statistics of a large number of events has yet to be proven and it is fade statistics that are of interest to the satellite system designer.

The prediction of attenuation and depolarization on slant paths typically requires knowledge of several parameters of a rainstorm model. These parameters describe:

Water Phase : Liquid or various mixtures with ice

Drop size distribution (DSD): Number of particles of a given equivalent drop diameter

Particle shape distribution: Number of particles with a given shape

Distribution of particle orientation: Number of particles with a given axis orientation

If we assume that two parameters are sufficient to describe a particular distribution then seven different parameters are required for the rainstorm model. In practice more than two parameters may be needed for a particular distribution. The gamma drop size distribution proposed by Ulbrich and Atlas [1982] requires three

parameters. Shape and orientation distributions are areas for further investigation.

The water phase and drop size distribution have the greatest impact on attenuation predictions while all the rainstorm information is necessary to predict depolarization, with particle shape and orientation being most important. A two parameters drop size distribution can be measured with a ZDR radar. Water phase may be inferred from range height (RHI) or bright band observations, if they exist. Skolnik, [1980]

Good theoretical models exist which relate drop size distribution (DSD) to attenuation and depolarization, however, determining the DSD from radar collected data has depended heavily on empirical relations adjusted for particular events. The use of more rigorous models requires a more accurate way to determine the rainstorm parameters.

There are two major objectives of our experiment. The first is to improve the theoretical model relating radar measurements to the DSD. The work in this area was presented in July of 1986, Stutzman et al [1986].

The second objective is to produce a data base which contains observations for at least 90% of the rainstorms in a year period. The data base will contain measured satellite link data and it will contain the corresponding radar observations.

For an individual fade event it is possible to estimate some of the unknown rainstorm parameters. This is done by adjusting them for the

best agreement between measured and predicted attenuation and depolarization. While this technique is useful it gives no information on the effect of parameter estimation on fade statistics.

The data base of rain events will be used to assess the validity of ground based radar as a tool for predicting fade statistics on an earth-space satellite path. The unknown parameters will be estimated so as to produce the most accurate fade statistics for the entire data base rather than the best event by event agreement.

This chapter will describe the equipment and methods used to obtain this data base.

2.1.3 EXPERIMENTAL SETUP

Figure 2.1 shows the equipment used for the survey. The radar is an S-Band long range tracking radar modified to be a fast-switched ZDR radar. The equipment and its modifications, and the Data Acquisition System (DAS) have previously been described in the literature, Marshall et al. [1981] and Andrews et al. [1983]. The VPI radar can not only measure ZDR, that is reflectivity in the horizontal plane, Z_h , and in the vertical plane, Z_v , but it is also capable of measuring Z in any one of eight polarizations spaced 22.5 ° apart. In our current study only the Z_h and Z_v are used, but data from the other polarizations is available for later analysis. This data will be used at some future time to obtain information on drop orientation.

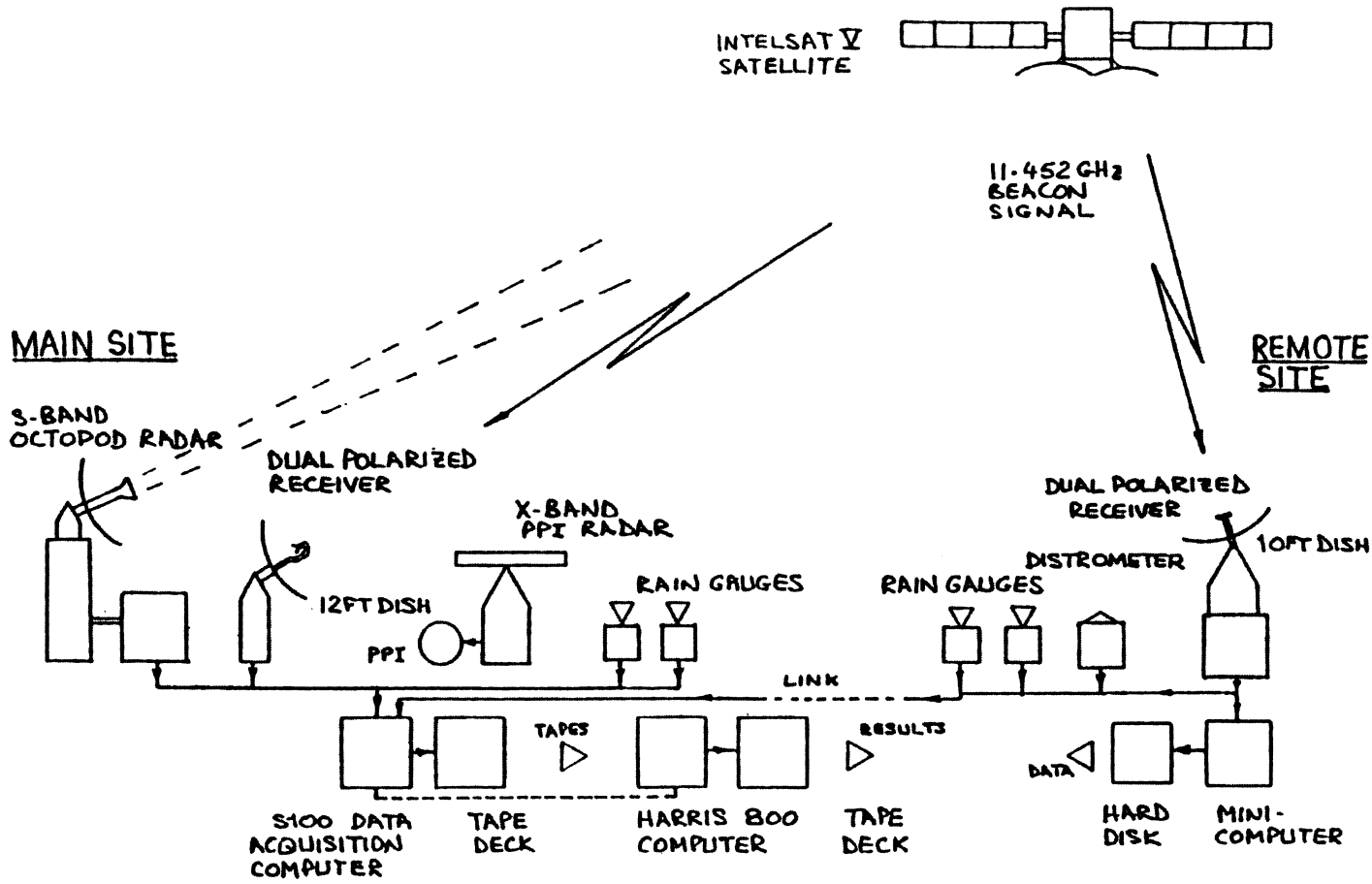


Figure 2.1 INTELSAT Experiment Organization

A system to point the antenna under computer control has been added to the radar. The system and circuitry to accomplish this task are described in a subsequent chapter of this paper. The pointing system permits the radar to do complex scans. In this case, it scans the slant path of a distant earth station.

Virginia Tech has two earth stations. One of them is colocated with the radar. The other is located 7.3 km distant. Each station monitors the strength of the co and cross polarized signals from a circularly polarized beacon (11.542 GHz) on an INTELSAT V satellite. The satellite has an elevation angle of 18°. During clear weather periods, these signal levels are sampled and recorded every 30 seconds by an S-100 bus computer located at the main site. An IBM PC at the remote site samples the remote receiver output at 30 second intervals. The PC also samples the weather instruments at the remote site, and transmits all this information over a dedicated phone line to the S-100 computer at the main site. When radar data is being collected the receivers at each site are sampled at approximately three second intervals rather than the clear weather 30 second rate.

The radar is programmed to execute a scan cycle over both the remote and main sites. Figure 2.2 shows the scan. The scan begins with the radar aimed directly over the remote site. Next the radar does an RHI over the remote site. The radar is then scanned up the remote site slant path. From there the antenna is pointed up the main site slant path. The radar then does an RHI over the main site and

returns to the main site slant path once again. The antenna is then swung back to the remote site slant path and scanned back down this path to the remote site where the cycle begins again. The entire cycle takes about 6.5 minutes. The measured antenna position is recorded for each point on the cycle to improve the accuracy of the slant path reconstruction from the radar data.

Weather instrumentation is included at each site. At the remote site there are two tipping bucket rain gauges, one of which has been modified to respond to low rain rates, a temperature sensor, and a distrometer. The distrometer is from the acoustic design of Flach [1972] and it was constructed from the description by Rowland [1975, 1976]. A description of the VPI adaptation of this distrometer can be found in Bottomely [1985].

Each time a rain drop strikes the distrometer head, there is a pulse output from the distrometer. This pulse output goes to a peak hold circuit which is sampled every 10 milliseconds by the remote site PC. This "captures" the largest impact in each 10 millisecond window. The resulting voltage is binned by the PC as a particular sized drop. The PC counts number of each sized drop and sends this information to the main site every 30 seconds as a drop size distribution. The radar looks directly over the remote site during one of the RHI scans. This permits comparison of distrometer and rain gauge data with the vertical structure of rain as observed by the radar.

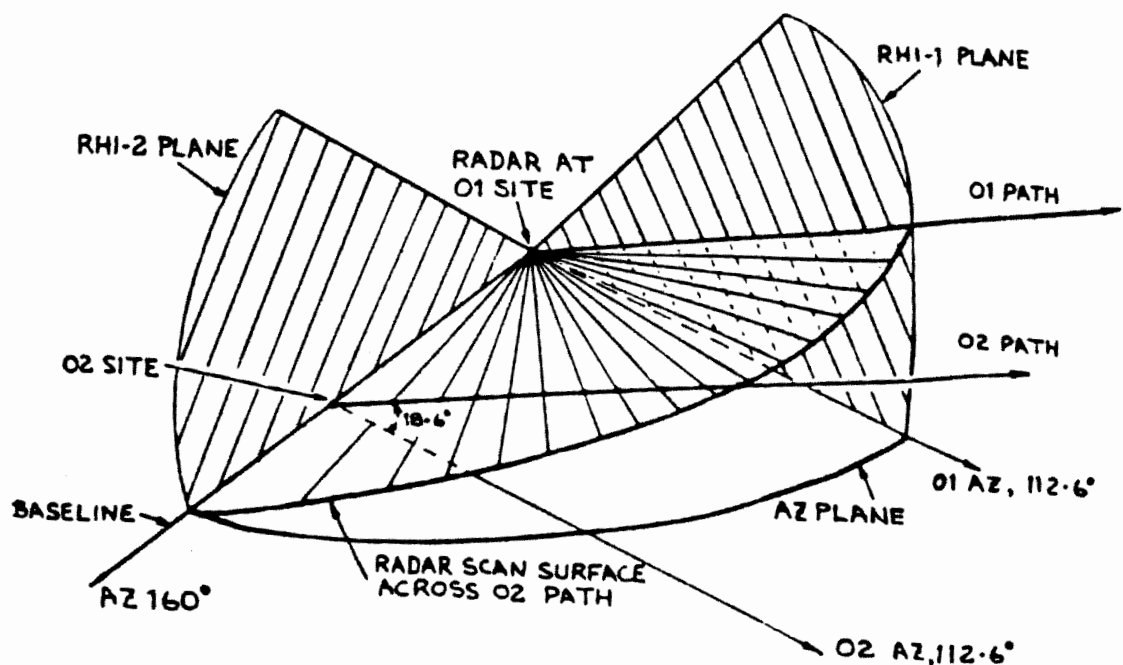


Figure 2.2 Radar Scan Sequence

At the main site there are two rain gauges similar to the ones of the remote site, a temperature and wind speed indicator, and a recording barometer. With the exception of the barometer and distrometer data, all the data from weather instruments is recorded with the receiver data at either 30 second or 3 second intervals.

2.1.4 DATA ANALYSIS

The data analysis is done in two stages. The first stage reduces the raw data to an "archive" tape. Each event has its own archive tape. This tape contains:

- * Drop size distribution data measured by the distrometer
- * Date, time, and radar antenna position for each point of the scan
- * Rain gauge rain rates for both sites and a remote site rain rate obtained from distrometer data
- * Measured attenuation and depolarization for both the main and the remote site
- * The Z values for 128, 250 meter range gates for eight different polarizations 22.5° apart

The second stage of the data processing is accomplished by extracting the Z information from the archive tape for each point on the desired path. ZDR is calculated for each point. This information is sent to the computer program "FORWARD." FORWARD is actually a set of programs. The first is BSCAT which converts the Z and ZDR to N_o and

Λ which are the parameters of the drop size distribution, Stapor and Pratt [1984]. BSCAT has the capacity to do this not just for the entire storm but for each point on the path. With the parameters obtained for the DSD in each range bin, the second program of FORWARD, MULTI, calculates the attenuation and depolarization for each point on the path and from there the attenuation and depolarization for the entire path. MULTI is based on multiple scattering theory, Tsolakis and Stutzman [1982].

Comparing the predictions with the measured attenuation and depolarization it is possible to adjust those rainstorm parameters that cannot be measured so as to produce the most accurate fade statistics.

2.2 DATA VALIDATION

2.2.1 INTRODUCTION

This is a complex experiment. Its success is dependent on having a valid data base from which to do the predictions. It is possible to calibrate the radar "statically," that is to measure transmitted power with a wattmeter, receiver sensitivity with a signal generator, and system operation with a calibrated sphere. Much of the work of this paper is directed toward that end. However there is an old proverb

that states that "the proof of the pudding is in the eating." Does the system actually measure ZDR?

The radar system measures the reflectivity factor Z for various polarizations and ZDR can be obtained from the horizontally and vertically polarized Z measurement. Z can be related to rain rate:

$$Z = ar^b \quad (2.1)$$

where r is rain rate and a and b are empirically derived constants. Attenuation can then be obtained from the rain rate, Battan [1973].

The difficulty with this relation is that it is empirically derived and it changes with the type of rain, Battan [1973], and it does not give a relationship between Z and ZDR. In addition, relating Z to measured rainfall rate is subject to its own errors since the rain that the radar "sees" may not be the rain that falls into the rain gauge.

It is necessary is to determine a relation between Z and ZDR and to compare that relation with the measured Z and ZDR.

From this relationship it can be shown whether the radar is obtaining the correct value of ZDR for each measured value of Z . This task is complicated by the statistical nature of Z and ZDR. The best that can be obtained is an average Z and ZDR since the radar reflections are the sum of reflections from randomly distributed rain drops in the radar pulse volume.

2.2.2 Z-ZDR RELATIONS

Examination of equation A.38 reveals that when ZDR is calculated one of the parameters of the DSD, N_o , is divided out and ZDR is a function of Lambda only. Since ZDR is in the range of 0 - 4 dB, Bringi et al. [1979], a reasonably accurate estimate of Z can be obtained by considering all the drops to be spherical and calculating Z from the following relationship:

$$Z = N_o \int_{D_{eq}}^{\infty} (D_{eq})^6 \exp(-\Lambda D_{eq}) dD_{eq} \quad (2.2)$$

If N_o is chosen there is a unique relationship between Z and ZDR for each Lambda, Seliga and Bringi [1976]. For each value of N_o there is a unique value of ZDR for each value of Z. The two are related through the drop size distribution (DSD).

Extensive work has been done by the Satellite Communications Group here at Tech, Stapor [1982], Stapor and Pratt [1982] and by others, Ulbrich [1984], relating Lambda to ZDR under various conditions.

It should be noted that ZDR is affected by the elevation angle to the drop and its canting angle. As the elevation increases the radar looks more at the "bottom" of the drop and it appears more round than oblate. High elevation angles have the effect of lowering ZDR. Canting angle is the angle between a drop axis and the incident wave and a canting angle other than zero also reduces ZDR. A third factor

that affects ZDR is the proportion of oblate drops, F . F is usually estimated to be in the range of 0.6 - 1.0.

Ulbrich's [1984] relation between Lambdas and ZDR is given by:

$$ZDR = 27.5(0.362\Lambda)1.55 \text{ dB} \quad (2.3)$$

This is for a Marshall and Palmer [1948] DSD, i.e. $\mu = 0$ in equation A.37. This is an empirical relation. The Stapor relations between Z and ZDR are obtained by numerical integration of equation A.38 corrected for elevation angle, canting angle and F . These relations are presented in graphical form in Stapor [1982]. Pratt also has a similar set of curves which at this time are unpublished.

Choosing $N_o = 8000$ (after Marshall and Palmer) it is possible to calculate Z from equation 2.2 for various values of Lambda. ZDR for these same values of Lambda was obtained from the sources described above. The results are plotted in figure 2.3.

2.2.3 ESTIMATING ZDR

The measured backscattered signal is the sum of the reflections from all the drops in the pulse volume. The drops are randomly distributed in the volume so that the returned signal is the sum of signals with random amplitudes and phases. The returned signal is given by:

$$(A_{h,v}) \exp(j\phi_{h,v}) = (C_{h,v}) \sum_{k=1}^N F_k(h,v) \exp(j\theta_{k(h,v)}) \quad (2.4)$$

where $A_{h,v}$ and $\phi_{h,v}$ are the received amplitude and phase at the horizontal and vertical polarizations respectively. $F_k(h,v)$ and $\theta_{k(h,v)}$ are the corresponding backscattered amplitude and phase of the k^{th} scatterer in the pulse volume, and $C_{h,v}$ is the radar constant, Bringi et al. [1983]. The returned signal will be distributed around some mean value. This mean value can be obtained by averaging the returned signal.

Bringi et al. [1983] have made a theoretical analysis of three different averaging schemes. They are the square-law estimator, the log ratio estimator, and the ratio estimator. The square-law estimator is given by:

$$ZDR = [1/m(\sum_{i=1}^m A_{hi}^2)] - [1/m(\sum_{i=1}^m A_{vi}^2)] \quad (2.5)$$

The log-ratio estimator is given by:

$$ZDR(\text{dB}) = (1/m) \sum_{i=1}^m 10 \log(A_{hi}/A_{vi})^2 \quad (2.6)$$

The ratio estimator is given by:

$$ZDR = (1/m) \sum_{i=1}^m (A_{hi}/A_{vi})^2 \quad (2.7)$$

The estimator presently being used in the VPI radar is the square-law estimator and Bringi et al. [1983] show that this estimator will have the lowest standard deviation of the three. For the 64 sample average

used in the VPI radar, the standard deviation should be in the 0.35 to 0.50 dB range.

The distribution of the returned signal is also affected by the cross correlation and the signal to noise ratio (SNR). In the time that it takes the radar to switch from horizontal to vertical, the rain drops may change position relative to the radar and thus the horizontal and vertical reflections will become uncorrelated. The amount of decorrelation increases as the switching time increases. The switching time for the VPI radar is 4.16 msec. This is considered "fast-switched" so the amount of decorrelation is small. Also the lower the Signal to Noise Ratio (SNR), the more noise is added to the returned signal. This has the effect of reducing the cross correlation. The SNR will be poorest for low values of Z. Both of these effects are difficult to quantify and were ignored for the sake of this analysis. This was justified by the fast-switching construction of the radar and by the fact that ZDR at higher values of Z, where the SNR is better, is of the most interest for this analysis.

2.2.4 ZDR FROM THE NOVEMBER 28, 1985 EVENT

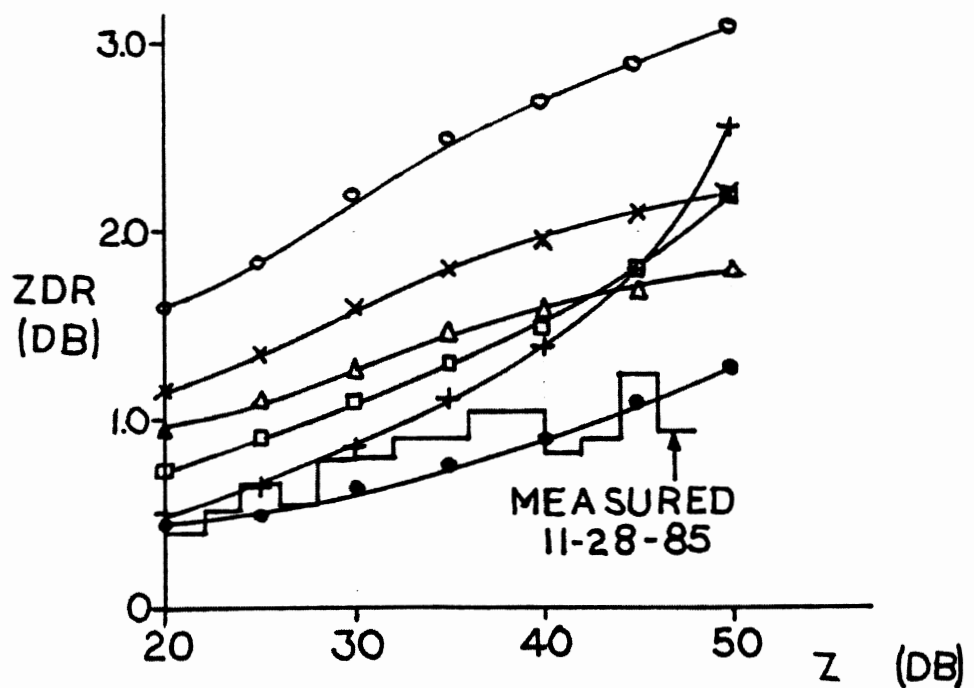
Data taken during a rainstorm which occurred on November 28-29, 1985 is used to determine whether or not the radar was measuring ZDR. A segment which spans 23:47 GMT, Nov 28 to 00:18 GMT, Nov 29 was

removed from this storm. This time represents a period of intense rain fall.

ZDR is calculated and averaged for Z values in 2 dB bands beginning at 20 dBZ and ending at 48 dBZ (Z=1 is 0 dBZ) To insure that the results were not contaminated by ground clutter or bright band only those range bins greater than 10 and less than 64, ($2.5\text{km} < \text{range} < 16\text{km}$), and those elevation angles greater than 15 degrees are used. The use of relatively high elevation angles will reduce the average ZDR somewhat. The results are plotted over the predicted values of ZDR in Figure 2.3 and tabulated in Table 2.1. A listing of the computer program used to do the calculation is to be found in Appendix 2.

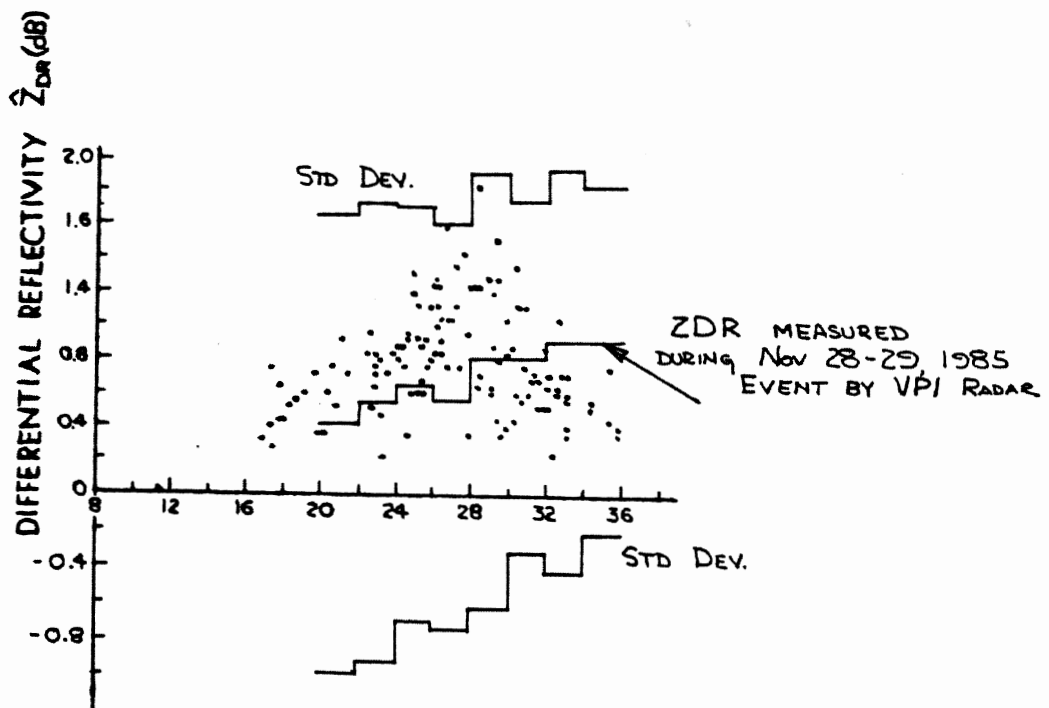
The measured values of ZDR for a particular Z agree well with the predicted range of ZDR. The measured ZDR is somewhat lower than the predicted ZDR but this is consistent with the previously noted limitations of the process used to analyze the measured data. The standard deviation of the ZDR is significantly higher than expected. There seems to be no immediate explanation for this.

Despite the higher than expected standard deviation, the measured ZDR falls in the expected range. Bringi et al. [1983] have published a scatter plot of ZDR verses Z. Figure 2.4 is a reproduction of that plot with the ZDR measured during the November 28-29 event superimposed on it. As figure 2.4 shows the range of ZDR measured by the VPI radar closely conforms to the range measured by Bringi et al.



Curve	Source	Elevation Angle	F_o	Canting Angle Ave.	Canting Angle Std. Dev.	μ
o	Stapor	0°	1.0	0°	0°	0
x	Stapor	30°	1.0	0°	0°	0
△	Stapor	0°	0.6	0°	0°	0
□	Pratt	0°	1.0	0°	0°	0
●	Pratt	0°	0.6	0°	0°	0
+	Ulbrich & Atlas	?	?	?	?	?

Figure 2.3 Z versus ZDR from various sources.



REFLECTIVITY \hat{Z} (dBz)
 Scatter plot of \hat{Z}_{DR} versus \hat{Z}

Figure 2.4 Scatter Plot after Bringi, Seliga, and Cherry [1983] with ZDR as measured by VPI RADAR supimposed.

Ave Z (dB)	Ave ZDR (Ratio)	ZDR (dB)	Std Dev ZDR (Ratio)	ZDR range (dB) $10\log(ZDR+Std Dev)$
20-22	1.097	0.40	0.36	-1.32 - 1.63 dB
22-24	1.127	0.52	0.36	-1.15 - 1.72
24-26	1.158	0.64	0.32	-0.77 - 1.69
26-28	1.132	0.54	0.30	-0.80 - 1.59
28-30	1.199	0.79	0.34	-0.66 - 1.87
30-32	1.202	0.80	0.28	-0.35 - 1.71
32-34	1.233	0.91	0.33	-0.44 - 1.94
34-36	1.232	0.90	0.28	-0.21 - 1.80
36-38	1.268	1.03	0.26	-0.03 - 1.84
38-40	1.271	1.04	0.37	-0.45 - 2.15
40-42	1.207	0.82	0.32	-0.52 - 1.84
42-44	1.229	0.90	0.29	-0.27 - 1.81
44-46	1.338	1.26	0.33	0.03 - 2.22
46-48	1.236	0.92	0.35	-0.53 - 2.00

Table 2.1

Z, ZDR, and the Standard Deviation from the
November 28th - 29th Event

2.2.5 ANTENNA CALIBRATION

The feed system used in the VPI radar is capable of producing a linear polarization in any plane. This is accomplished by first launching a linearly polarized wave in a circular waveguide. With a polarizer this mode is then converted into a circularly symmetric waveguide mode. This mode is converted back into the linear mode by a second polarizer. Since the second polarizer can be rotated, the polarization angle of the linear polarization produced by this

polarizer is a function of its position, Andrews et al. [1983]. In an ideal world the coupling between the circularly symmetric mode and the polarizer would be independent of position. This is the real world however and the coupling does depend on position. The net effect is that the antenna gain will change with polarization.

It is necessary to correct for this effect before accurate ZDR measurements can be made. This was done by using several hours of data taken February 3, 1986 during a very light rain. A light rain has very small drops. Small drops remain more spherical as they fall and thus there will be very little ZDR. Any average ZDR that is measured can then be attributed to a gain change in the antenna.

A procedure similar to the one described in Section 2.2.3 was used to determine this change in gain. Vertical polarization was defined as the reference polarization. The difference between the Z measured in the vertical polarization and the Z's measured in the other seven polarizations was calculated and averaged. The effect of the ZDR attributable to the rain drops was reduced by restricting Z to values between 20 and 25 dB. If the antenna gain is the same in each polarization and the rain drops are spherical, then the average difference in the various polarizations would be zero. If the rain drops are assumed to be spherical then any average difference that does occur is a result of differences in antenna gain for each polarization. The results of this test are plotted in the scatter plot of Figure 2.5. A listing of the computer program used to do the

calculation is in Appendix 3. Each point on the plot represents the average ZDR of 1000 values of Z between 20 and 25 dB. From the curve an appropriate factor was obtained to correct for differences in antenna gain in different polarizations. These correction factors were used when ZDR was calculated in the procedure of Section 2.2.3.

Another and possibly more accurate method to determine antenna channel gain difference was suggested by Seliga and Bringi [1979]. They calibrated out the antenna gain differences by aiming the antenna directly up. This looks at the "bottom" of the rain drops, and from the bottom all the drops will appear circular independent of their size. This procedure would permit the use of higher Z values and the greater signal to noise ratio that accompanies them. This would result in less noise in the averaging process.

Seliga and Bringi found the gain difference in their antenna, which used vertical and horizontal polarization only, to be 0.42 dB. The gain corrections for the VPI antenna are of the same order of magnitude.

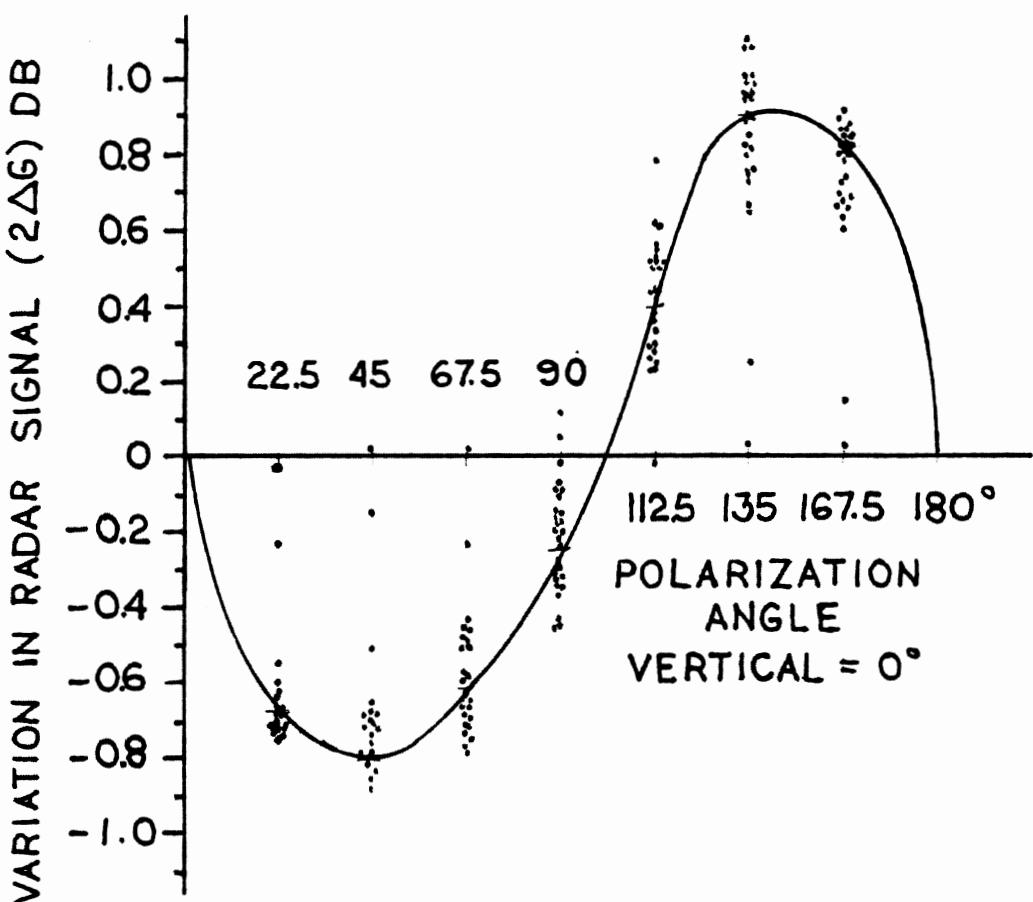


Figure 2.5 Variation in RADAR Signal with Polarization

CHAPTER 3 RADAR ANTENNA POINTING SYSTEM

3.1 INTRODUCTION

The scan cycle for the INTELSAT experiment described in chapter 2 requires some type of antenna position controller. The modified VERLORT (VERy LOng Range Tracking) radar in use at VPI has a complex antenna pointing system. This system was capable of tracking a target and performing various kinds of scan patterns, as well as permitting manual pointing of the antenna. However it was not possible to electrically command a given position. For the INTELSAT project it was necessary to devise a way to point the antenna under computer control.

This is accomplished by an electromechanical interface between the controlling computer, an IBM PC, and the VERLORT manual pointing system. The computer reads the antenna position through a Synchro to Digital converter (S/D), compares that position to the desired position, and then runs a small DC gear motor mechanically linked to the manual position hand wheel to bring the antenna to the desired position. Figure 3.1 is a block diagram of the system. This may seem a bit crude in the age of "hi-tech" but this arrangement has some significant advantages. It is relatively simple to implement, it avoids the necessity of interfacing the computer with high current, high voltage machinery, and it avoids the problem of stabilizing a sample data

feedback system. The last problem is particularly acute, not because such systems are difficult to stabilize but because many of the time constants in this system are unknown.

3.2 VERLORT ANTENNA POINTING SYSTEM

3.1.1 INTRODUCTION

The radar antenna pointing system is described in some detail in the VERLORT operating manual, Reeves Instrument Corporation [1960], however the system is 1940's technology and makes extensive use of rotating machinery and vacuum tube circuitry. For these reasons a more basic description of the major components of the system will be included.

Figure 3.2 is a simplified circuit diagram of the manual pointing system. There are two almost identical systems, one for azimuth and one for elevation. The parts of the two systems which are different are of no consequence for manual operation and Figure 3.2 shows the system for one axis only.

In Figure 3.2, the synchro transmitter and the synchro control transformer are connected as an error detector to generate an AC voltage whose amplitude and phase is proportional to the amount and direction of mechanical displacement between the two synchros. The synchronous detector, which is called a "commutator" in the original VERLORT

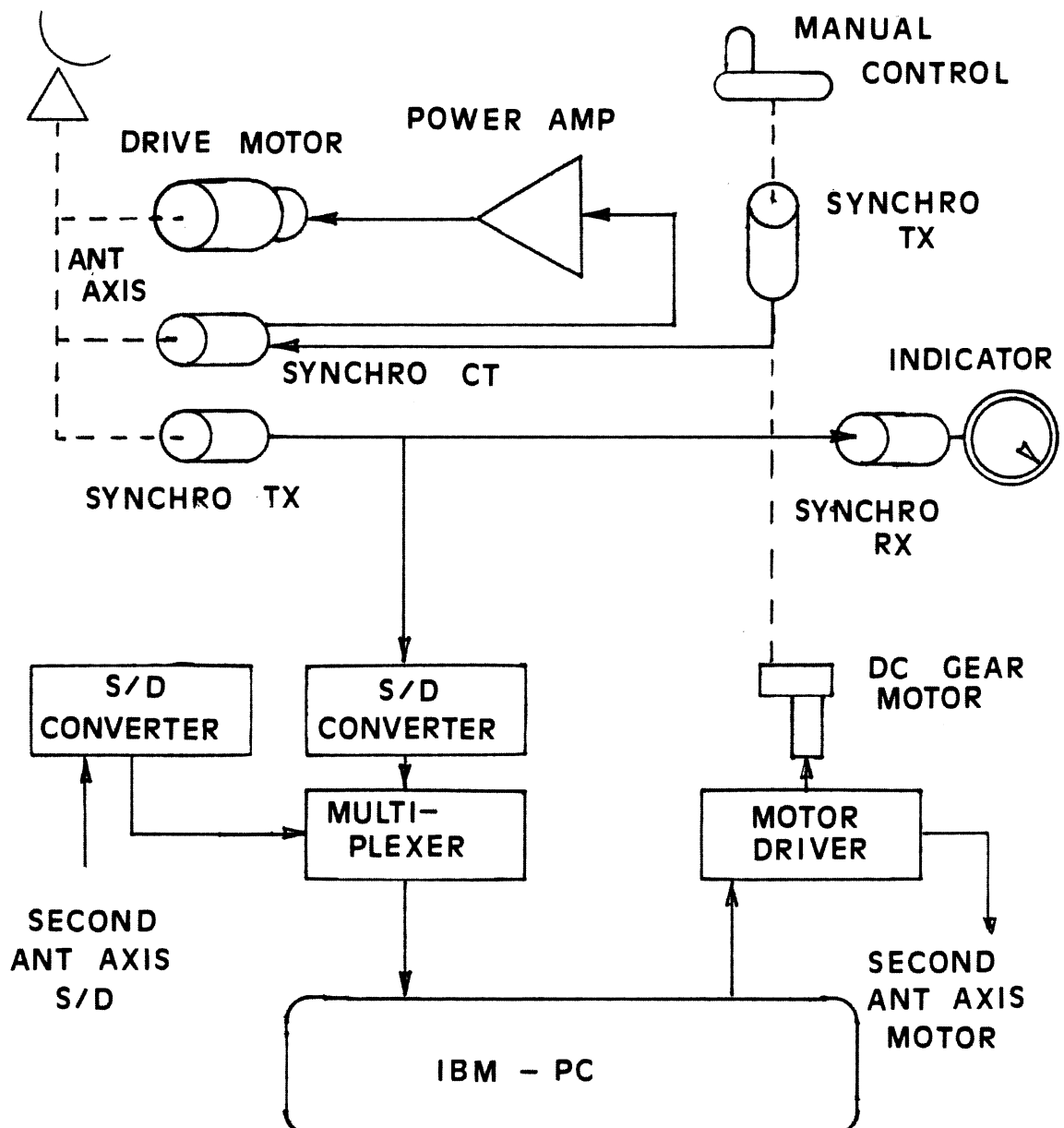


Figure 3.1 Antenna Pointing System

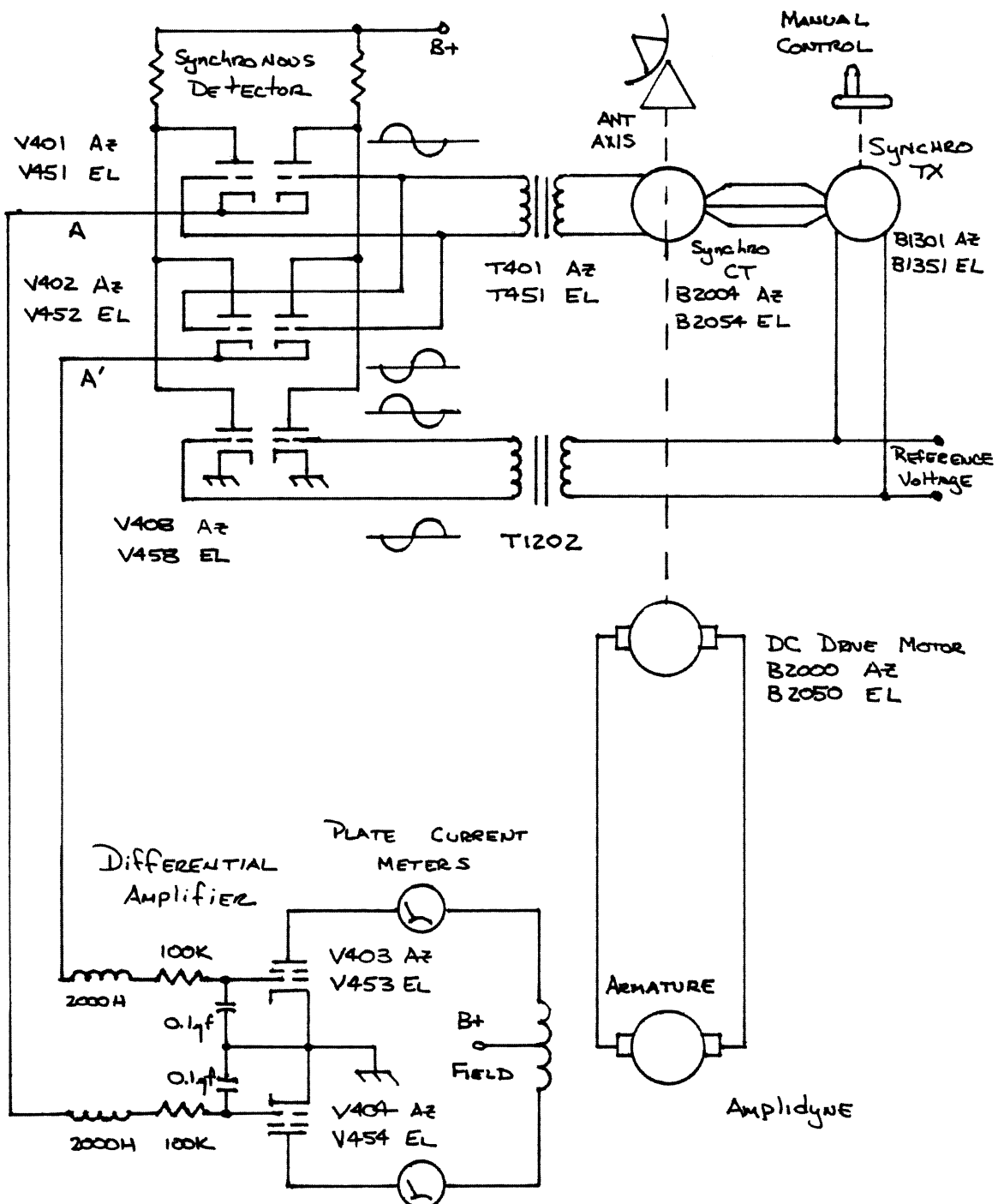


Figure 3.2 Simplified Schematic of VERLORT Antenna Pointing System

documentation, converts the AC voltage into a DC voltage which is amplified by a vacuum tube differential amplifier. This amplifier controls the field current in the amplidyne. The amplidyne then generates a voltage which causes the DC drive motor to run. This motor is connected through a gear box back to the syncro control transformer, and to one of the antenna axes. The drive motor runs to minimize the mechanical displacement between the synchro control transformer on the antenna axis and the synchro control transmitter connected to the manual hand wheel. When the antenna reaches the desired position the mechanical displacement between the control transmitter is zero. The error voltage produced by the synchro pair is then zero, the amplitidyne output ceases, and the drive motor then stops the antenna in the desired position.

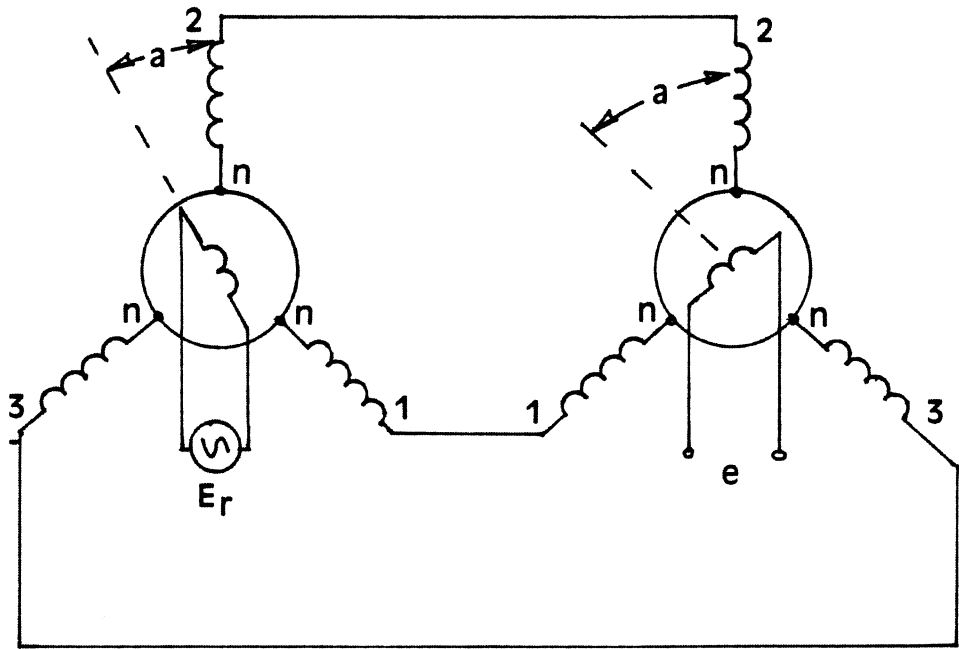
3.2.2 SYNCHRO OPERATION

The synchros may be unfamiliar devices so their operation will be described. There are four different kinds of synchros: control transmitters (CX), control transformer (CT), control receivers (CR), and differential synchros. They all consist of a stator and a rotor. On the transmitter stator there is a balanced three phase winding and the rotor is dumbbell shaped with a single phase winding on it. The rotor winding is brought out through slip rings to external connections. The transmitter syncro is very similar in construction to a 3-phase generator or synchronous motor. For the synchros however, single phase AC rather

than DC is applied to the rotor winding. Through transformer action there is coupling between the rotor and the stator windings. Since the rotor winding can move with respect to the stator, the coupling between the rotor and any stator winding is a function of position. The defined "zero" position for the transmitter is when there is maximum coupling between the rotor and winding 2 as shown in figure 3.3. However, there are two positions where this condition is satisfied. An unambiguous zero is defined by the winding dots. Mechanically, the rotor orientation is defined by a small notch cut in the syncro shaft.

The control transformer (CT) is very similar to the control transmitter, with two important exceptions. The rotor is more cylindrical with an umbrella shaped cross section and a very small air gap. This reduces the magnetizing current required for the CT. Also the stator windings are of higher impedance so that several CT's could be connected to one CX. Secondly, zero is defined in a different way. For the CT, zero is defined where the coupling between the rotor and winding 2 in Figure 3.3 is a minimum.

The control receiver (CR) is identical to the CX electrically. Its only difference is mechanical in that the CR has a damper, often in the form of a lead washer, attached to the rotor shaft. The damper is to reduce overshoot. In normal use the respective stator windings of the CX and the CR are connected together and both rotors are excited from a common source. The CR will then follow any mechanical movement of the CX.



Synchro Control
Transmitter (CX)

Synchro Control
Transformer (CT)

Figure 3.3 Synchro Error Detector

The differential syncro has a balanced three phase winding on both the rotor and the stator. While there are several differential synchros in the VERLORT system they are not of interest here. The differential introduces a phase shift between the three phase voltage applied to the rotor and the corresponding voltage induced in the stator. This phase shift is a function of the the relative positions of the rotor and stator windings.

The transformer action between the rotor and stator winding of the synchros will induce a voltage in each of the stator windings. These voltages will be of the same frequency as the applied field and proportional to the coupling between each phase and the rotor. So

$$E = rE_r \quad (3.1)$$

where r is the effective stator to rotor turns ratio and E_r is the applied rotor voltage. Referring to the CX in figure 3.3, the RMS voltage induced in winding 2 is given by

$$E_{2n} = E \cos(a) \quad (3.2)$$

Correspondingly E_{1n} and E_{3n} can be written in the following way:

$$E_{1n} = E \cos(a - 120^\circ)$$

(3.3)

$$E_{3n} = E \cos(a + 120^\circ)$$

This is consistent with our definition of electrical zero resulting in maximum coupling when $a=0$. Using Equations (3.2) and (3.3) with the appropriate trig identities, it is now possible to write the terminal voltages for the device.

$$E_{12} = E_{1n} + E_{n2} = E_{1n} - E_{2n}$$

(3.4a)

$$E_{12} = \sqrt{3} \cos(a - 150^\circ)$$

$$E_{23} = E_{2n} + E_{n3} = E_{2n} - E_{3n}$$

(3.4b)

$$E_{23} = \sqrt{3} \cos(a - 30^\circ)$$

$$E_{31} = E_{3n} + E_{1n} = E_{3n} - E_{1n}$$

(3.4c)

$$E_{31} = \sqrt{3} \cos(a + 90^\circ)$$

It is clear that the terminal voltages of the device are affected by rotor displacement. Because the device is reciprocal the opposite is also true, that for a given set of applied voltages the rotor voltage is a function of rotor position.

3.2.3 SYNCRO ERROR DETECTOR

Figure 3.3 also shows the control transmitter and the control transformer connected as an error detector. This is the same manner in which the control transformer and the control transmitter are connected in figure 3.2. The CX supplies magnetizing currents to the CT so the same currents flow in both the CT and CX. This means that a field which exactly corresponds to the field in the CX is set up in the CT. Recall that the CT zero is defined for minimum coupling between the rotor and winding 2 of the stator. If the rotor of the CX was locked in its zero position then the voltage induced in the CT will be

$$e = E_r \sin(a) \quad (3.5)$$

With both rotors mechanically free to rotate, the voltage induced in the CT rotor is a function of the difference of the displacements from their respective zero positions.

$$e = E_r \sin(a_x - a_t) \quad (3.6)$$

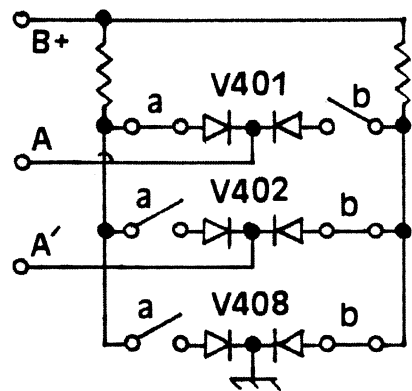
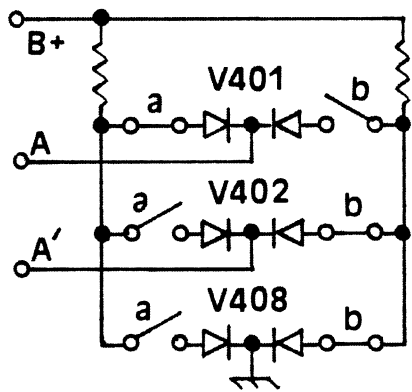
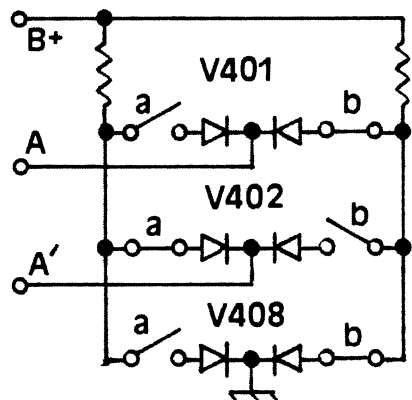
where a_x is the displacement from zero of the CX and a_t is the same for the CT. It is clear that when the two devices have the same mechanical position with respect to their zeros then the CT output voltage is zero.

Notice that the induced voltage can be either positive or negative depending on the direction of the displacement. The sign of the sine can be translated into a phase difference which indicates the direction of the displacement. The VERLORT pointing system uses a synchronous detector as a phase sensitive detector to recover this information. The result is a DC voltage whose sign indicates the proper direction for the drive motor to run and whose amplitude tells the motor how fast to run.

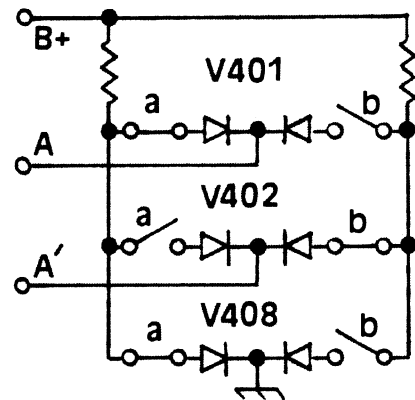
3.2.4 SYNCHRONOUS DETECTOR, THE VERLORT COMMUTATOR

The VERLORT operation manual speaks of this phase detector as a "commutator." It can also be thought of as a multiplier or balanced mixer. To gain a better grasp of its operation, the synchronous detector circuit of figure 3.2 has been redrawn in Figure 3.4 with the tubes replaced with a series of switches and diodes. The negative portion of the wave form applied to the grid turns the tube off while the positive portion turns it on. The triodes that form the network in figure 3.4 can be thought of as voltage controlled current sources much like FET's although their "on" resistance is much higher. To look at the tubes as switches is somewhat an over simplification but it is useful for understanding the circuit's operation.

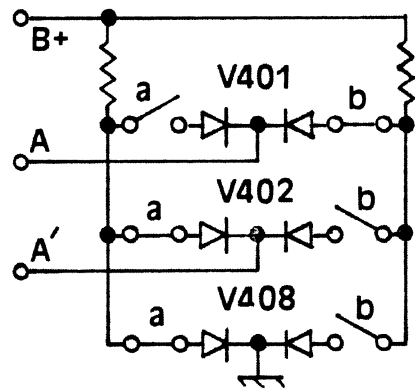
Since there are two identical systems, the operation of the detector will be described in terms of the azimuth channel only. What is said



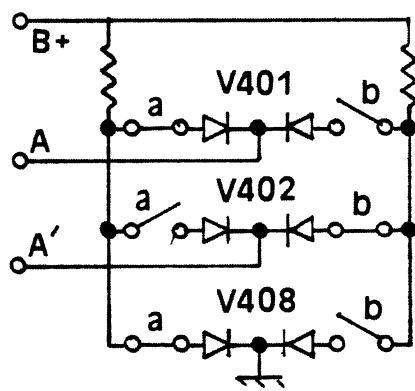
1st half cycle



In Phase



Out of Phase



Input Zero

2nd half cycle

Figure 3.4 VERLORT Commutator Operation

of the azimuth channel is also true of the elevation channel only with different part numbers.

The excitation voltage applied to the CX is also applied to the grids of V408 through transformer T1202. This is the "reference" voltage. T1202 supplies a push-pull output thus insuring that when one half of the tube V408 is on, the other half must be off. Transformer T401 is used to do the same thing to the "error" voltage coming from the CT B2004.

Figure 3.4A shows what happens when the error and reference voltages are in phase. During the first half cycle of the reference, V408b is on. This pulls the supply rail on the right low so even though V401b is also on there is no output at point A. V402a is on and V408a is off so the left supply rail is high and current flows through V402a to the output which causes point A' to be more positive than point A. During the second half of the cycle shown in figure 3.4A, the situation is exactly reversed but point A' is still more positive than A. V408b is off and the right supply rail is high. Point A' is connected to the supply rail that is high through V402b.

When the error voltage is out of phase with the reference, figure 3.4B shows that during the first half cycle V408a is off and V408b is on. The left supply rail is then high. V401a and V402b are on and V401b and V402a are off. Since the left supply rail is high, current flows through V401a making point A more positive than A'. During the second half of the cycle the opposite occurs. The right supply rail is high

because V408b is off. V401a and V402b are off and V401b and V402a are on, however point A is still more positive because V401b connects it to the right rail which is high.

There is one additional condition to investigate and that is when the error voltage is zero. This is shown in Figure 3.4C. With zero volts on the grids, the tubes will still conduct. The tube sections are not exactly identical however, so one side will conduct more heavily than the other. For example, say V401a and V402b conduct more heavily. During the first half cycle V401a will be on and A is more positive than A'. During the second half cycle A is more positive because V402b conducts more heavily than V401b. The average difference between A and A' is then zero over the whole cycle.

The output of the commutator is filtered by a low pass filter in the grid circuit of V403 and V404, Figure 3.2. It is tempting to look at these components as determining the dynamics of the feedback system. Empirical tests, however, suggest that these components have little effect on the loop. The loop dynamics appear to be determined primarily by the mechanical time constants of the system.

3.2.5 DIFFERENTIAL AMPLIFIER AND AMPLIDYNE

The detected error voltage from the filter is applied to the grids of V403 and V404 which form the differential amplifier. The plate current of these two tubes flow through a differential field winding

in the amplidyne. If the error voltage is zero the plate currents will be equal and no net field is produced in the amplidyne. An error voltage from the CT will cause the plate currents to become unbalanced in one direction or the other. This will produce a net field and an output from the amplidyne.

The amplidyne is a rotating current amplifier. It consists of a 3-phase motor driving a DC generator. The polarity and the voltage of the output are determined by the direction and magnitude of the current imbalance in the field winding. The generator portion is capable of producing over 200 volts at 100 amperes. Given that the field currents are only about 25 millamps, this is a rather healthy amplifier. The amplidyne also has the advantage of being almost indestructible.

The output of the amplidyne drives the motor armature which is geared to the control transformer and one of the antenna axes. The gearings and the polarities are such that when the motor runs the error voltage produced by the angular displacement between the hand wheel CX and the antenna axis CT is minimized, thus there is a closed loop system. An error voltage can be generated either by the operator moving the hand wheel to command the antenna to move to a new position, or by wind or another force trying to move the antenna from its current position. In either case the system forces the antenna axis angle to agree with the position sent by the CX.

3.3 RADAR POINTING SYSTEM TO PERSONAL COMPUTER INTERFACE

3.3.1 SYNCRO TO DIGITAL CONVERTERS

For the computer control system it is necessary to supply antenna position information in a form that the PC can use. This is done by the Synchro to Digital converter referred to in Figure 3.1.

Apart from the feedback control system in the VERLORT radar there is an additional synchro transmitter and receiver for each axis. This additional CX is ganged with the CT that is part of the feed back loop and the additional synchro receiver is mounted on the control console with a position indicator dial. The CX "transmits" the antenna position down to the display. The IBM PC used to control the antenna "reads" the antenna position through a synchro to digital converter (S/D) connected to the display CX-CR pair. The S/D is a specialized A/D converter. Since there is a unique voltage on each phase for each synchro position, it is possible to sample the vector sum of the phase voltages and produce a digital word that is related to the synchro position.

The S/D is a packaged device with 12 bit resolution manufactured by Computer Conversions Corporation, Synchro Conversion Handbook [1982]. It is desired that the antenna position be known to $\pm 0.25^\circ$. The resolution of the S/D is

$$\frac{360^\circ}{2^{12}} = 0.08789^\circ \quad (3.7)$$

It is therefore necessary to position the antenna within ± 3 counts in order to obtain the $\pm 0.25^\circ$ pointing accuracy required for the INTELSAT scan routine.

Figure 3.5 is the S/D converter card. The converters are self contained and only require ± 15 volts and $+5$ volts. This voltage is supplied by regulators on the card, U3, U4, and U5.

It is necessary to inhibit the S/D converter during the time it is being read. If this is not done it is possible that the value could change during the read cycle. As long as there is no change in the antenna position the converter is quiescent. As soon as it detects some change it begins the conversion process and this is not synchronized with the computer.

The rest of the circuitry in Figure 3.5 is LED's and their drivers to display the current S/D output. These were added as a trouble shooting aid.

3.3.2 S/D MULTIPLEXER

The IBM PC is equipped with a Metrabyte PIO12 parallel I/O card shown in figure 3.6, Metrabyte [1985]. This card has 24 bits of parallel I/O and it could have been used to handle both of the 12 bit S/D converters directly, but some of the bits were needed for other tasks. Port PA and lower half of port PC are dedicated to the S/D converters.

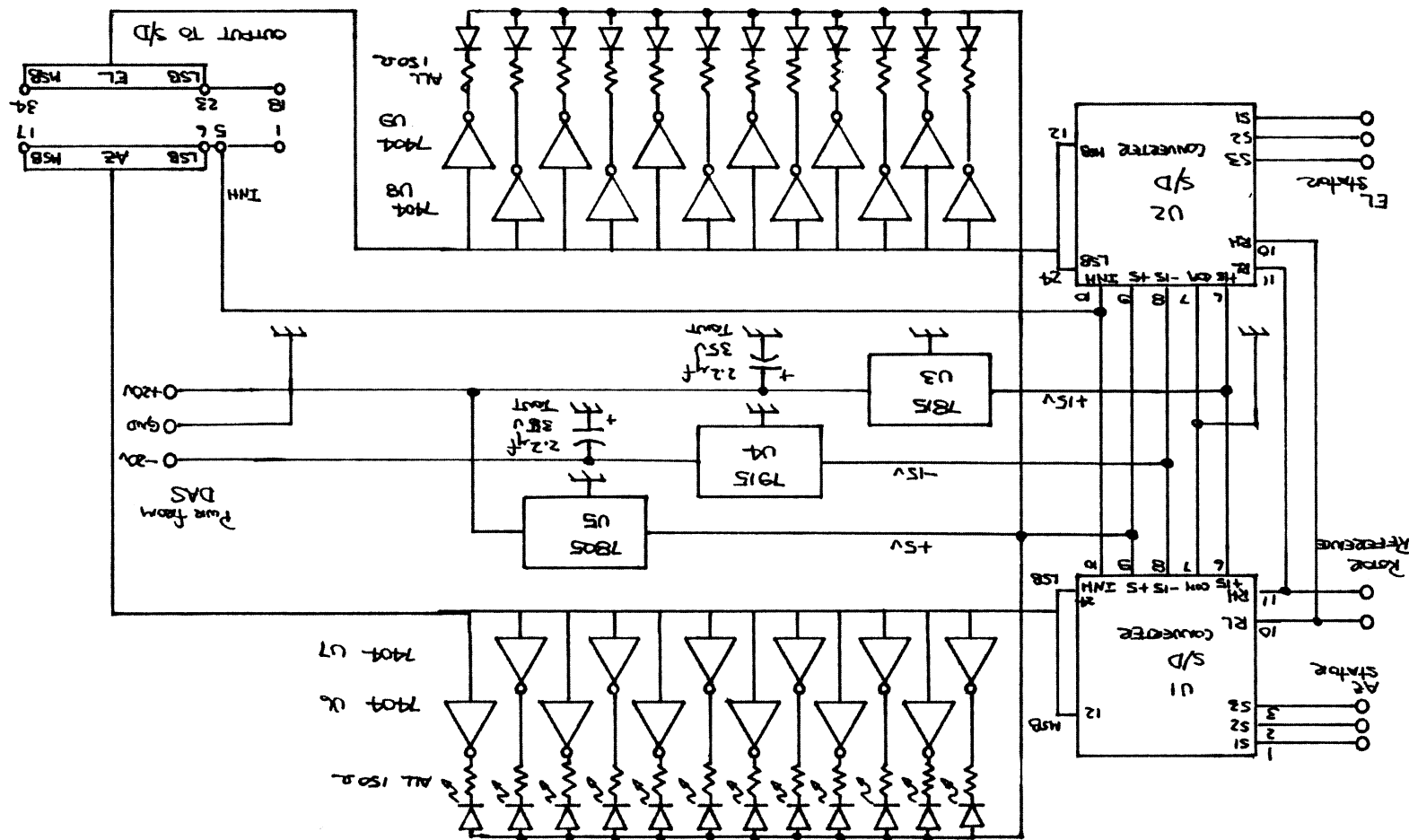


Figure 3.5 Synchro to Digital Converter Circuit

These two ports supply the required 12 bits but it was necessary to multiplex the information from the elevation and azimuth S/D converters on to the same 12 bits. This is the function of the the multiplex card shown in Figure 3.7.

The multiplex card is built around 74LS241 tristate bus drivers; U1, U2, and U4. They form a 12 pole double throw switch. Forcing pin 1 low and pin 19 high on the 74LS241 chip activates the output of the bus driver, and it acts as a noninverting gate. When the output is deactivated the bus driver appears as an open circuit. When U1 and the lower half of U4 are selected the 4 least significant bits of the azimuth S/D are connected to the lower nibble of port PC on the Metrabyte card and the upper 8 bits of the azimuth S/D are connected to port PA of the Metrabyte card. If U2 and the upper half of U4 are selected, the same thing happens only this time with the elevation S/D converter.

This selection process takes place through the upper nibble of port PC. As Figure 3.6 shows, port PC can be divided into two separate 4 bit nibbles. The lower nibble of port PC is configured as an input and the upper nibble is programmed as an output. A BCD to 10 line decoder, U3 in Figure 3.7, is connected to the upper nibble of port PC. Table 3.1 shows the effect of various outputs to port PC.

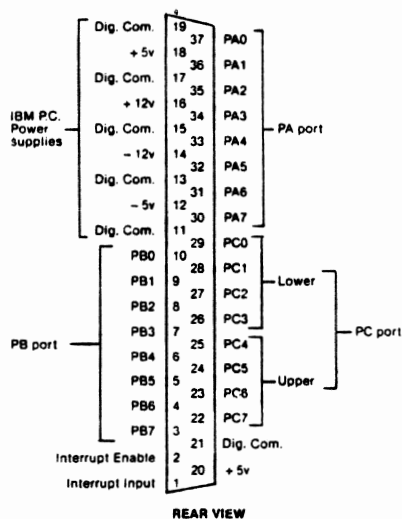
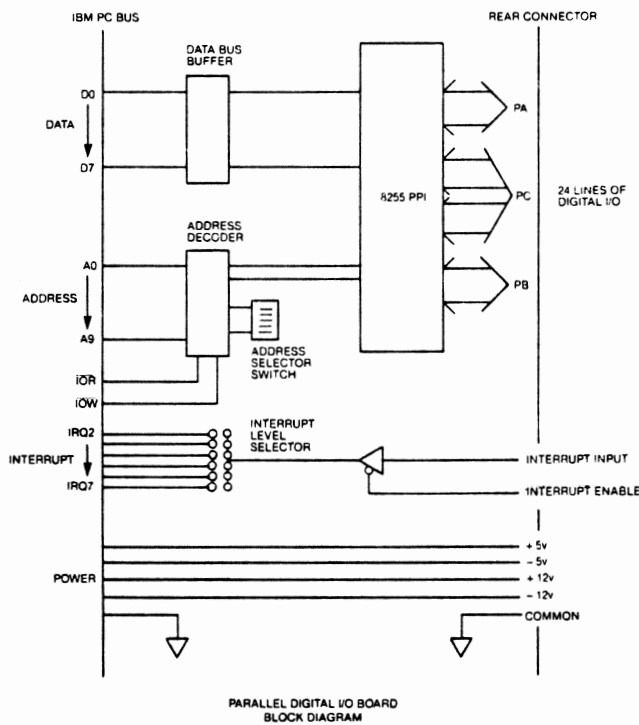


Figure 3.6 Metrabyte Card

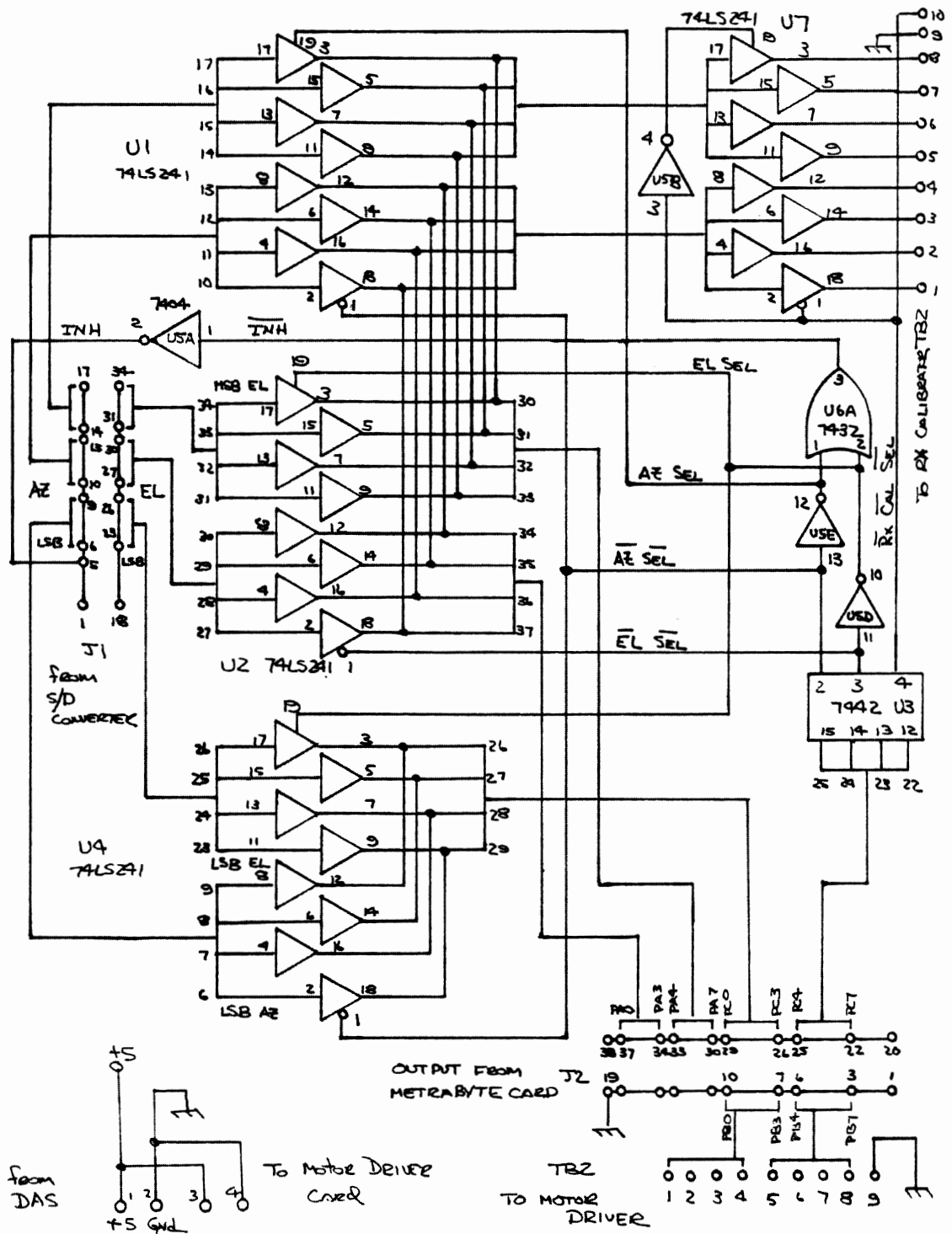


Figure 3.7 Synchro/Digital Multiplexer

Output to Port PC	U3 output	Selection
10H	pin 2 low	lower U4 and U1 Azimuth channel
20H	pin 3 low	upper U4 and U2 Elevation channel
30H	pin 4 low	U7 Receiver calibrator

Table 3.1

Metrabyte Card I/O Structure

Inverters, U5D and U5E, are used to supply the proper level to the select pins of the bus drivers. Their outputs are also ORed together with U6A and then inverted in U5A. The output of U5A will go low any time either of the S/D's is selected. This signal is used to inhibit the S/D's. Both converters are inhibited while one is read. The multiplex card also contains the output port that controls the receiver calibrator. More will be said about the receiver calibrator subsequently.

3.3.3 PC OUTPUT TO VERLORT MECHANICAL INTERFACE

Once the PC has selected and read the appropriate S/D, the resulting value is compared with the desired antenna position that is stored in a computer lookup table. If the difference is more than three counts the computer determines the direction that the antenna must go and writes

the appropriate command to Port PB of the parallel I/O card. Port PB is used to control a small DC gear motor that rotates the hand wheel CX.

The VERLORT manual pointing system is used intact. The desired movement is obtained by mechanically coupling a DC gear motor to the CX's, B1301 and B1302, that are part of the manual pointing system. These two CX's are unique in that both the rotor and the stator can be mechanically moved. In the original VERLORT system the stator is connected through a 10/1 gear train to a 2 phase servo motor. This motor is used as part of the scanning system. The rotor of the CX was connected through another gear train to the manual hand wheel. Moving either rotor or stator will cause the antenna to move.

The 2 phase servo motor could not be used because of the slower speed required for the INTELSAT scan and the complexity of the original servo system. The DC gear motor is connected directly to the shaft of the servo motor. The drawer that contains this machinery was modified by drilling several holes in the frame and bringing an extension shaft through the front panel. The two DC gear motors were mounted on the front panel and connected to the extension shaft with a small flexible coupling. Figure 3.8 shows the mechanical arrangement.

3.3.4 MOTOR DRIVER

Port PB of the Metrabyte card is configured as an output. The outputs from Port PB go to the motor driver card. The schematic

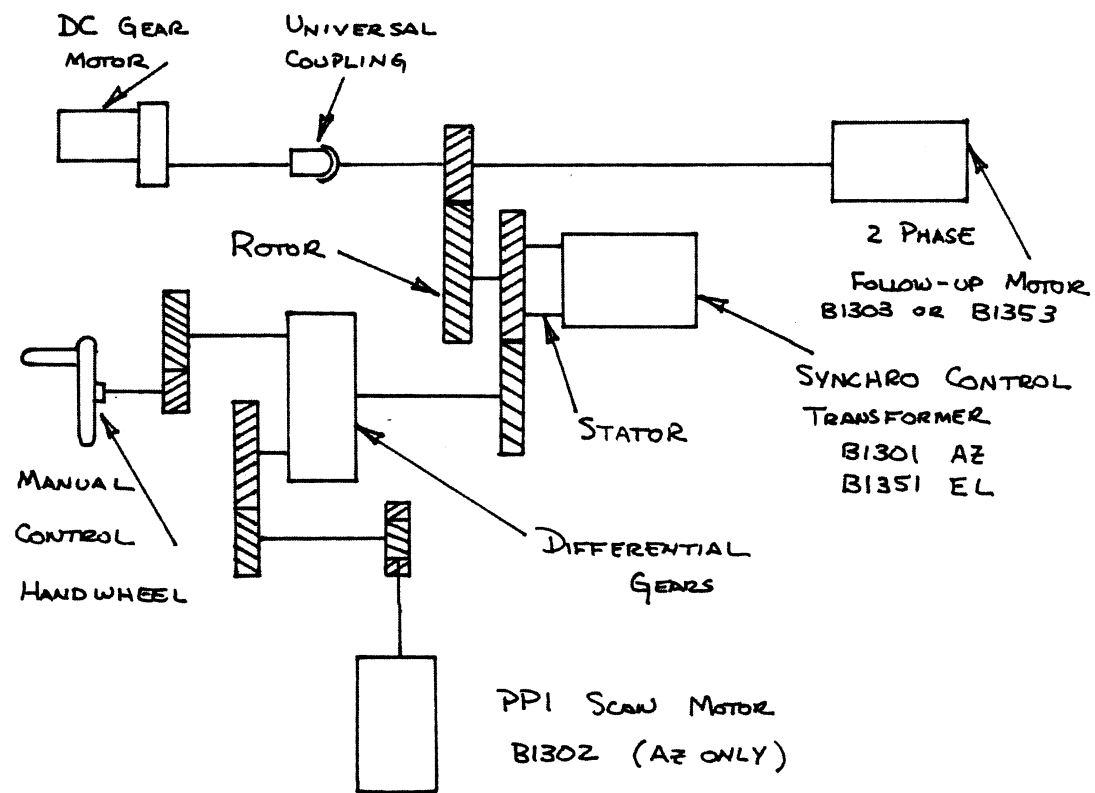


Figure 3.8 Mechanical Connection

for the motor driver card is shown in Figure 3.9. There are two identical drivers, one for elevation and one for azimuth. They each consist of a 7442 decoder, four opto-isolators, and four power transistors connected as switches. There is also an adjustable plus and minus voltage regulator, U3 and U4. These regulators supply the lower voltage for the motor "slow" speed.

The operation of both drivers is the same, so only the azimuth driver will be described. A BCD 1 applied to U2 will pull pin 2 low and turns on opto-isolator I8. This connects the the base of Q8 through a 100 ohm current limiting resistor to the -6 volt supply rail. Q8 conducts and the -6 volt supply is applied to the azimuth motor. If a BCD 2 is applied to U2, pin 3 will be low and I7 and Q7 will be on. The +6 volt supply is now connected to the azimuth motor and it will then run in the opposite direction. A BCD 3 will apply -12 volts to the motor and BCD 4 will apply +12 volts.

The nature of the internal decoding of the 7442 allows only one output to be low at one time. If anything other than BCD 1-4 is applied, all the opto-isolators will be cutoff and nothing will happen. A BCD 0 is used as the stop command.

Port PB is divided into two nibbles. The upper four bits are used for the azimuth and the lower four bits are dedicated to the elevation. Since only five commands per axis are needed only three of the 4 bits are used.

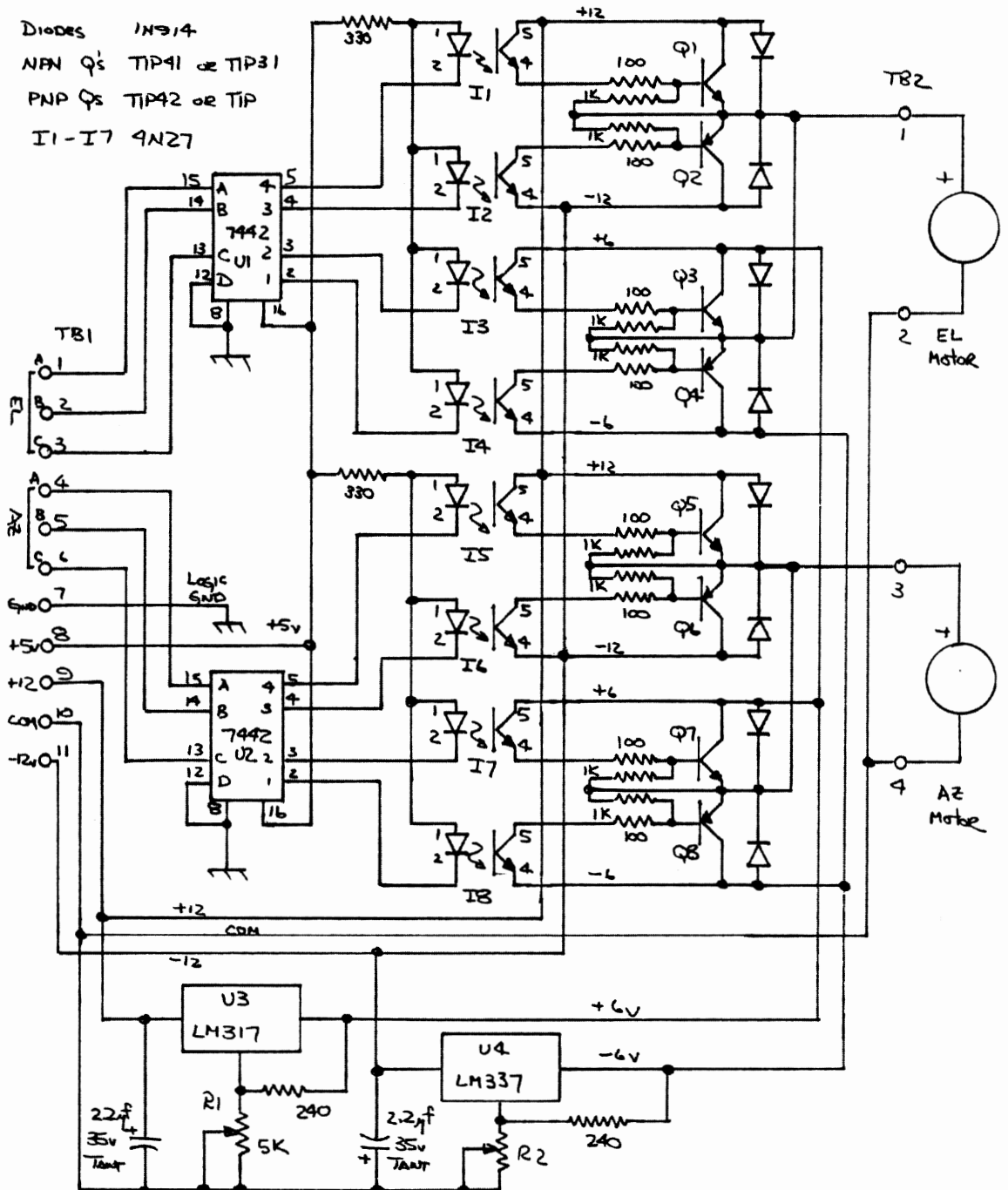


Figure 3.9 Motor Driver Circuit

Port PB output		Action
xxxxx000B	x0H	Az stop
xxxxx001B	x1H	Az CW slow
xxxxx010B	x2H	Az CCW slow
xxxxx011B	x3H	Az CW fast
xxxxx100B	x4H	AZ CCW fast
x000xxxxB	0xH	E1 stop
x001xxxxB	1xH	E1 down slow
x010xxxxB	2xH	E1 up slow
x011xxxxB	3xH	E1 down fast
x100xxxxB	4xH	E1 up fast
x - don't care		

Table 3.2

Motor Driver input function table

If the x's are all made zeros then the elevation and azimuth commands could be ANDed together in the software to provide independent control of the two axes.

3.4 ANTENNA CONTROL SOFTWARE

The software was written in TURBO Pascal for the IBM PC. The program complete listing is included in Appendix 4. The procedure for programming of the Metrabyte card and the synchro read procedure may be of greater general interest so they will be described in some detail.

3.4.1 INPUT/OUTPUT CONSIDERATIONS

To read the S/D converter it is necessary to do the following operations: initialize the Metrabyte card, select the correct S/D, read the upper eight bits, read the lower four bits, and combine the result into one number.

The Metrabyte card uses four addresses in the address space of the IBM PC. 300H was chosen as the base address. Programming the base address is accomplished by setting a dip switch on the card. The choice of address is somewhat arbitrary, but the Metrabyte documentation suggests addresses below 255H should be avoided because the PC uses some of these addresses for internal I/O. The Metrabyte I/O is organized as follows:

Base address (300H)	+0	PA port	read/write
	+1	PB port	read/write
	+3	PC port	read/write
	+4	Control port	write only

Table 3.3

I/O Addresses and Functions

Before any port can be used it is necessary to write an instruction to the control word port. This tells the I/O which ports are inputs and which ones are outputs. Writing 91H to this port will initialize PA as an input, PB as an output, PC 0-3 as an input, and PC 4-7 as an output. This conforms to the circuitry already described.

3.4.2 SYNCHRO READ PROCEDURE

```

PROGRAM ElevationRead ;

CONST porta = 300H;      (Input, upper 8 bits)
    portb = 301H;      (Output, motor control)
    portc = 302H;      (hi nibble - S/D select,
                        lo nibble - S/D lower 4 bits)
    portc = 303H;      (control port, out 91H to it)

VAR   e1 : integer ;

PROCEDURE elev(var e1 : integer) ;  (Read the elevation)

    Var hi, lo : byte ;

BEGIN
    PORT[portc] := 20H; (select the elevation S/D)

```

```

hi := PORT[porta] ; (read the upper 8 bits)
lo := PORT[portc] ; (read the lower 4 bits)
lo := lo AND 0fH: (upper 4 bits of portc are
                     undefined so mask them out)
el := 16*hi + lo ; (multiply with upper 8 bits by
                     16 to shift them to the right
                     4 bits and add the lower 4 bits)
PORT[portc] := 0H; (Deselect the elevation S/D)
END;

BEGIN          (Begin main program)

    PORT[portd] := 91H; (Initialize the Metrabyte card)

    elev(el);          (Call the elevation read
                         procedure)

END.

```

In the program above the variable el will contain the value of the elevation S/D. This value will be an integer between 0 and 4095. This number can be converted to degrees in the following way:

$$\text{Elevation(degrees)} = \frac{\text{el(counts)}}{4096} (360) \quad (3.8)$$

The azimuth could be read in a similar way by outputting 10H to portc.

3.5 SYSTEM PERFORMANCE

For such a "crude" system it performs very well. In the slow mode it will routinely point the antenna within a ± 1 count ($> \pm 1^\circ$) of the desired position. The system has operated reliably for approximately six months. At the present writing the "fast" mode still does not work reliably. The

"fast" mode causes unexpected failure of the "fast" switching transistors. The switching transients produced by the higher voltage applied to the motors in the fast mode may cause the transistors to fail. A possible fix would be to put a small, about 10 ohm, resistor in series with the motor to limit the current. Until the cause of this failure is found a somewhat longer scan cycle must be tolerated because the "fast" mode cannot be used.

CHAPTER 4. RADAR CALIBRATION

4.1 INTRODUCTION TO RADAR MEASUREMENT ERRORS

The Virginia Tech radar measures the backscattered power from rain drops in a particular range cell. This received power can be related to the radar reflectivity factor, Z, through the radar equation:

$$P_r = \frac{\pi^5 P_t G(ct) |K|^2}{1024(\ln 2) R^2 \lambda^2 L_r L_t} Z = C Z / R^2 \quad (4.1)$$

where

P_r	power received
P_t	power transmitted
c	velocity of light
t	pulse width
R	range
λ	wavelength
L_r	losses associated with receiver
L_t	losses associated with transmitter
C	Radar constant
$ K ^2$	$(\epsilon - 1) / (\epsilon + 2)$ where ϵ is the dielectric constant of the rain drops

The radar constant C is usually invariant for any particular system but it must be accurately known because the received power is directly proportional to C.

The radar reflectivity factor can easily be calculated if the received power, range, and C are known. Errors in Z can be associated with processing errors and errors inherent in the modeling as well,

but this chapter will deal primarily with reducing radar constant errors.

Pulse width and wavelength are related to the radar circuitry and any variation in them should be so small as to be ignored. The two quantities most subject to change are the transmitter power and the receiver sensitivity. This chapter describes a transmitter average and peak power monitor and a receiver calibrator that are incorporated into the radar system to reduce errors from these two sources.

Transmitter power is sampled in the output waveguide through a directional coupler and attenuated to an appropriate level for a thermistor power meter for the average power measurement. Part of this power sample is also applied to a diode square law detector for peak power measurement.

Given the nature of the data collection system, there is an additional requirement that the peak power information be placed in range gate zero of the receiver. The function of the peak power monitor is to properly multiplex the transmitter power sample and the receiver output.

The receiver calibration is done by injecting a signal of a known power into the output waveguide. The signal is generated by a packaged microwave oscillator. A programmable attenuator reduces the oscillator signal to the appropriate level for the receiver. This signal is injected through a directional coupler into the output waveguide. The attenuator is controlled by an IBM PC programmed to perform the

calibration cycle. The receiver calibration is initiated by an operator on an occasional basis.

If the transmitter power and receiver sensitivity are known, it is possible to obtain antenna gain by measuring the power reflected from a calibrated target. A target used for this purpose is a metallic sphere. The radar equation for the sphere target is given by:

$$P_r = \frac{P_t G^2 \lambda^2 \sigma}{(4\pi)^3 R^4} \quad (4.2)$$

where σ is the radar cross section of the target and the quantities in equation 4.2 are defined as in equation 4.1 above. Assuming that the range to the target, the transmitter power, the received power, and the target cross section are all known, it is possible to solve for the antenna gain.

The computer program described in Appendix 1 was used to calculate the radar cross section of the six inch diameter sphere that is used for the calibration of the VPI radar. At the radar's operating frequency of 2800 MHz, the sphere has the following characteristics:

$$ka = 4.4686 \quad \sigma/\pi a^2 = 1.0443 \quad \sigma = 0.01905 \text{ m}^2$$

A six inch calibration sphere for 2800 MHz is a good choice because $\sigma/\pi a^2$ is often estimated as equal to one.

The waveguide loss from the radar to the antenna is an unknown but it is not necessary to know it explicitly. The transmitter power

measurement and the receiver sensitivity measurement are done at the same point in the waveguide. Since this point is beyond the T-R switch in the radar, the transmission line losses are equal for both transmit and receive. Since the antenna gain is equal for both transmit and receive, the line losses can then be lumped in with the antenna gain. The antenna gain measured by the sphere calibration will be reduced by the line losses.

4.2 THE MEASUREMENT OF RADAR TRANSMITTER POWER

4.2.1 SYSTEM REQUIREMENTS

Transmitter output is characterized by both a peak and an average power. For the INTELSAT project it is necessary to measure and record both. Since the measured peak power value goes in range gate zero, an interface with the DAS is required for the peak power measurement. The average power is recorded once for each radar data point. Since it is necessary to record radar data, transfer it to the S-100 computer, and move the antenna to the next point, the average power measurement is only done every 8-10 seconds. This is adequate for the present application. The actual measurement is done under control of the IBM PC which handles the task of antenna control.

4.2.2 AVERAGE POWER MEASUREMENT

It is common practice, Handbook of Microwave Measurements [1963], at microwave frequencies to measure power by using directional couplers and/or attenuators to reduce the power level to a range where it can be converted to heat in a heat sensitive device such as a thermistor. Such devices have a relatively long thermal time constants, HP8487 Users Manual [1983]; long in terms of the pulse length and repetition time of the radar pulse. This means that thermistor power meters will respond to the average of the transmitter power in the following way:

$$P_{ave} = (t)(prf)P_{peak} \quad (4.3)$$

where t is the pulse length and prf is the pulse repetition frequency.

An HP 432A power meter and an HP 8487B thermistor mount are used for the average power measurement. The power meter has a 0-1 volt recorder output which is sampled by an A/D converter in the antenna control PC. The PC transfers this value to the DAS, along with the current antenna position.

Transmitter power is approximately 100 watts average (50 dBm) or 250 kw peak (84 dBm), but 10 mw (10 dBm) is the highest range on the power meter. The transmitter has a 27 dB coupler in the output waveguide so additional attenuation is needed to bring the power into the power meter's range. A power sample for peak power measurement

and a way to inject the receiver calibration signal is also needed. Figure 4.1 shows the system used to accomplish this.

At this point a word of caution is in order. Most attenuators, power meters, and other RF devices have both a peak and an average power rating. Exceeding either one can result in the destruction of the device. Atten 1 of figure 4.1 is a device rated for 20 watts average even though it is subjected to only 0.15 watts average. It is however subjected to approximately 500 watts peak. Atten 1 was originally a 2 watt average, 200 watt peak, device. The excess peak power soon destroyed it so an attenuator with a higher peak power rating is necessary. The HP 8478B power meter head is rated for 37 dBm microseconds. It operates at 36 dBm microseconds in this system. One hopes that HP's usual conservative rating applies in this case.

4.2.3 PEAK POWER MEASUREMENT

It is a simple matter to obtain the peak power from the measured average in the following way:

$$P_{\text{peak}} = \frac{P_{\text{ave}}}{(t)(\text{prf})} \quad (4.4)$$

This however does not fully satisfy the need to measure peak power. Each pulse is an independent event since each pulse is transmitted in a different polarization. Even though the echoes from each

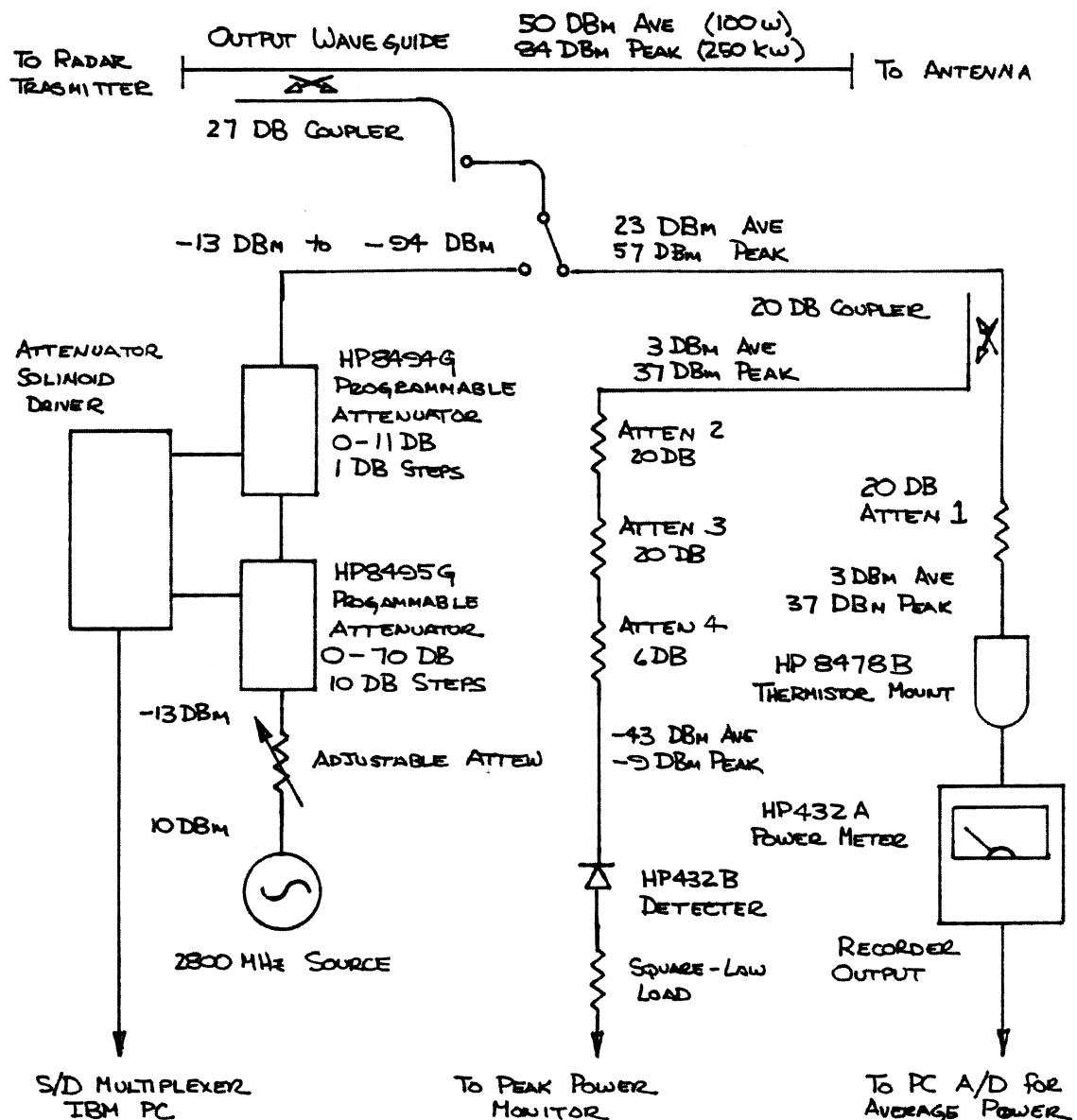


Figure 4.1 Power Monitor and Receiver Calibrator System

polarization are averaged over 64 samples, each of these samples is eight pulses apart. For this reason it is not desirable to use the average power measurement to obtain peak power. It is desirable to sample each pulse individually.

There are a number of methods of peak power measurement, Handbook of Microwave Measurements [1963], however most of them use the integrating properties of a CRT. One method that requires no integration and thus can measure the power of individual pulses is a square law detector and a Sample/Hold circuit

Square law detection is normally done with diode rectifiers. The output current of the diode can be written as:

$$I_o = aV_{in} + bV_{in}^2 + cV_{in}^3 + \dots \quad (4.5)$$

If the applied voltage is small enough, it is possible to ignore the 3rd and higher order terms. Then if the diode is presented with an appropriate resistive load and the AC components of the output are filtered out, the output voltage is proportional to the square of the applied voltage and thus proportional to power.

A Schottky barrier diode was chosen for this application because it has a very low junction capacity so it will not stretch out the short transmitter pulse. It is also much less susceptible to high power burnout which is particularly important in a pulse application, and it

is available packaged for microwave use. An HP432B coaxial crystal detector is such a device and was chosen for this application.

4.2.4 PEAK POWER DETECTOR AND SAMPLE/HOLD CIRCUIT

The detector requires a high impedance load and it produces a relatively small output voltage so buffering and amplification are required to bring the detector output up to the desired level. The peak power sampler consists of two amplifiers, U1 and U2, followed by a sample/hold circuit, U3, as shown in Figures 4.3 and 4.4.

U1 is a high speed FET voltage follower with a gain of 1. It supplies the high impedance load for the detector. R1 trims the offset voltage of U1. Since U1, U2, and U3 are all DC coupled, R1 is used to trim the offset of all three amplifiers.

U2 is an inverting amp with a gain of 50. It supplies the gain necessary to bring the 50 mv detector output up to 2.5 v. This voltage is applied to the sample/hold U3. The transmitter pulse is 800 nsec wide so to prevent distortion of the pulse it is necessary to use very fast op-amps for U1 and U2. These amplifiers will operate to 100 MHz and careful decoupling is necessary to insure stable operation.

U3 is a high speed sample/hold. It holds the detected peak until it can be sampled by the DAS. Even though the transmitter pulse occurs only every two milliseconds or so, the sample/hold must follow the short pulse and it must be able to dump the hold in less than the time

required for one range gate, or 1.7 micro-seconds. For these reasons U3 must be a high speed S/H. The one being used for the power sample is the same as the one used in the video channel of the DAS.

4.2.5 POWER MONITOR DAS INTERFACE

The sampled value of the peak power must be placed in range gate zero so it can be recorded with the echoes from that pulse. This is accomplished by an analog multiplexing of the sampled transmitter pulse with the receiver video.

The rising edge of trigger pulse starts the cycle that turns on the transmitter. There is approximately a one micro-second delay before transmitter output actually appears due to delay in the radar modulator. It is necessary to introduce a delay in the peak power sampler so that the sample is taken at the maximum of the transmitter pulse. The detected voltage is then added to the receiver video and it must be held until sampled by the DAS for range gate zero. The receiver must be turned off during this hold period because its output goes to +5 volts due to transmitter leak-through and ground clutter echoes received immediately after the transmitter fires. The receiver function must be restored for the next range gate sample. Figure 4.2 shows the timing necessary to accomplish this.

Figures 4.3 and 4.4 contain the circuitry needed for the DAS power sampler interface. The time at which the transmitter sample is taken

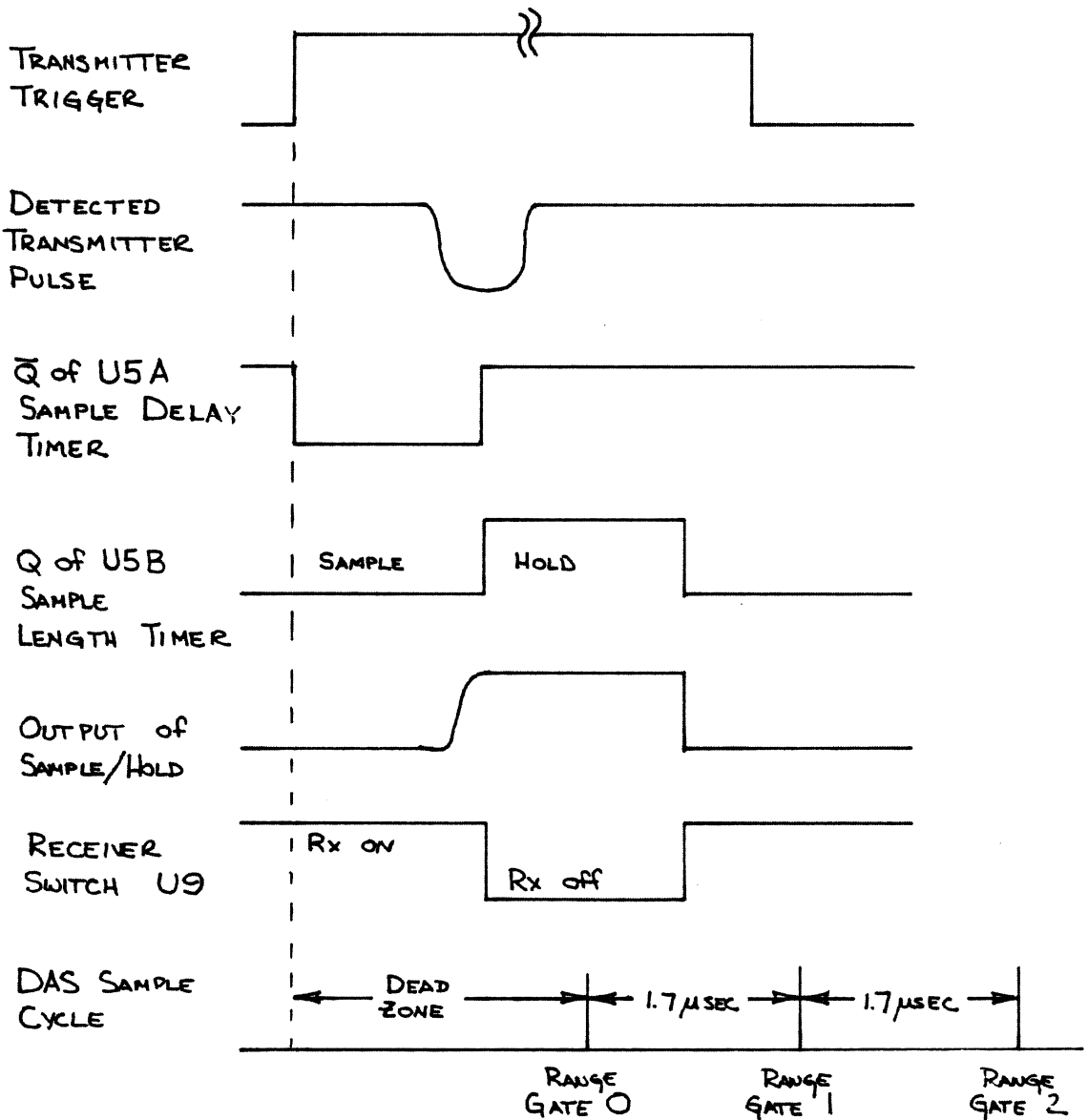


Figure 4.2 Power Monitor Timing Diagram

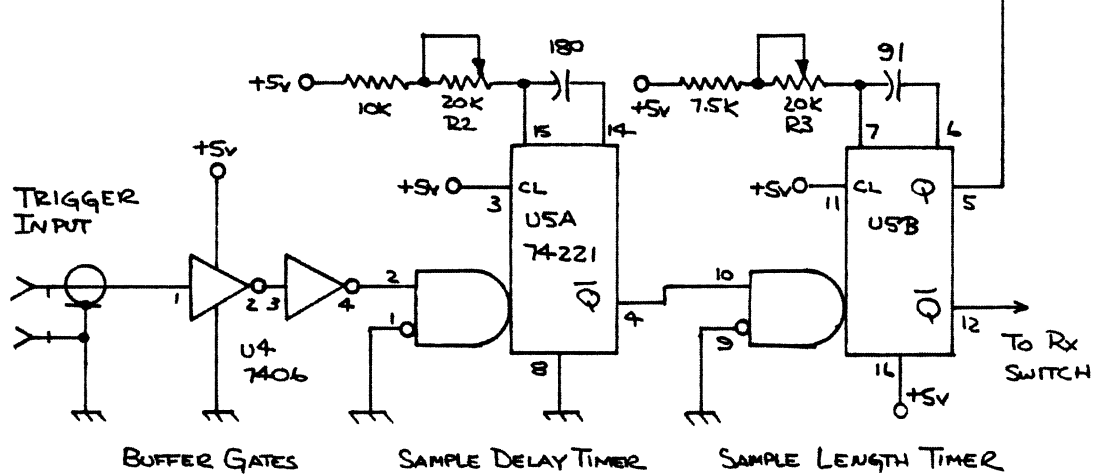
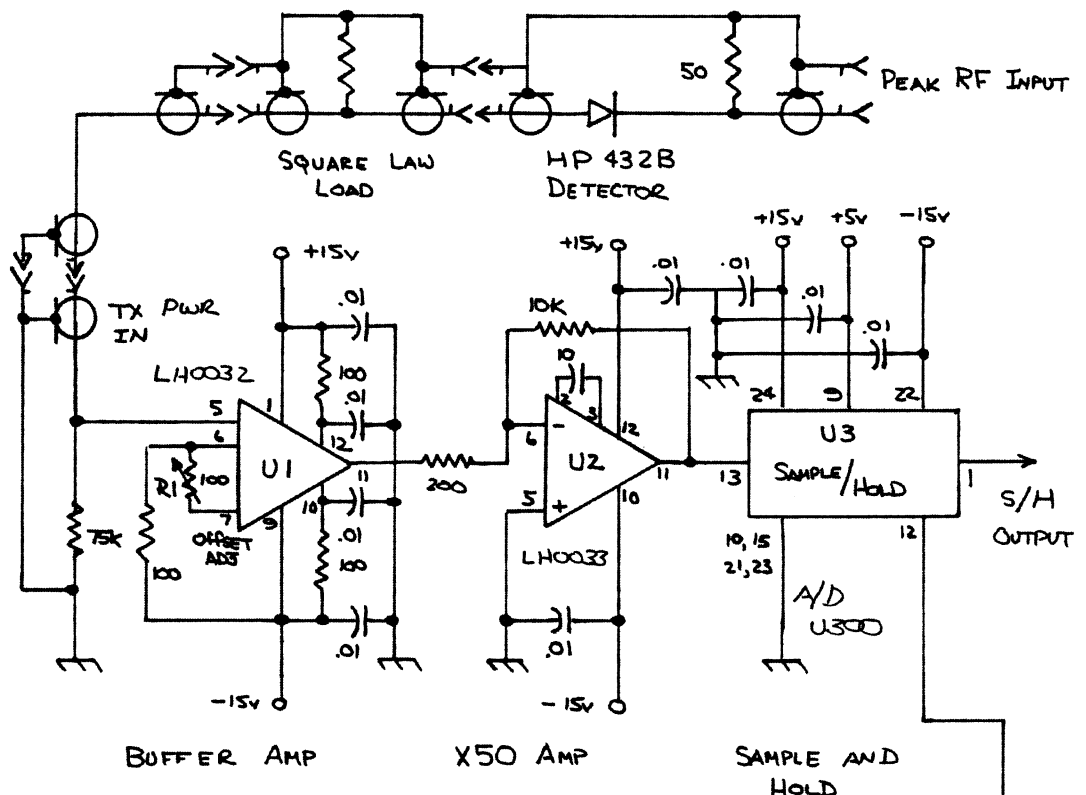


Figure 4.3 Peak Power Sampler

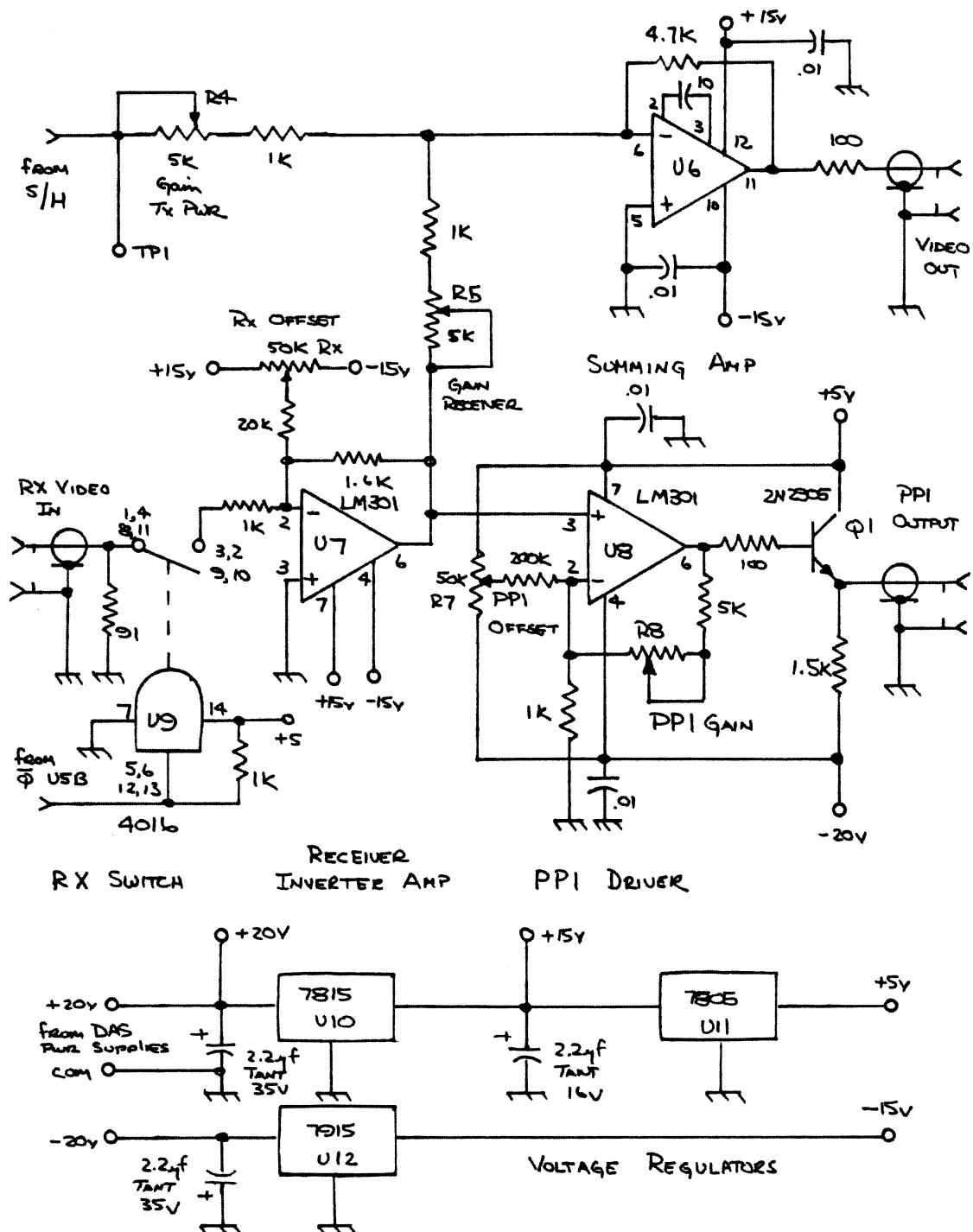


Figure 4.4 Peak Power Sampler

is controlled by the sample delay timer U5A. The sample delay is set so that the hold begins at the most negative value of the detected pulse. The sample delay is determined by the time it takes for RF power to appear after triggering. The hold time is determined by the DAS dead zone, the sample delay, and the sampling rate of the DAS. The sample delay and sampling rate are more or less fixed so any change in the dead zone will necessitate a change in the peak power sample time.

4.2.6 DAS INTERFACE CIRCUIT OPERATION

Referring to Figure 4.3, the transmitter trigger is applied to U4 of the peak power sampler which acts as a buffer. The rising edge of the trigger starts the sample delay timer, U5A. This forces its \bar{Q} output low. After it times out, its output goes high again. This starts the hold timer U5B. When this timer starts, its Q output goes high and places the Sample/Hold U3 in the hold mode. In the sample mode, U3 appears as a follower type amp. In the hold mode, the output is held at its current value.

The hold timer, U5B, controls the time that the transmitter sample is held. It must be held long enough so that when the DAS samples range gate zero it samples the voltage held from the transmitter power detector. The hold must end and the receiver must be reconnected before the DAS samples range gate 1 some 1.7 microseconds later.

When the hold timer is started its \bar{Q} output also goes low and turns off the analog switch of U9 of Figure 4.3. This disconnects the receiver from summing amplifier, U6. The summing amp adds the receiver output and the output of the sample/hold. During the hold period the analog switch is open so the receiver contribution to the summing amplifier output is zero and the output of U6 contains only the value of the sampled transmitter power. After the transmitter hold ends the receiver is reconnected. With the transmitter output zero, the output of the summing amp is the receiver video alone.

The inverter amp, U7, has a gain of about 1.6 to make up for a small amount of loss in the analog switch U9. It also inverts the receiver video so that after it goes through the inversion of the summing amp it will appear with the correct polarity for the DAS A/D converter.

The PPI display requires a video voltage between zero and -15 volts. To obtain this voltage swing, U8 and Q1, which form the PPI driver, are used with asymmetrical supplies of +5 and -20 volts.

Finally U10 and U11 are positive voltage regulators which supply +15 and +5 volts respectively. U12 is a -15 volt regulator. The ± 20 volt power is obtained from the DAS power supplies.

4.2.7 ADJUSTMENT PROCEDURE

The power sampler and DAS interface should be adjusted according to the following procedures.

The amplifier offsets should be set first. TP1 of Figure 4.4 is supplied for this purpose. The transmitter offset is set as follows: with the diode detector connected but with the transmitter off, R1 is adjusted for zero voltage at TP 1. The receiver offset is set by first setting the transmit offset, then with the transmitter off and the receiver disconnected, R6 is adjusted for zero voltage at the VIDEO output.

Adjustment of the power sampler is accomplished by disconnecting the receiver and the DAS from the power monitor and connecting a scope to the VIDEO output. With the transmitter running, R2, which controls the sample delay time, is adjusted for a maximum height pulse. The DAS is then reconnected to the VIDEO output and the RADCAL program is run from the S-100 computer. R3 is now adjusted until the power sample value appears in range gate zero. It may be necessary to adjust the dead zone in order to make this happen. All the other range gates should be zero or close to it. Disconnecting the diode detector from TX PWR jack on the power monitor should cause all the range gates to go to zero. After adjustment the receiver should be reconnected to the RX jack and the power monitor is now be ready for use. With the receiver connected,

the transmitter sample should appear in range gate zero with receiver noise or ground clutter appearing in their normal positions.

As already noted, U6 is a summing amp. Its inverting terminal is an effective ground so the gain of the transmitter sampler and the receiver video can be set independently. R4 sets the gain of the transmitter sampler, and R5 sets the gain for the receiver video.

The adjustment of R4 and R5 is accomplished as follows. The offset in both the transmitter and receiver channels should be set as described above. R4 is then set so the the transmitter sample is a hundred or so counts less than the DAS saturation value while RADCAL is running. R5 is set so that the maximum of the receiver video is just less than 5 volts at the VIDEO output. There is some slight interaction of R4 and R5 so it is necessary to recheck the other channel after any adjustment. The best situation is not to readjust gain once it has been set unless absolutely necessary. Receiver and transmitter recalibration can be done by changing the slope and intercept, M and B, in the data processing programs rather than trying to set the calibrations to some value.

The PPI driver, U8, is adjusted to produce the most pleasing display. R7 adjusts the offset and R8 sets the gain for the driver.

4.3 RECEIVER CALIBRATOR

4.3.1 THE RADAR RECEIVER

The VPI radar uses a single conversion superheterodyne receiver with an intermediate frequency of 30 MHz and a logarithmic detector. The log detector gives it a dynamic range between 70 and 80 dB. Figure 4.5 is a block diagram of the receiver. The only parts of the receiver left from the original VERLOT radar are the duplexer, the image filter, and the mixer.

4.3.2 RECEIVER CALIBRATOR

The calibrator has two functions. The first function is to measure the sensitivity of the receiver and the second function is to determine its linearity. The calibrator injects a signal of a known power into the receiver waveguide. From this signal, the absolute sensitivity of the receiver can be obtained. This power can be adjusted in 1 dB steps over an 81 dB range with step attenuators to determine receiver linearity.

The receiver's operating range is -40 dBm to -110 dBm. The signal source generates about +10 dBm. The waveguide coupler and two HP step attenuators reduce the signal level to the proper range. There is an adjustable attenuator at the output of the signal source to isolate the source from the step attenuators and to set the source output. Figure

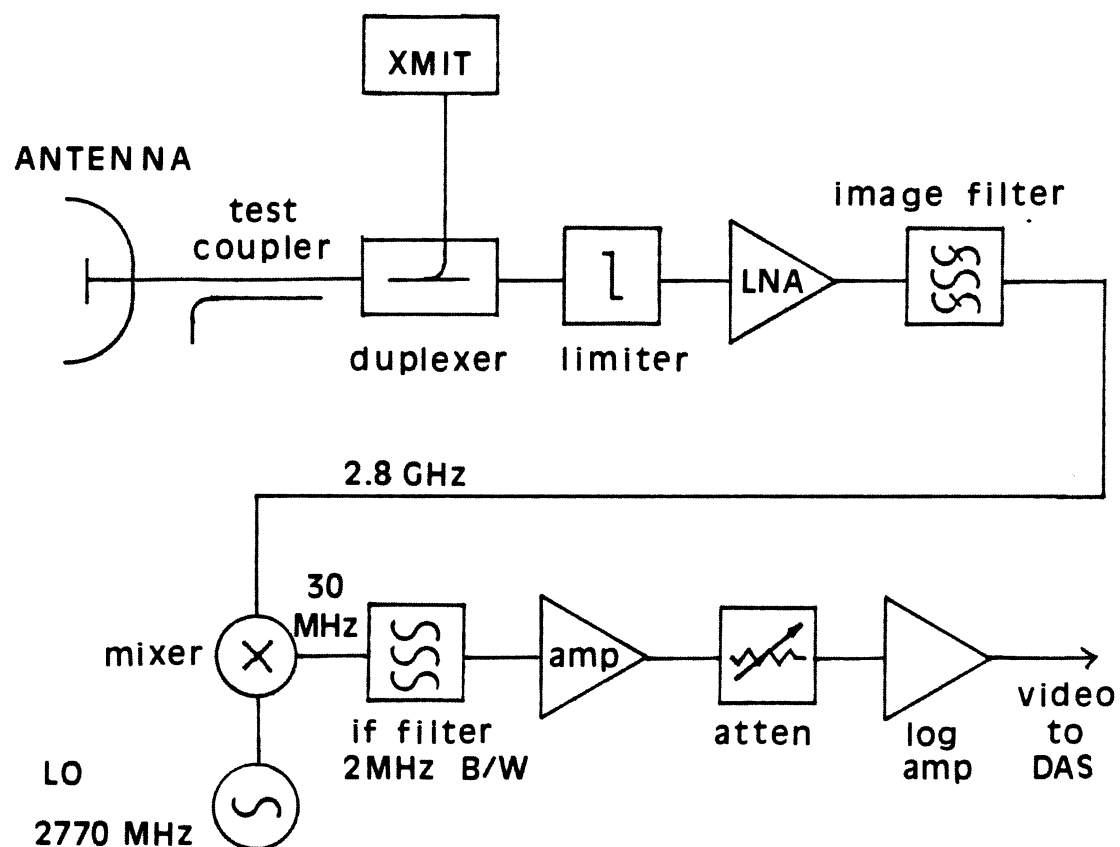


Figure 4.5 Radar Receiver.

4.1 shows the arrangement of source and attenuators along with approximate signal levels. The co-ax switch in Figure 4.1 selects either the transmitter power monitor or the receiver calibrator. This switch is controlled by the program which does the receiver calibration.

The test signal is generated by a microwave signal source. The source is phase locked to a crystal reference. This should make it stable with frequency. The source was not specially designed for output level stability, however its output was monitored for several hours with a power meter and its output stability seems as good as the power meter stability. The normal procedure would be to set the calibrator output with the power meter each time the calibrator is used. Under these conditions the power stability of the source should be more than adequate.

The step attenuators are controlled by the PC which does the antenna control. With proper calibration the program will calculate the signal level at each step or supply a desired signal level. The PC controls the step attenuators through port PA of the Metrabyte card. This was described in Section 3.3.2.

4.3.3 CALIBRATION AND USE

To set up and use the calibrator it is necessary that the transmitter is off. Care should be taken not to run the transmitter while the receiver calibrator is connected to the output waveguide

lest damage be done to the attenuators and the signal source. The calibration program makes this difficult but not impossible.

To use the calibrator, it is first necessary to calibrate its output with a power meter. The source should be turned on several hours before use so that it can stabilize. It is best to leave the source off when not in use. The source runs at the receiver frequency so there is the possibility of interference.

4.3.4 COMPUTER INTERFACE

Port PA of the Metrabyte card, Figure 3.6 , is configured as an output. This is accomplished by outputting 81H to the control register of the Metrabyte card. For more details on programming see Section 3.4. The S/D multiplexer, Figure 3.7, has an extra 8 bit output that is addressed by writing a BCD 3 to the upper nibble of Port PC. When this output is selected Port PA is connected through a 74LS241 bus driver, U7 of Figure 3.7, to the programmable attenuator solenoid drivers. Also when this output is selected, pin 4 of U3 of Figure 3.7 goes low. This low is used to control the co-ax switch which connects the receiver calibrator output to the waveguide.

The HP 8490 series step attenuators are controlled by 24v solenoids. The HP 8495 contains three attenuator cards arranged in attenuations of 10, 20, and 40 dB. It can easily be programmed in BCD for a maximum attenuation of 70 dB. The HP 8494 contains four

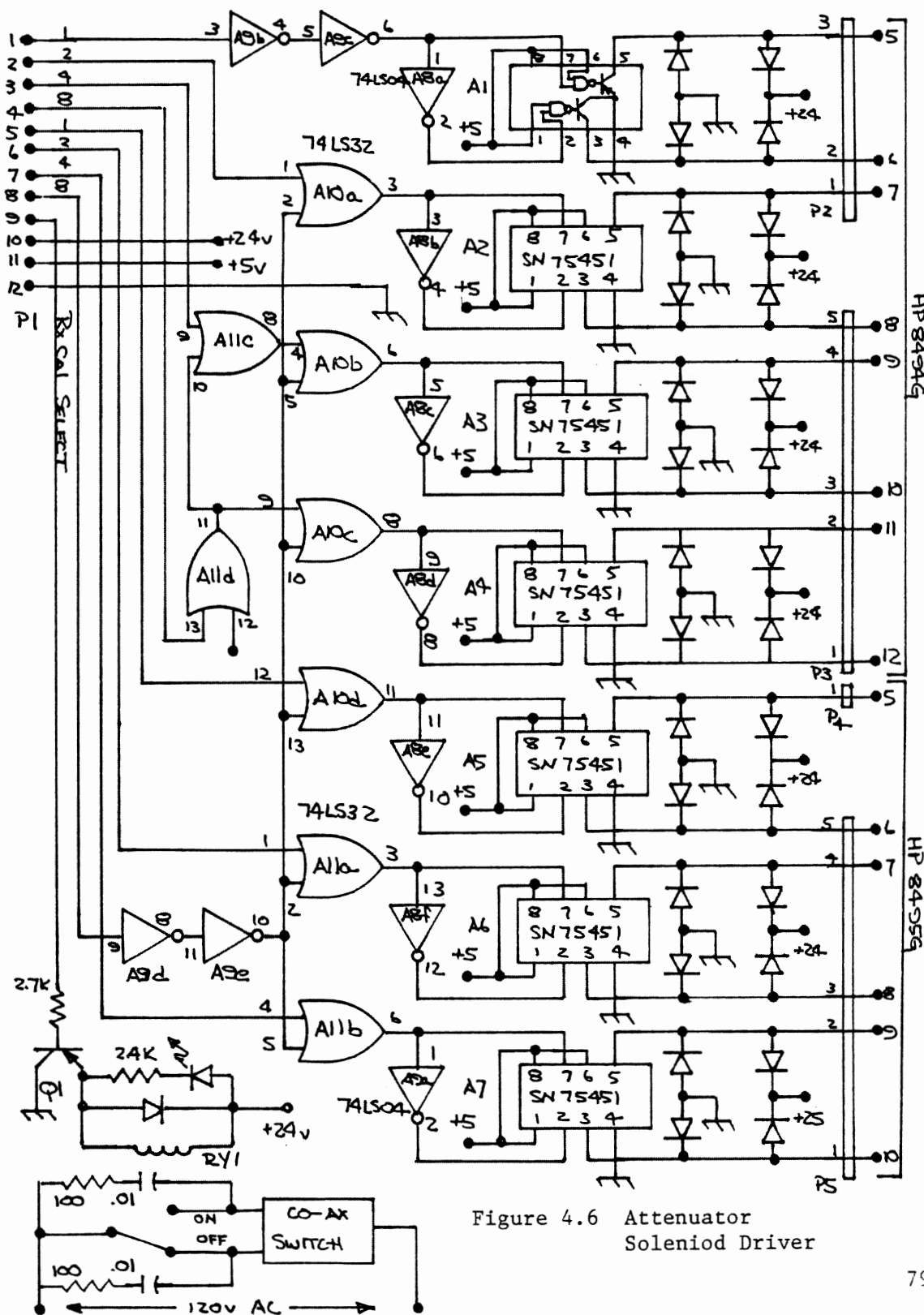


Figure 4.6 Attenuator
Solenoid Driver

attenuator cards arranged in attenuations of 1,2,4,4 dB. This is not quite BCD but with some simple decoding it is possible to program it in BCD.

Figure 4.6 is the circuit diagram for the attenuator driver card. U10 and U11 perform the logic to permit programming the attenuators BCD. U11C OR's the "4" and "8" line together. If the "4" is high only one of the 4 dB sections will be actuated and if the "8" line is high both 4 dB sections are actuated through U11C. U10, U11A, and U11B are wired such that a BCD "80" will actuate all the attenuator sections except the 1 dB section. This will give 80 dB of attenuation. The extra gates of U9 and U11D are used for buffering.

Each of the solenoids of the attenuator requires 24 volts at about 125 ma. The solenoids are magnetically latching. That means that the solenoids need be energized only long enough to latch them in position. As soon as one solenoid is latched in position, contacts internal to the attenuator disconnect power from it. Another set of contacts are closed so that the unlatching solenoid can be energized. This arrangement forms a kind of mechanical set-reset flip-flop. Figure 4.7 shows a diagram of one section of the attenuator.

U1-U7 of Figure 4.6 are drivers for the solenoids. Each driver chip contains two switches which are capable of handling the voltage and current required by the solenoids. With the aid of a 74LS04 inverter gate these switches are arranged as a SPDT switch. The diodes associated with each driver are to protect the transistors in the

switches from the inductive kick generated each time the solenoid current is interrupted.

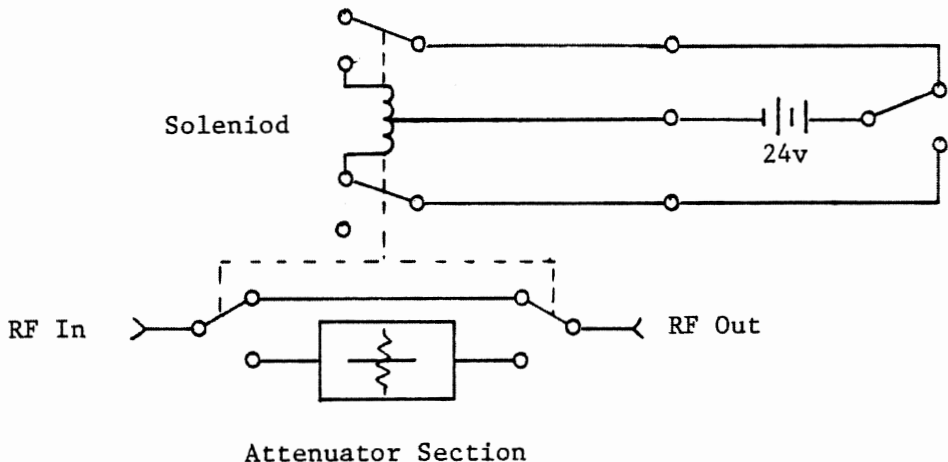


Figure 4.7

Attenuator Solenoid Operation

The relay, RY1 and its associated switch, Q1, control the co-ax switch. An LED is connected across the relay coil to indicate when the receiver calibrator is connected to the radar waveguide. Some thought was given to this circuit so that the more likely failure modes would cause the co-ax switch to remain connected to the transmitter power monitor. This will reduce the likelihood of the transmitter being turned on while the step attenuators are connected to the output waveguide.

CHAPTER 5. CONCLUSIONS

The complexity of the VPI radar and statistical nature of rain echoes make the direct verification of ZDR difficult. A method was developed to compare measured ZDR with predicted values of ZDR and ZDR from previously published work. The ZDR measured by the VPI radar is in the correct range.

The validity of fade statistics developed from the data base of radar observations and measured link performance depend on the validity of the radar observations. Initial predictions of rain induced fading on the main site slant path were published in July of 1986, Stutzman et al. [1986]. These predictions show good agreement between the measured values of attenuation and the attenuation predicted from radar Z, ZDR measurements. This agreement is further confirmation that the radar measures and records ZDR correctly.

Several pieces of specialized hardware were developed for the INTELSAT experiment. The most significant piece of hardware is the antenna pointing system. The need for very accurate pointing, a simple reliable PC controlled system, and the complexity of interfacing with 1940's technology represented a serious engineering challenge.

The original VERLORT radar pointing system is used intact. The PC obtains the necessary position information by reading the stator voltages of the VERLORT position indicator synchros with an

analog to digital converter. The PC moves the antenna through an electromechanical interface. This interface is a small DC motor that moves the synchro which causes the VERLORT manual pointing system to reposition the antenna. In six months of observations this simple system has performed very well. It has proven to more accurate and more reliable than originally expected.

REFERENCES

1. Abramowitz, M. and Irene A. Stegun, Handbook of Mathematical Functions, Dover, 1965, 1045 pp.
2. Andrews, J.H., T. Pratt, R.E. Porter, and D.M. Imrich, "The VPI&SU Multiple Polarization Plane ZDR Radar - The Octopod Radar," 21st Conference on Radar Meteorology, Amer. Meteor. Soc., Boston, pp. 364-368, 1983.
3. Battan, L. J., Radar Observation of the Atmosphere, University of Chicago Press, Chicago, 1973, 324 pp.
4. Bottomley, L.J., "The Application of IBM PC's and Distrometers in a Satellite Propagation Experiment," Masters Thesis, Virginia Polytechnic Institute and State University, 1985.
5. Bowman, J.J., T.B.A. Senior, and P.L.E. Uslenghi, Electromagnetic and Acoustic Scattering by Simple Shapes, North-Holland Publishing, 1969, 728 pp.
6. Bringi, V.N., Thomas A. Seliga, and S.M. Cherry, "Statistical Properties of the Dual-Polarization Differential Reflectivity (ZDR) Radar Signal," IEEE Trans. Geosci. Remote Sensing, vol Ge-21, pp. 215-220, 1983.
7. Flach, T.E., "An Automated System for the Measurement and Analysis of Raindrop Size Distributions," Masters Thesis, University of Illinois, Urbana, 1972.
8. Harrington, R. F., Time-Harmonic Electromagnetic Fields, McGraw-Hill, New York, 1961, 479 pp.
9. Hewlett Packard, Operating and Service Manual, HP8495 Attenuator, 1981.
10. Hewlett Packard, Operating and Service Manual, HP8487 Thermistor Mount, 1983.
11. ILC Data Device Corporation, Synchro Conversion Handbook, Third Printing, 1982.
12. Marshall, J.S., and W.M.K. Palmer, "The Distribution of Raindrops with Size," J. Atmos. Sci., 5, pp 165-166, 1948.

13. Marshall, R.E., E.A. Manus, P.H. Wiley, and C.W. Bostian, "An S Band Radar for Studying the Effects of Weather on the SIRIO and COMSTAR Satellite Downlink Signals," 20th Conference on Radar Meteorology, Amer. Meteor. Soc., Boston, pp. 498-501, 1981.
14. Metrabyte Corporation, Data Acquisition and Control Interfaces, 1985 Engineering Catalog.
15. Pruppacher, H.R. and K.V. Beard, "A Wind Tunnel Investigation of the Internal Circulation and Shape of Water Drops Falling at Terminal Velocity in Air," Quarterly Journal of the Royal Meteorological Society, 96, pp. 247-256, 1970.
16. Lord Rayeigh, Phil. Mag, 41, p 107,274,447, 1881.
17. Reeves Instrument Corporation, Technical Manual, VERLORT Radar System, Models LRT-2 and LRT-3, NASA Contract NAS5-3060, 1960.
18. Rowland, J.R., "Comparison of Two Different Raindrop Distrometers," 17th Conference on Radar Meteorology, Amer. Meteor. Soc., Boston, p. 398, 1976.
19. Rowland, J.R., L.W. Bennent, and R.E. Miller, "Description of the APL Disdrometer - Raingauge System," Memorandum of APL, John Hopkins University, 26 September 1975.
20. Seliga, T.A. and V.H. Bringi, "Potential Use of Radar Differential Reflectivity Measurements at Orthogonal Polarizations for Measuring Precipitation," Journal of Applied Meteorology, 15, pp. 69-76, 1976.
21. Seliga, T. A., Bringi, V. N., And H. H. Al-Khatib, "Differential Reflectivity Measurement in Rain: First Experiments," IEEE Trans. on Geosci., Vol. GE-17, No. 4, pp. 240-244, 1979.
22. Seliga, T.A., V.N. Bringi, and H.H. Al-Khatib, "A Preliminary Study of Comparative Measurements of Rainfall Rate Using the Differential Reflectivity Radar Technique and a Raingage Network," Journal of Applied Meteorology, 20, pp. 1366-1368, 1981.
23. Skolnik, Merrill I., Introduction to Radar Systems, Second Edition, McGraw-Hill, New York, 1980, 581 pp.
24. Stapor, D.P. and T. Pratt, "Dual Polarized Radar for Propagation Research," Proceedings of USRI Commission F Open Symposium on

Multiple-Parameter Radar Measurements of Precipitation, pp. 43-48, 1982.

25. Stratton, J.A., Electromagnetic Theory, McGraw-Hill, New York, 1941, 615 pp.
26. Stutzman, W.L., M. Starr, T. Pratt, and C.W. Bostian, "The Calculation of Rain Effects on Earth Space Slant Path Attenuation and Depolarization," Proceedings of URSI Commission F Open Symposium on Wave Propagation: Remote Sensing and Communications, pp. 10.1.1-10.1.4, 1986.
27. Sucher, M. and Jerome Fox, ed., Handbook of Microwave Measurements, Third Edition, Volume 1, Polytechnic Press, New York, 1963, 416 pp.
28. Tsolakis and Stutzman, W.L., "Multiple Scattering of Electromagnetic Waves by Rain," Radio Science, 47, pp. 1495-1502, 1982.
29. Ulbrich, C.W., "The Effects of Drop Size Distribution Truncation on Rainfall Integral Parameters and Empirical Relations," 22nd Conference on Radar Meteorology, Amer. Meteor. Soc., Boston, pp 332-337, 1980.
30. Ulbrich, C.W. and David Atlas, "Assessment of the Contribution of Differential Polarization of Improved Rainfall Measurements," Proc. of URSI Commission F Open Symposium on Multiple-Parameter Radar Measurements of Precipitation, pp 1-8, 1982.
31. Ulbrich, C.W. and David Atlas, "Assessment of the Contribution of Differential Polarization to Improve Rainfall Measurements," Radio Science, Vol 19, Number 1, pp. 49-57, 1981.
32. Van de Hulst, H. C., Light Scattering by Small Particles, John Wiley, New York, 1957, 470 pp.

APPENDIX 1 ELECTROMAGNETIC SCATTERING FROM CONDUCTING SPHERES AND RAIN DROPS

A.1 INTRODUCTION

This appendix contains a solution to the problem of electromagnetic scattering by spheres and a development of the basic theory of differential reflectivity (ZDR) and its relation to drop size distributions (DSD).

The spherical scattering problem is solved for a conducting sphere. From this solution a computer program is developed that will compute the radar cross section (RCS) of a conducting sphere. Since conducting spheres are used as radar calibration targets, it is important that their RCS be accurately known. The results of this program are used for calibrating the VPI radar.

The results of the problem of scattering by conductive spheres is extended to scattering by dielectric spheres. Rain drops can be modeled as dielectric spheres. They are not perfectly spherical however. They become distorted by air pressure as they fall through the atmosphere so the spherical scattering model must be modified to account for this distortion. This modification is the basis for the differential reflectivity (ZDR) concept of Seliga and Bringi [1976].

The main body of this thesis uses the concept of ZDR with only a minimal definition. The development of the ZDR concept is included in this appendix for sake of completeness.

A.2 THE SPHERICAL SCATTERING PROBLEM

Solutions to the problem of scattering by spheres are abundant, Stratton [1941], Van de Hulst [1957], and Harrington [1961], however numerical results in other than graphical form are more difficult to obtain. An understanding of the solution is necessary in order to obtain numerical results. The form of the solution will follow the development of Harrington.

A.2.1 THE SPHERICAL WAVE EQUATION

The full solution requires solving the Helmholtz wave equation.

$$\frac{1}{r^2} \frac{\partial}{\partial r} \left(r^2 \frac{\partial \psi}{\partial r} \right) + \frac{1}{r^2 \sin \theta} \frac{\partial}{\partial \theta} \left(\sin \theta \frac{\partial \psi}{\partial \theta} \right) + \frac{1}{r^2 \sin^2 \theta} \frac{\partial^2 \psi}{\partial \phi^2} + k^2 \psi = 0 \quad (\text{A.1})$$

is the wave equation in spherical co-ordinates.

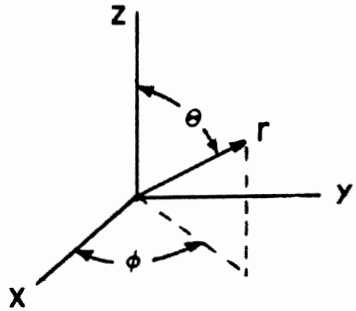


Figure A.1

Spherical Co-ordinate System

Figure A.1 shows the co-ordinate system. The wave equation can be solved by the technique of separation of variables. This means that the solution should take the form:

$$\psi = R(r) H(\theta) \Phi(\phi) \quad (A.2)$$

and it produces a set of three independent differential equations. After the separation process the resulting equations are:

$$\frac{d}{dr} \left(r^2 \frac{dR}{dr} \right) + [(kr)^2 - n(n+1)] R = 0 \quad (A.3a)$$

$$\frac{1}{\sin \theta} \frac{d}{d\theta} \left(\sin \theta \frac{dH}{d\theta} \right) + [n(n+1) - \frac{m^2}{\sin^2 \theta}] H = 0 \quad (A.3b)$$

$$\frac{d^2 \Phi}{d\phi^2} + m^2 \Phi = 0 \quad (A.3c)$$

Each of these equations has a known solution, Stegun and Abramowitz [1965].

The Φ equation, equation A.3c, is the simple harmonic equation. Since ϕ goes from 0 to 2π on a sphere, solutions of this equation must be periodic on this range. Linear combinations of $\sin(m\phi)$ and $\cos(m\phi)$ or $e^{-jm\phi}$ or $e^{jm\phi}$ are suitable solutions for equation A.3c.

The H equation, equation A.3b, is very similar to Bessel's equation and its solutions are spherical Bessel functions of the form:

$$b_n(kr) = \sqrt{\frac{\pi}{2kr}} B_{n+1/2}(kr) \quad (A.4)$$

where $B_{n+1/2}$ is any Bessel function of fractional order. While any of the spherical Bessel functions will work, only $j_n(kr)$ is finite when $r=0$, thus it is the only one that results in a physically realizable solution at the origin. The functions $h_n^{(1)}(kr)$ and $h_n^{(2)}(kr)$ are spherical Bessel functions that can be used to describe inward and outward traveling waves respectively.

The solutions to the R equation, equation A.3a, are associated Legendre functions, $P_n^m(\cos\theta)$ or $Q_n^m(\cos\theta)$. These functions must be finite for $0 \leq \theta \leq \pi$. Only $P_n^m(\cos\theta)$, with n integer, meets this condition.

If a is the radius of the sphere, then for $r < a$, that is inside the sphere, the resulting solution for the wave equation is of the form:

$$\psi_{mn} = j_n(kr) P_n^m(\cos\theta) e^{jm\phi} \quad (A.5)$$

Outside the sphere, in the absence of sources, the fields must go to zero at infinity. This requires that $j_n(kr)$ to be replaced with $h_n^{(2)}(kr)$, so:

$$\psi_{mn} = h_n^{(2)}(kr) P_n^m(\cos\theta) e^{jm\phi} \quad (A.6)$$

A.2.3 SOLUTIONS OF MAXWELL'S EQUATIONS IN SPHERICAL CO-ORDINATES

Now that we have a solution for the spherical wave equation, it is now possible to use this result to solve Maxwell's Equations for the desired fields. The general procedure is to write Maxwell's equations in terms of a magnetic vector potential \bar{A} and an electric vector potential \bar{F} .

$$\bar{E} = -\bar{\nabla} \times \bar{F} + \frac{1}{j\omega\epsilon} \bar{\nabla} \times \bar{\nabla} \times \bar{A} \quad (A.7a)$$

$$\bar{H} = \bar{\nabla} \times \bar{A} + \frac{1}{j\omega\mu} \bar{\nabla} \times \bar{\nabla} \times \bar{F} \quad (A.7b)$$

In rectangular co-ordinates, $\bar{A} = \hat{u}_z$ and $\bar{F} = 0$ produces fields TM to z and $\bar{F} = \hat{u}_z$ and $\bar{A} = 0$ produces fields TE to z and any arbitrary field can be expressed by a combination of these two fields. The rectangular components of these fields can be rewritten in spherical co-ordinates. This is not very convenient and unfortunately $\bar{A} = \hat{u}_r \psi$ and $\bar{F} = \hat{u}_r \psi$ are not solutions to the spherical wave equation. However it can be shown that $A_r/r = \psi$ and $F_r/r = \psi$ will satisfy the spherical wave equation, so let

$$\bar{F} = \hat{u}_r r\psi \quad (A.8a)$$

$$\bar{A} = \hat{u}_r r\psi \quad (A.8b)$$

The spherical Bessel functions can be modified to incorporate this factor of r:

$$\hat{B}_n(kr) = kr b_n(kr) = \sqrt{\frac{\pi kr}{2}} B_{n+1/2}(kr) \quad (A.9)$$

It is now possible to calculate the desired fields using equations A.7 and A.8.

A.2.4 PLANE WAVE SCATTERING FROM SPHERES

In the case of a radar, the incident field on the spheres is locally a plane wave. While the wave can come from any direction, the easiest to describe is a z-traveling x-polarized wave. Again, figure A.1 shows the geometry. This wave has the following components:

$$E_x^i = E_o e^{-jkz} = E_o e^{-jkrcos\theta} \quad (A.10a)$$

$$H_y^i = \frac{E_o}{\eta} e^{-jkz} = \frac{E_o}{\eta} e^{-jkrcos\theta} \quad (A.10b)$$

The i superscript indicates the incident field and η is the intrinsic impedance of free space. In order to obtain A_r and F_r it is desirable to write the above plane wave as the sum of waves TM and TE to r . This can be done in the following way :

$$E_r = \cos(\phi)\sin(\theta)E_x^i = E_o \frac{\cos\phi}{jkr} \frac{\partial}{\partial\theta} (e^{-jkrcos\theta}) \quad (A.11)$$

This last step may not be immediately obvious. This result was obtained by applying $\bar{\nabla} \times \bar{H}$ in spherical co-ordinates to the \bar{H} component of the wave to obtain the resulting component of E_r .

It is possible to write equation A.11 in terms of spherical functions.

$$E_r^i = -j \frac{E_o \cos\phi}{(kr)^2} \sum_{n=1}^{\infty} j^{-n} (2n+1) \hat{J}_n(kr) P_n^1(\cos\theta) \quad (A.12)$$

This looks very much like the ψ function, equation A.5. With the plane wave in these terms it is possible to work backwards through equation A.7 to obtain \bar{A} and \bar{F} . This results in:

$$A_r^i = \frac{E_0}{\omega\mu} \cos\phi \sum_{n=1}^{\infty} a_n \hat{J}_n(kr) P_n^{-1}(\cos\theta) \quad (\text{A.13a})$$

$$F_r^i = \frac{E_0}{k} \sin\phi \sum_{n=1}^{\infty} a_n \hat{J}_n(kr) P_n^{-1}(\cos\theta) \quad (\text{A.13b})$$

where

$$a_n = \frac{j^{-n}(2n+1)}{n(n+1)} \quad (\text{A.14})$$

The form of the scattered wave will be very similar to the incident wave except that it must go to zero at infinity and it may have a different amplitude. The first condition may be met by replacing $\hat{J}_n(kr)$ in equation A.13 with $\hat{H}_n^{(2)}(kr)$ and the second is met by a new set of constants:

$$A_r^s = \frac{E_0}{\omega\mu} \cos\phi \sum_{n=1}^{\infty} b_n \hat{H}_n^{(2)}(kr) P_n^{-1}(\cos\theta) \quad (\text{A.15a})$$

$$F_r^s = \frac{E_0}{k} \sin\phi \sum_{n=1}^{\infty} c_n \hat{H}_n^{(2)}(kr) P_n^{-1}(\cos\theta) \quad (\text{A.15b})$$

If equations A.13 and A.15 are added the resulting expression will be the potentials of the total field.

$$A_r = \frac{E_0}{\omega\mu} \cos\phi \sum_{n=1}^{\infty} [a_n \hat{J}_n(kr) + b_n \hat{H}_n^{(2)}(kr)] P_n^1(\cos\theta) \quad (\text{A.16a})$$

$$F_r = \frac{E_0}{k} \sin\phi \sum_{n=1}^{\infty} [a_n \hat{J}_n(kr) + c_n \hat{H}_n^{(2)}(kr)] P_n^1(\cos\theta) \quad (\text{A.16b})$$

All that is left is to determine the coefficients b_n and c_n . This can be done by noting that if the sphere is a perfect conductor, E_θ and E_ϕ must be zero at $r = a$. This results in

$$b_n = -a_n \frac{\hat{J}_n'(ka)}{\hat{H}_n^{(2)'}(ka)} \quad (\text{A.17a})$$

$$c_n = -a_n \frac{\hat{J}_n(ka)}{\hat{H}_n^{(2)}(ka)} \quad (\text{A.17b})$$

The solution is now complete and any of the desired fields can be found with equation A.7.

A.2.5 RADAR CROSS SECTION OF SPHERES

What is desired is the backscatter from the sphere since that is what the radar measures. In general the backscatter area or radar cross section (RCS) is given by:

$$\sigma = \lim_{r \rightarrow \infty} (4\pi r^2 |E_x^s| / |E_o|) \quad (A.18)$$

To calculate the RCS, it is necessary to obtain the scattered field, E_x^s . Since the radar is a long distance from the sphere it is permissible to use a far field approximation. In the far field $H_n^{(2)}(kr)$ can be replaced by its asymptotic approximation $j^{n+1} e^{-jkr}$. Making this approximation it is now possible to calculate the scattered field from equation A.7 and A.15.

$$E_\theta^s = j \frac{E_o}{kr} e^{-jkr} \cos\phi \sum_{n=1}^{\infty} j^n [b_n \sin(\theta) P_n^{(1)}(\cos\theta) - c_n P_n^{(1)}(\cos\theta) / \sin(\theta)] \quad (A.19)$$

A similar expression could be obtained for E_ϕ^s , but notice that

$$E_x^s = E_\theta^s \left| \begin{array}{l} \theta = \pi \\ \phi = \pi \end{array} \right. = E_\phi^s \left| \begin{array}{l} \theta = \pi \\ \phi = -\pi/2 \end{array} \right.$$

As $\theta \rightarrow \pi$, the associated Legendre functions can be replaced with their limit values:

$$\lim [P_n^1(\cos\theta)/\sin\theta] = (-1)^n n(n+1)/2$$

$$\lim [\sin\theta P_n^1'(\cos\theta)] = (-1)^n n(n+1)/2$$

Now a complete expression for the field backscattered in the direction of the incident radiation can be found.

$$E_x^s = \frac{E_0}{kr} e^{-jkr} \sum_{n=1}^{\infty} \left[(-1)^n (2n+1) \frac{(J_n(ka)\hat{H}_n^{(2)}(ka) - J_n'(ka)\hat{H}_n^{(2)}(ka))}{H_n^{(2)}(ka)H_n^{(2)*}(ka)} \right] \quad (A.20)$$

Equation A.20 can be reduced further by using the Wronskian of the spherical Bessel function.

$$W(j_n(ka), h_n^{(2)}(ka)) = j_n(ka)h_n^{(2)*}(ka) - h_n^{(2)}(ka)j_n'(ka) = i/ka^2$$

$$(A.21)$$

Recall that the Bessel functions were modified by multiplying them by the factor ka , so equation A.21 simply becomes the factor i . Now equation A.18 which gives the echo area can be completed:

$$\sigma = \frac{\lambda^2}{4\pi} \left| \sum_{n=1}^{\infty} \frac{(-1)^n (2n+1)}{\hat{H}_n^{(2)}(ka) \hat{H}_n^{(2)}(ka)} \right|^2 \quad (A.22)$$

This is Harrington's result. For very small spheres, only the first term of the summation in equation A.22 is significant. The echo area can then be approximated by:

$$\sigma = \frac{9\lambda^2}{4\pi} (ka)^6 \quad (A.23)$$

This scattering that is a function of λ^{-4} is called the Rayleigh scattering.

The original object was to calculate the RCS for a given sphere. Equation A.22 was evaluated with a simple computer program. Appendix 5 contains the listing for the program used to do that calculation. The Bessel functions are obtained from standard recursion relations. The number of terms in the summation is determined by the desired accuracy of the result. The program continues to sum until two successive sums differ by less than .05%. This means that the results are accurate to three decimal places. The program can easily be modified to obtain other degrees of accuracy.

In order to test the program it is necessary to compare its output with some published results. The RCS is often normalized by the factor πa^2 since πa^2 is the limit value of the RCS when the sphere is very large with respect to the wavelength. The RCS normalized by πa^2 is often

plotted with respect to ka where $k=2\pi/\lambda$. Figure A.2 is such a plot generated by the sphere echo area program. It agrees with published plots of Bowman et al. [1969] and Skolnik [1962].

A.2.6 SCATTERING FROM RAIN DROPS

It is possible to solve the spherical scattering problem for a dielectric sphere. A rain drop can be thought of as a dielectric sphere. The solution of this problem is slightly more difficult because with the dielectric sphere there will be fields interior to the sphere. To obtain a solution it is necessary to obtain the field components both interior and exterior to the sphere and match the field components at $r = a$.

Harrington points out that for dielectric spheres that is very small with respect to a wavelength, the resulting scattered fields can be written as if they were the combination of fields from a small electric and magnetic dipole. In the case of a small dielectric nonmagnetic ($\epsilon_r = 1$) sphere, the scattered field is due to the electric dipole alone.

$$p = \frac{4\pi j}{\eta k^2} E_0 (ka)^3 \frac{m-1}{m+2} \quad (A.24)$$

where p is the electric dipole moment and m is the refractive index of the particle. The dipole moment $p = \Delta x I$, where Δx is the length

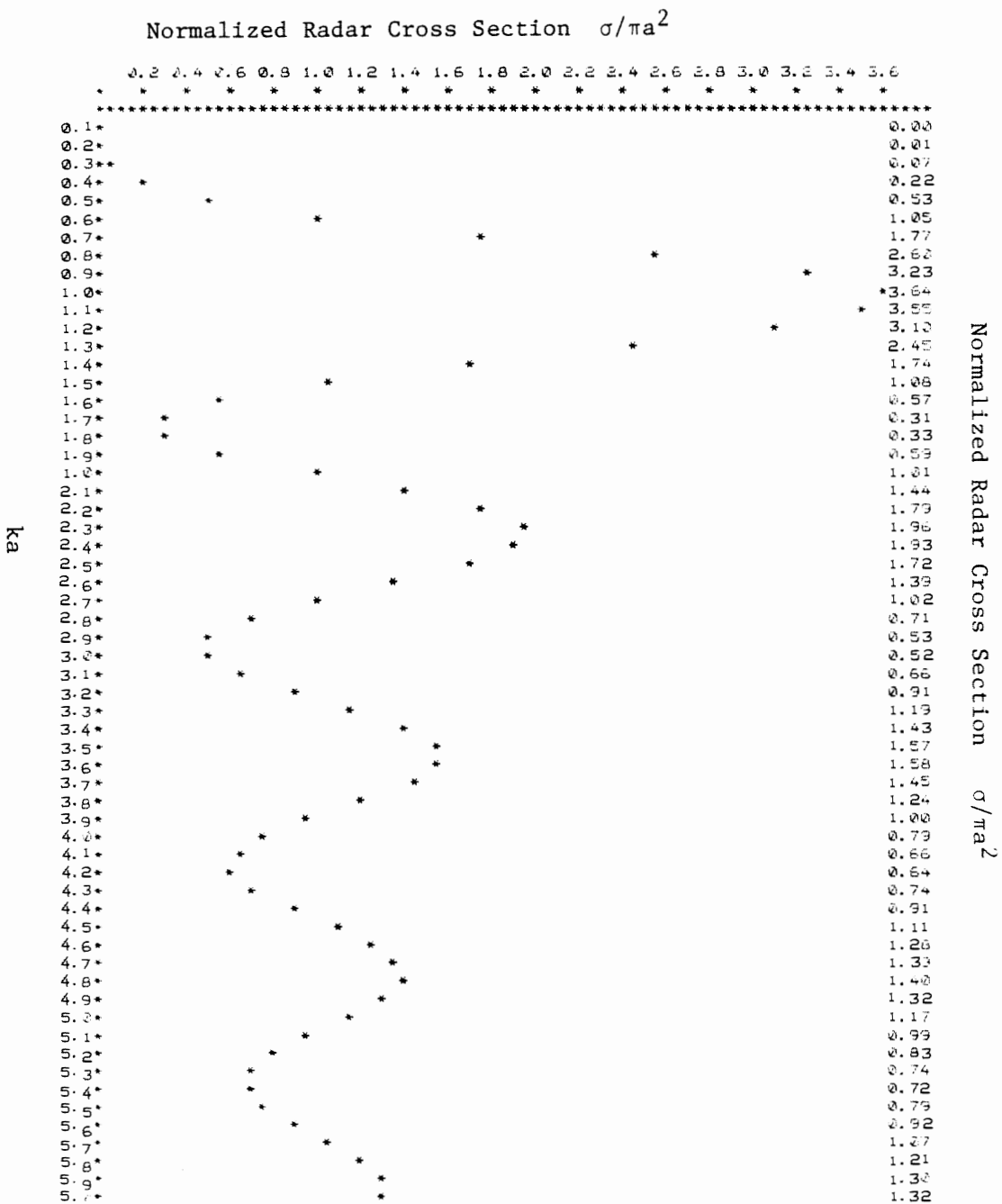


Figure A.2 Normalized Radar Cross Section Versus ka .

and I is the current of an equivalent dipole. The incident radiation is x -directed so the particle radiates as if it were an x -directed dipole Δx long with a current I flowing in it.

This suggests a way of modeling non-spherical rain drops. Since the larger rain drops become slightly flattened as they fall, they will exhibit different dipole moments depending on incident polarization. This is the basis of the Seliga and Bringi [1976] technique for measuring differential reflectivity.

Falling rain drops become oblate spheroids. The dipole moment of these spheroids is given by:

$$\begin{aligned} p_v &= (4\pi \epsilon_0) g' E_{ho} \\ p_h &= (4\pi \epsilon_0) g E_{vo} \end{aligned} \quad (A.25)$$

where E_{ho} and E_{vo} are the incident electric fields, p is the dipole moment, and v , h denote the vertical and horizontal polarizations respectively. The g' and g factors can be obtained from Van De Hulst [1957] :

$$\begin{aligned} g &= V(m^2 - 1) / [4 + (m^2 - 1)P] \\ g' &= V(m^2 - 1) / [4 + (m^2 - 1)P'] \end{aligned} \quad (A.26)$$

V is the volume of the drop and m is the index of refractions. The P and P' are also given by Van De Hulst and they are related to the geometry of the oblate spheroid:

$$P = 4 - 2P' = (4/e^2)(1 - [(a/b)/e]\sin^{-1}e) \quad (A.27)$$

The factor e is the eccentricity of the cross section where $e^2 = 1 - (a/b)^2$, and a and b are the respective distances from the major and minor axis of the drop. The figure A.3 shows the geometry.

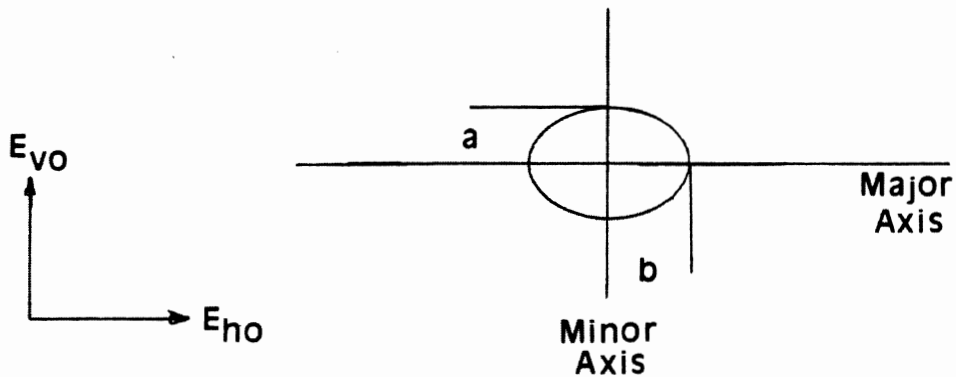


Figure A.3

Rain Drop and Polarization Geometry

Experimental work has been done that relates the a/b ratio to the diameter of an equivalent spherical drop. Pruppacher and Beard [1970] found as a result of wind tunnel tests that:

$$a/b = \begin{cases} 1.0 & 0 < D_{eq} < 0.028\text{cm} \\ [1 - (9/32)D_{eq}\rho_m v^2/\mu]^{0.5} & 0.28 < D_{eq} \leq 0.1\text{ cm} \\ 1.03 - 0.62 D_{eq} & 0.1 < D_{eq} \leq 1.0\text{ cm} \end{cases}$$

$\rho_m = 1.1937 \cdot 10^{-3} \text{ g cm}^{-3}$, density of water vapor in
saturated air

$\mu = 72.75 \text{ erg/cm}^2$, surface tension of water

v = terminal velocity of the drop

(A.28)

Since this equation is written in terms of an equivalent spherical drop diameter, D_{eq} , it is handy define the drop volume in terms of the equivalent drop diameter:

$$V = \frac{4\pi}{3} \left(\frac{D_{eq}}{2}\right)^3 \quad (\text{A.29})$$

The scattered field from the drop can now be described in terms of its geometry.

The magnitude of the backscattered field in the far field produced by the p_h , p_v dipole moments is given by :

$$\begin{aligned} |E_{sh}| &= 1/4(\pi\epsilon_0) (k^2/r) |p_h| \\ |E_{sv}| &= 1/4(\pi\epsilon_0) (k^2/r) |p_v| \end{aligned} \quad (\text{A.30})$$

Using equation A.30 in A.18, and with A.25, A.26 and A.27 it is possible to calculate the radar cross section for each axis of the drop:

$$\begin{aligned} \sigma_h &= (16/9)(\pi^7/\lambda^4)(D_{eq})^6 \left| \frac{(m^2-1)}{[4+(m^2-1)p']} \right|^2 \\ \sigma_v &= (16/9)(\pi^7/\lambda^4)(D_{eq})^6 \left| \frac{(m^2-1)}{[4+(m^2-1)p]} \right|^2 \end{aligned} \quad (\text{A.31})$$

where σ_v and σ_h are the radar cross sections for vertical and horizontal polarization respectively.

With the radar cross section it is possible to obtain the average backscattered power at a range r due to horizontally and vertically polarized incident waves.

$$P_{h,v}(r) = (C/r^2) \int_{D_{eq}} \sigma_{h,v} N(D_{eq}) dD_{eq} \quad (A.32)$$

C is the radar constant and $N(D_{eq})$ is the number of drops with diameter D_{eq} . From A.32 is it also possible to obtain a radar reflectivity factor Z for each polarization:

$$z_h = \int_{D_{eq}}^{\infty} (D_{eq})^6 \left| \frac{m^2 - 1}{4 + (m^2 - 1)P'} \right|^2 N(D_{eq}) dD_{eq} \quad (A.33)$$

$$z_v = \int_{D_{eq}}^{\infty} (D_{eq})^6 \left| \frac{m^2 - 1}{4 + (m^2 - 1)P} \right|^2 N(D_{eq}) dD_{eq}$$

The backscattered power becomes:

$$P_{h,v}(r) = (C^*/r^2) z_{h,v} \quad (A.34)$$

where $C^* = C(16/9)(\pi^7/\lambda^4)$. Seliga and Bringi [1976] then define the differential reflectivity, or ZDR as:

$$ZDR = 10 \log(z_h/z_v) \quad (A.35)$$

ZDR and z_h are two independent parameters of the rain that the radar can measure.

A.3 DROP SIZE DISTRIBUTIONS

From the previous discussion of the backscatter from raindrops, it should be clear that the backscattered power from a volume of space is determined by the size, the shape, and the number of rain drops in the volume. In order to actually calculate the backscattered power it is necessary to have a value of $N(D_{eq})$. It is common to use a truncated

exponential distribution, after Marshall and Palmer [1948], to estimate the number of drops of a particular size in a given volume.

$$N(D_{eq}) = N_o \exp(-\Lambda D_{eq}) \quad 0 < D_{eq} < D_{max} \quad (A.36)$$

where N_o and Λ are parameters of the distribution. Such a drop size distribution (DSD) is characterized by two parameters. More recently Ulbrich and Atlas [1982] have suggested using a gamma DSD:

$$N(D_{eq}) = N_o (D^{\mu}) \exp(-\Lambda D_{eq}) \quad 0 < D_{eq} < D_{max} \quad (A.37)$$

where μ is an extra parameter in the distribution. Notice that equation A.37 becomes equation A.36 if $\mu = 0$. Ulbrich [1984], and Ulbrich and Atlas [1984] point out that the variability of the empirical relation between radar reflectivity and rain rate ($Z = ar^b$) can not be accounted for with a drop size distribution (DSD) which has the same shape for all storms. The extra parameter μ in the distribution changes the distribution shape. In addition the Marshall and Palmer DSD predicts a finite number of infinitely small drops. This runs counter to the physical situation where the number of drops of zero diameter must be zero. The gamma DSD fulfills this physical requirement for any μ greater than zero.

If the Marshall and Palmer DSD is used then equation A.33 becomes:

$$Z_h = N_o \int_{D_{eq}} (D_{eq})^6 \left| \frac{m^2 - 1}{4 + (m^2 - 1)P} \right|^2 \exp(-\Lambda D_{eq}) dD_{eq} \quad (A.38)$$

$$Z_v = N_o \int_{D_{eq}} (D_{eq})^6 \left| \frac{m^2 - 1}{4 + (m^2 - 1)P} \right|^2 \exp(-\Lambda D_{eq}) dD_{eq}$$

Since ZDR is obtained from the ratio of Z_h and Z_v , N_o does not appear in the ZDR calculation. ZDR is a function of Lambda only. Z and ZDR are measurable quantities. From ZDR, Lambda can be obtained, and with Lambda and Z_h , N_o can be calculated.

N_o , Lambda, and μ describe the DSD. It is the DSD that is desired since it is the basis of attenuation and depolarization calculations. While Ulbrich suggests that the distribution can be different for different rainstorms, it is reasonable to add that the distribution will also vary within a particular storm. If the radar resolution is fine enough, it is possible to measure differences within the same storm. The ZDR radar can measure two of the distribution parameters in any part of its observing volume. If a reasonable estimate can be made for μ , a DSD can be obtained from any part of the rainstorm that can be observed by the radar and this should result in a more accurate determination of attenuation and depolarization than using one DSD to describe the entire storm.

APPENDIX 2

ZDR VERSUS Z PROGRAM: ZDRPLT

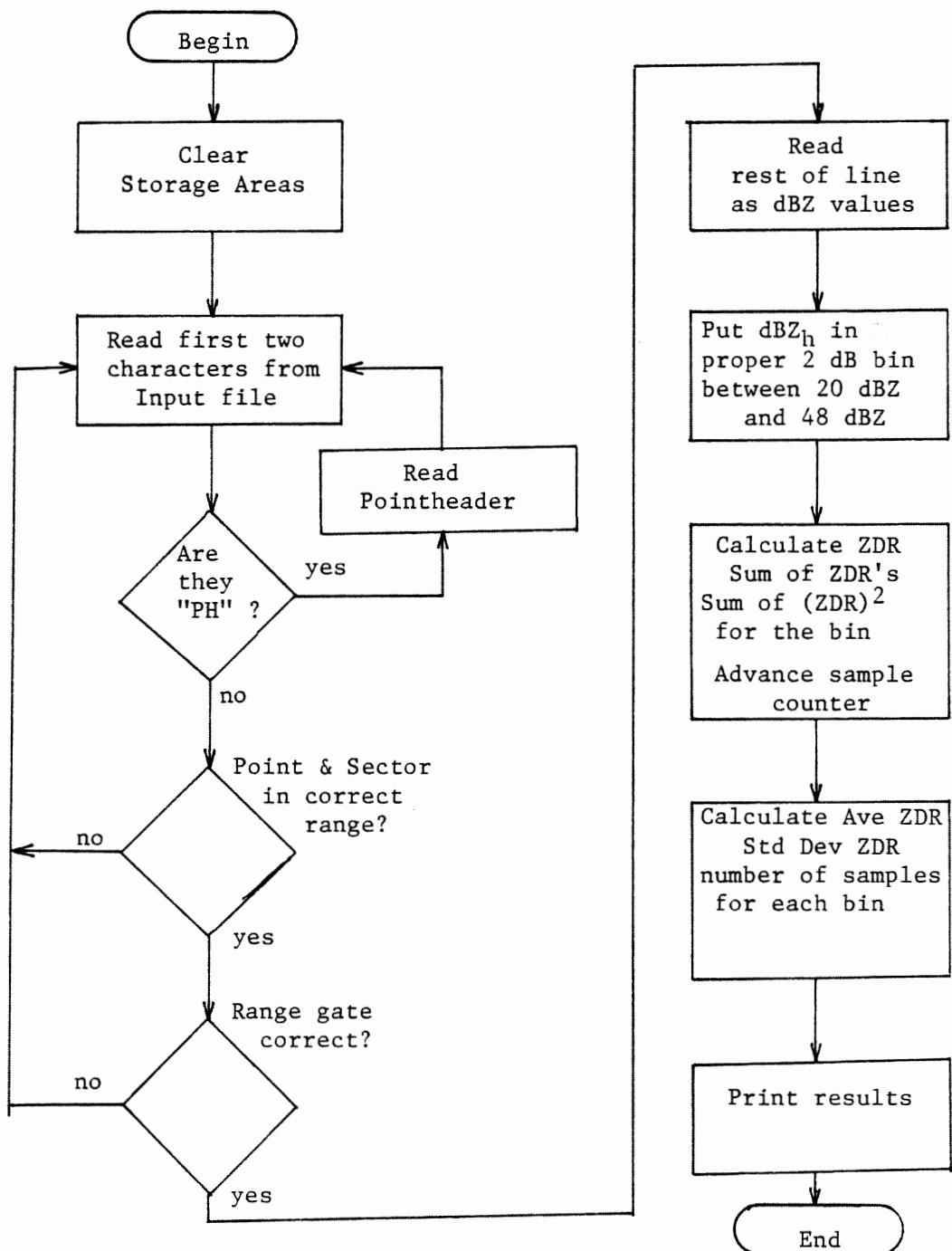


Figure A.2.1 Flow diagram for Program ZDRPLT

```

PROGRAM      ZDRPLT(SMPLIN(LFN=12, LineLength=66),
                      SMPLOUT(LFN=13,LineLength=132)) ;

(*****)

Program:   ZDRPLT calculates the average value of ZDR
           for values of Z in 2dB bins between 20-48 dBZ

Written by: Dennis Sweeney

Date: Febraury 1986

Language: Harris Pascal

Machine: Harris 800
         Minimum configuration: 256K memory page

*****)

TYPE Ar = Array[1..4] of Real ;
Br = Array[0..7] of Real ;

StoreArray=Record
  ZDR :      Real ;
  ZDRSQRD :   Real ;
  CNT :      Integer ;
End ;

VAR Store :      Array[1..35] of StoreArray ;
AZ,EL :          Integer ;
AP,LN10 :        Real ;
Date :          Packed Array[1..8] of Char ;
PointCount :    Integer ;
Time :          Packed Array[1..11] of Char ;
Sector, Point : Integer ;
SMPLOUT, SMPLIN : Text ;
DATA :          Packed Array[1..64] of Char ;
c :              char ;
LC :          Packed Array[1..2] of Char ;
A,B,BIN,I,K : Integer ;
HiZ,LoZ :        Integer ;
STATUS :        Integer ;
Z,ZDRMAX :      Array[0..7] of Real ;
CHNGN :        Br ;

```

```

Procedure DoZ(K:Integer);
Var
  ZDR : Real ;
Begin
  ZDR:=(Z[A]-CHNGN[A])-(Z[B]-CHNGN[B]) ;
  {calculate ZDR and correct for channel gain difference}

  IF ZDR<6.0 Then Begin           {Ignor any ZDR > 6dB}
    ZDR:=Exp(ZDR*ln10/10.0) ;

    If ZDR>ZDRMAX THEN ZDRMAX:=ZDR ;   {Save largest ZDR}

    Store[K].ZDR:=Store[K].ZDR+ZDR ;   {Sum of ZDR}
    Store[K].ZDRSQRD:=Store[K].ZDRSQRD+Sqr(ZDR) ; {Sum of ZDR*ZDR}
    Store[K].CNT:=Store[K].CNT+1 ;      {Number of samples}

  End ;
End ;

BEGIN

A:=4 ; B:=0 ;   {ZDR=(Z[A]-CHNGN[A])-(Z[B]-CHNGN[B]) }
Chngn[1]:=-0.670 ; Chngn[2]:=-0.80 ; Chngn[3]:=-0.62 ; Chngn[4]:=-0.25 ;
Chngn[5]:=0.40 ; Chngn[6]:=0.90 ; Chngn[7]:=0.82 ; Chngn[0]:=0.0 ;

Bind(SMPLIN,'3000SAVE*SAMPLE ',Status) ; {Input file}
Reset(SMPLIN) ;

Bind(SMPLOUT,'3000ZDR*ZDRPLT ',Status) ; {Output file}
Rewrite(SMPLOUT) ;

ZDRMAX := 0.0 ;
FOR K:=1 to 35 Do Begin
  Store[K].ZDR:=0.0 ;
  Store[K].ZDRSQRD:=0.0 ;
  Store[K].CNT:=0
End ;
LN10:=LN(10.0) ;

  WHILE Not EOF(SMPLIN) DO BEGIN
    REPEAT Read(SMPLIN,c) ; UNTIL (c<>' ') or eoln(SMPLIN) ;
    IF not eoln(SMPLIN) THEN Begin ;
      LC[1]:=c ;

```

```

READ(SMPLIN,LC[2]) ;
IF LC>>'RD' THEN begin
  If LC='PH' THEN
    Read(SMPLIN,Date,Time, PointCount,AP,AZ,EL,Sector,Point) ;
End
ELSE begin
  IF (Sector=1) OR (Sector=4) AND (Point>=6)
    OR (Sector=3) THEN BEGIN
    Read(SMPLIN,BIN) ;
    IF (BIN>=10) AND (BIN<64) THEN BEGIN

      {Choose ZDR in scan sectors and range gates such
      that there will be no ground clutter}

      FOR I:=0 to 7 DO  Read(SMPLIN,Z[I]) ;

      K:=Trunc((Z[0]-20.0)/2.0) ;
      IF K>=0 Then Begin ;
        K:=K+1 ;
        DoZ(K) ; {Calculate values}
      End ;
      End ;
    End ;
  End ;
ReadLn(SMPLIN) ;
End ;

WriteLN(SMPLOUT,'ZDR=Z[,A:1,]-Z[,B:1,]' ) ;
WriteLN(SMPLOUT) ;
WriteLN(SMPLOUT,' Z Ave ZDR Dev ZDR ZDR DB Dev DB Samples') ;

For K:=1 to 15 Do Begin
  HiZ:=20+2*K ;
  LoZ:=HiZ-2 ;
  IF (Store[K].CNT=0) or (Store[K].CNT=1) Then Begin
    WriteLN(SMPLOUT,LoZ:2,'-',HiZ:2,Store[K].ZDR:8:3,
           ',Store[K].CNT:8) ;
  End
  ELSE Begin

    {Calculate statistics and print results}

    Store[K].ZDRSQRD:=Sqrt((1.0/(Store[K].CNT-1))*(Store[K].ZDRSQRD-
      Sqr(Store[K].ZDR)/Store[K].CNT)) ;

```

```
Store[K].ZDR:=Store[K].ZDR/Store[K].CNT ;
Write(SMPLOUT,LoZ:2,'-',HiZ:2,Store[K].ZDR:8:3,
      Store[K].ZDRSQRD:8:3) ;
Store[K].ZDR:=LN(Store[K].ZDR)*10.0/LN10 ;
Store[K].ZDRSQRD:=LN(Store[K].ZDRSQRD)*10.0/LN10 ;
WriteLN(SMPLOUT,Store[K].ZDR:8:3,Store[K].ZDRSQRD:8:3,
        Store[K].CNT:8) ;

End ;
End ;
WriteLN(SMPLOUT,ZDRMAX:8:3) ;
END.
```

APPENDIX 3

RADAR ANTENNA CHANNEL GAIN DIFFERENCE PROGRAM: CHNGN

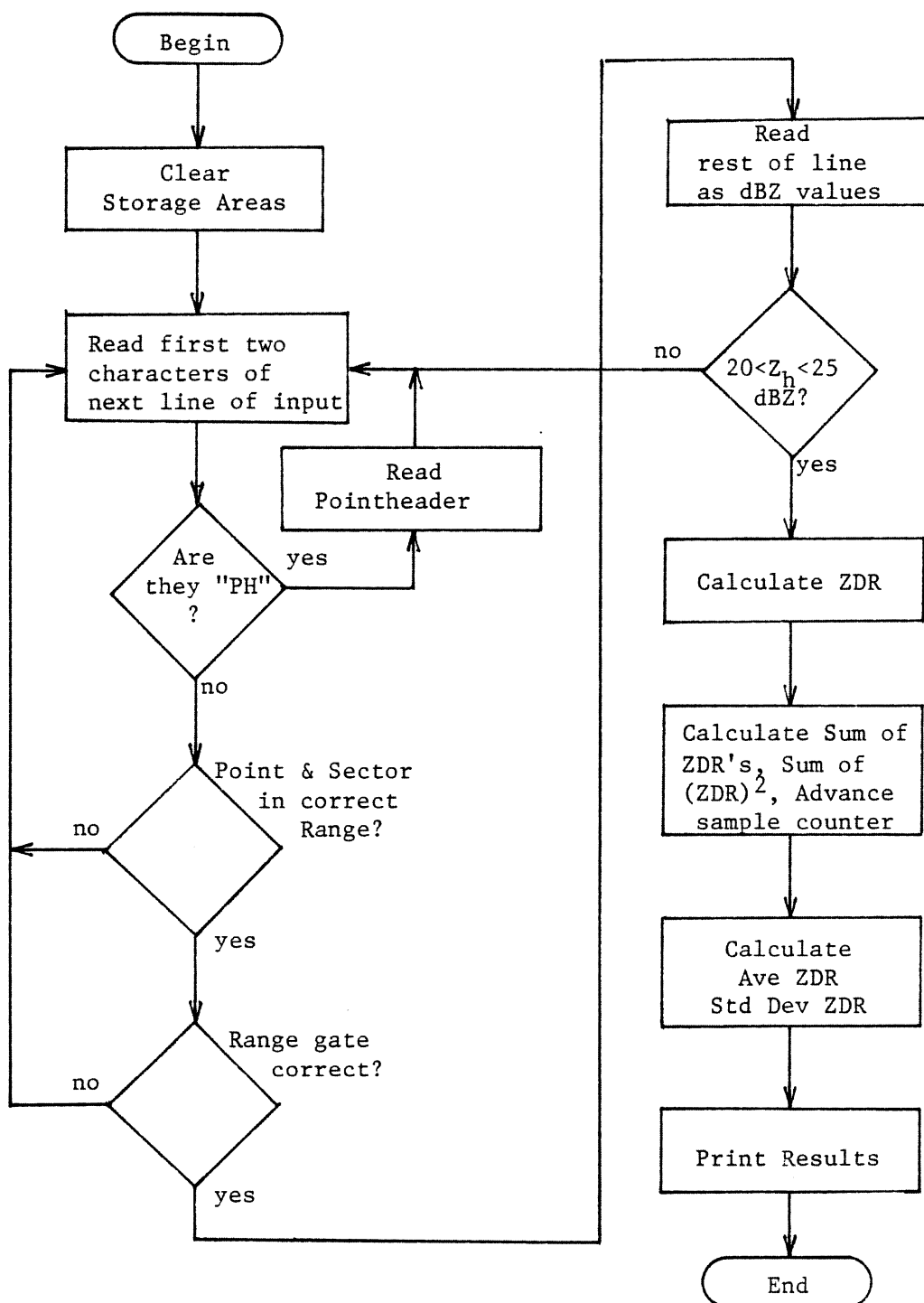


Figure A.3.1 Flow diagram for Program CHNGN

```
PROGRAM CHANNELGAIN(SMPLIN(LFN=12, LineLength=66),  
                      SMPLOUT(LFN=13,LineLength=132)) ;
```

```
(*****
```

Program: CHANNELGAIN calculates average ZDR for each polarization. If the ZDR data is taken during light rain, ie. ZDR=0, the result will be the difference in antenna gain with polarization.

Written by: Dennis Sweeney

Date: February 1986

Language: Harris Pascal

Machine: Harris 800
Minimum configuration, 256K memory page

```
*****}
```

TYPE

```
Ar = Array[1..4] of Real ;  
Br = Array[1..7] of Real ;
```

VAR

```
AZ,EL : Integer ;  
AP,ZO,LN10 : Real ;  
Date : Packed Array[1..8] of Char ;  
PointCount : Integer ;  
Time : Packed Array[1..11] of Char ;  
Sector, Point : Integer ;  
SMPLIN, SMPLOUT : Text ;  
DATA : Packed Array[1..64] of Char ;  
c : char ;  
LC : Packed Array[1..2] of Char ;  
BIN,I,K,STATUS : Integer ;  
SumZDRSQRD : Ar ;  
SumZDR : Ar ;  
SumDELTAZ : Br ;  
SumDELTAZSQRD : Br ;  
Z : Array[0..7] of Real ;  
ZDR : Ar ;  
CHNGN : Br ;
```

```

Procedure Clear4(var S1,S2:Ar) ;

Var
  I : Integer ;

Begin
  For I:=1 to 4 do begin
    S1[I]:=0.0 ;
    S2[I]:=0.0 ;
  End ;
End;

Procedure Clear7(var S1,S2:Br) ;

Var
  I : Integer ;

Begin
  For I:=1 to 7 do begin
    S1[I]:=0.0 ;
    S2[I]:=0.0 ;
  End;
End ;

Procedure PrintZDR(var SumZDR,SumZDRSQRD:Ar; K: integer) ;

Var
  I : Integer ;
  AveZDR : Array[1..4] of Real ;
  DevZDR : Array[1..4] of Real ;

Begin
WriteLN(SMPLOUT,'V-H ZDR is channel 1');
WriteLN(SMPLOUT,' Chan',' Ave ZDR ',' Dev ZDR ',' Ave DB ');
FOR I:=1 to 4 DO BEGIN
  AveZDR[I]:=SumZDR[I]/K ;
  DevZDR[I]:=(1.0/(K-1))*(SumZDRSQRD[I]-SQR(SumZDR[I])/K) ;
  Write(SMPLOUT,I:5,' ',AveZDR[I]:8:3,' ',DevZDR[I]:8:3) ;
  AveZDR[I]:=LN(AveZDR[I])*10.0/LN(10.0) ;
  WriteLn(SMPLOUT,' ',AveZDR[I]:8:3) ;
End ;
WriteLN(SMPLOUT) ;
End;

```

```

Procedure PrintZ(var SumDELTAZ, SumDELTAZSQRD :Br; K :Integer) ;

Var
  I    : Integer ;
  AveZ : Array[1..7] of Real ;
  DevZ : Array[1..7] of Real ;

Begin
  WriteLN(SMPLOUT,'Reference Channel is channel 0') ;
  Write(SMPLOUT,' Chan',' Ave Diff ',' Dev Diff') ;
  WriteLN(SMPLOUT,' Ave DB ') ;

  For I:=1 to 7 Do Begin
    AveZ[I]:=SumDELTAZ[I]/K ;
    DevZ[I]:=(1.0/(K-1))*(SumDELTAZSQRD[I]-SQR(SumDELTAZ[I])/K) ;
    Write(SMPLOUT,I:5,' ',AveZ[I]:8:3,' ',DevZ[I]:8:3) ;
    AveZ[I]:=LN(AveZ[I])*10.0/LN(10.0) ;
    WriteLN(SMPLOUT,' ',AveZ[I]:8:3) ;

  End;

  WriteLN(SMPLOUT) ;
  WriteLN(SMPLOUT) ;
End;

BEGIN  {Main prgram}

Chngn[1]:=-1.414 ; Chngn[2]:=-3.538 ; Chngn[3]:=-0.859 ;
Chngn[4]:=-0.569 ; Chngn[5]:=0.287 ; Chngn[6]:=0.372 ;
Chngn[7]:=0.491 ;

          {Channel gain differences}

Bind(SMPLIN,'3000arc*SAMPLE  ',Status) ; {Input file}
Reset(SMPLIN) ;

Bind(SMPLOUT,'3000zdr*CHNGN ',Status) ; {Output file}
Rewrite(SMPLOUT) ;

Clear4(SumZDR,SumZDRSQRD) ;

Clear7(SumDELTAZ,SumDELTAZSQRD) ;

```

```

LN10:=LN(10.0) ;
K:=0 ;
WHILE Not EOF(SMPLIN) DO BEGIN
    REPEAT Read(SMPLIN,c) ; UNTIL (c<>' ') or eoln(SMPLIN) ;
    IF not eoln(SMPLIN) THEN Begin ;
    LC[1]:=c ;
    READ(SMPLIN,LC[2]) ;
    IF LC<>'RD' THEN begin (Determine if line is RADAR data)
        If LC='PH' THEN
            Read(SMPLIN,Date,Time, PointCount,AP,AZ,EL,Sector,Point) ;
    End
    ELSE begin
        IF (Sector=1) OR (Sector=4) AND (Point>=6)
            OR (Sector=3) THEN BEGIN
            Read(SMPLIN,BIN) ;
            IF BIN>=10 THEN BEGIN
                (* Choose bin and sector to avoid ground clutter *)
                Read(SMPLIN,Z[0]) ;
                IF (Z[0]>=20.0) AND (Z[0]<=25.0) THEN BEGIN
                    (Choose Z between 20 and 25 dBZ)
                    FOR I:=1 to 7 DO Begin
                        Read(SMPLIN,Z[I]) ;
                    End ;
                    FOR I:=1 to 4 DO begin
                        (Calculate ZDR, sum ZDR and sum ZDR*ZDR
                         for statistics)
                        ZDR[I]:=Z[I+3]-Z[I-1] ;
                        IF ZDR[I]<6.0 THEN BEGIN
                            ZDR[I]:=EXP(ZDR[I]*LN10/10.0) ;
                            SumZDRSQRD[I]:=SumZDRSQRD[I]+
                                Sqr(ZDR[I]) ;
                            SumZDR[I]:=SumZDR[I]+ZDR[I] ;
                        End ;
                    End ;
                    Z0:=EXP(Z[0]*LN10/10.0) ;
                    FOR I:=1 to 7 DO begin
                        Z[I]:=Z[I]-Z[0] ;
                        IF Z[I]<6.0 THEN BEGIN
                            Z[I]:=EXP(Z[I]*LN10/10.0) ;
                            SumDELTAZ[I]:=SumDELTAZ[I]+Z[I] ;
                        End ;
                    End ;
                End ;
            End
        End
    End
End

```

```

        SumDELTAZSQRD[I]:=SumDELTAZSQRD[I] +
        SQR(Z[I]) ;
        END ;
        End ;
        K:=K+1 ;
        End ;
        End ;
        End ;
        End;
        End ;
        ReadLn(SMPLIN) ;

If ((K mod 1000)=0) and (K<>0) Then Begin

PrintZDR(SumZDR,SumZDRSQRD,K) ;
PrintZ(SumDELTAZ,SumDELTAZSQRD,K) ;
For I:=1 to 4 do WriteLN(SMPLOUT,SumZDR[I],SumZDRSQRD[I]) ;
WriteLN(SMPLOUT) ;
For I:=1 to 7 do WriteLN(SMPLOUT,SumDELTAZ[I],
SumDELTAZSQRD[I]) ;

WriteLN(SMPLOUT,'K=',K) ;
WriteLN(SMPLOUT) ;
WriteLN(SMPLOUT) ;
Clear4(SumZDR,SumZDRSQRD) ;
Clear7(SumDELTAZ,SumDELTAZSQRD) ;
K:=0 ;
End;
End;

PrintZDR(SumZDR,SumZDRSQRD,K) ;
PrintZ(SumDELTAZ,SumDELTAZSQRD,K) ;
For I:=1 to 4 Do WriteLN(SMPLOUT,SumZDR[I],SumZDRSQRD[I]) ;
For I:=1 to 7 Do WriteLN(SMPLOUT,SumDELTAZ[I],SumDELTAZSQRD[I]) ;
WriteLN(SMPLOUT,'K=',K) ;
END.

```

APPENDIX 4

ANTENNA SCAN PROGRAM: ANTENNA

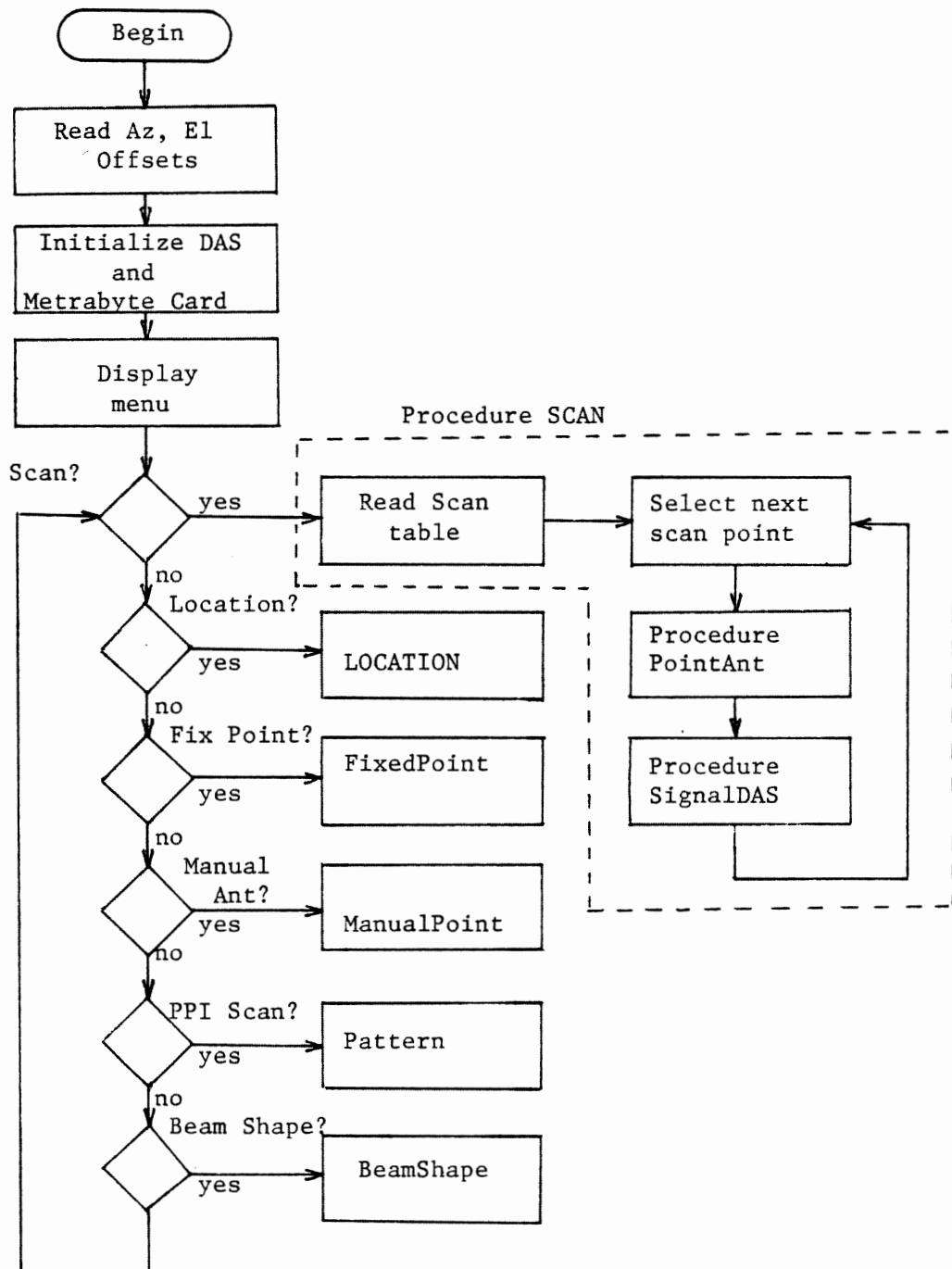
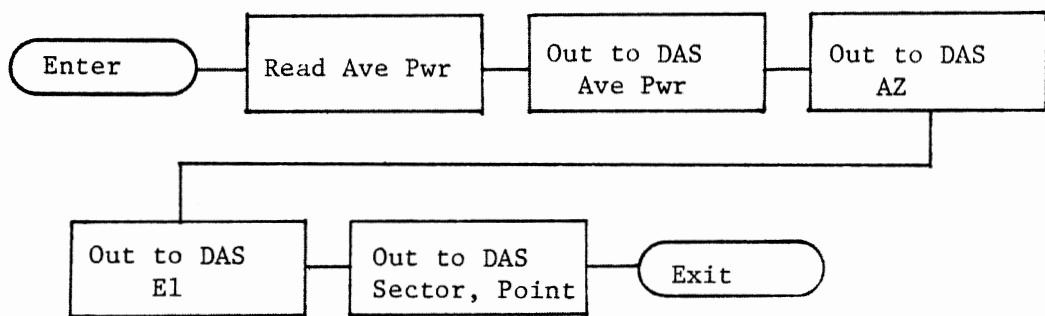
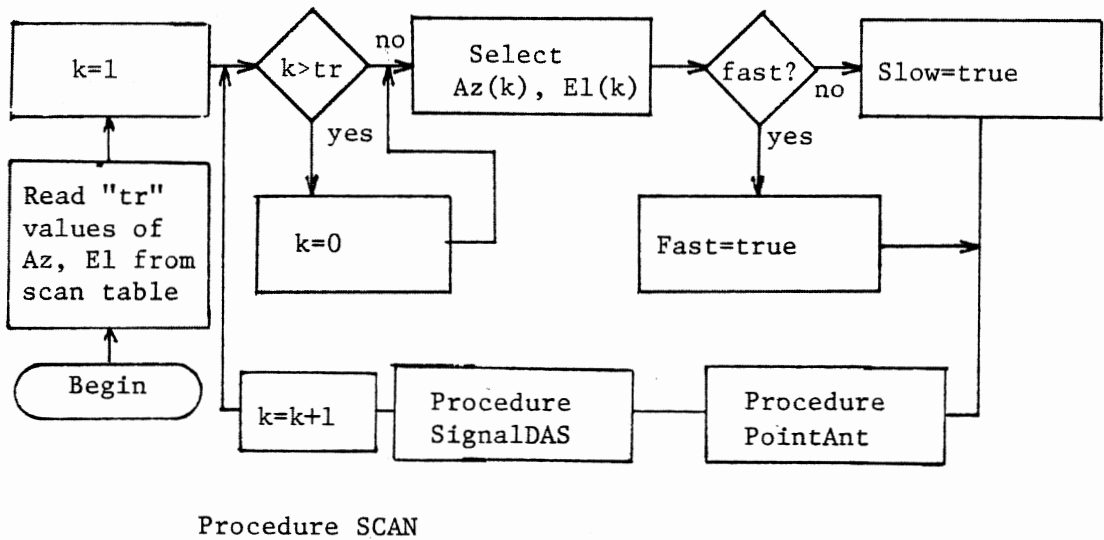


Figure A.4.1 Flow Diagram for Program ANTENNA



Procedure SignalDAS

Figure A.4.2 Flow Diagram for Procedures SCAN and SignalDAS

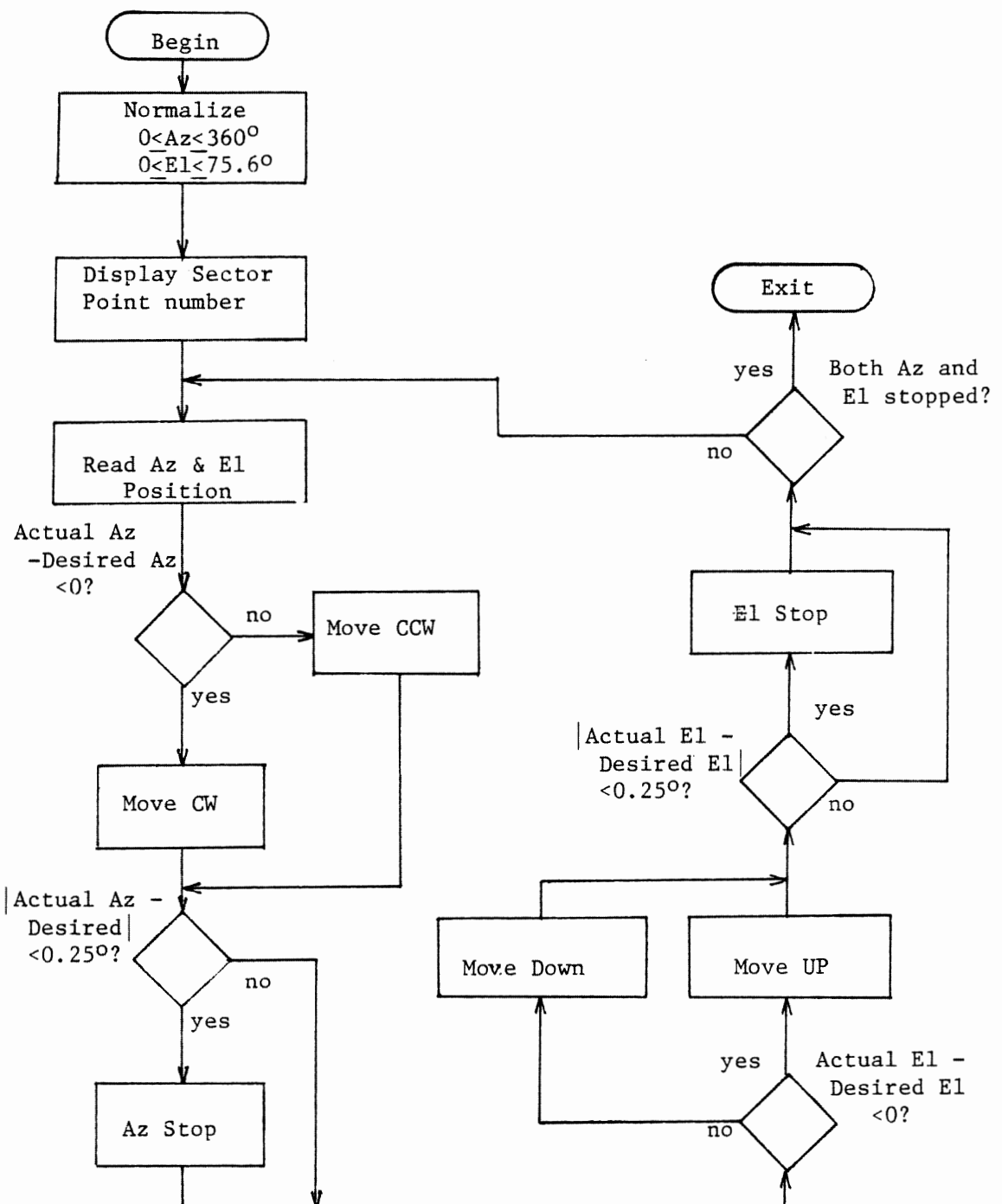


Figure A.4.3 Flow Diagram for PProcedure PointAnt

```

PROGRAM Antenna(input,output,PntFile) ;

{*****}

Program: ANTENNA controls the radar antenna
scan sequence

Written by: Bob Porter

Date: October 1985

Language: Turbo Pascal

Machine: IBM PC 128K

Additional Hardware : Metrabyte POI12 Card
                     24 bit PIO
                     Data Translation DT2808
                     A/D Card

Additional File: Antenna.dat
containing AZ and El positions

*****}

CONST DataReg      = $2EC ;      { DAS IO CONTROLLER ADDRESSES }
  CmdReg       = $2ED ;
  StatusReg    = $2ED ;

  SetInCmd     = $04 ;      { Controller Commands           }
  SetOutCmd    = $05 ;
  ReadCmd      = $06 ;
  WriteCmd     = $07 ;
  StopCmd      = $0F ;
  ResetCmd     = $00 ;
  ClearErrCmd  = $01 ;
  ReadAnalog   = $0C ;

  porta = $300 ;          { Input 8 bits - 24 bit card        }
  portb = $301 ;          { lo nib - cw/ccw hi nib - up/down   }
  portc = $302 ;          { hi nib - cntl / lo nib - s/d lo 4 bits }
  portd = $303 ;          { port control reg - out $91 to it     }

  dtc = 11.37778 ;        { * degrees to counts             */

```

```

TYPE PointRec = RECORD
    azdeg,eldeg : real ;
    azc,elc : integer ;
    sector : integer ;
    num : integer ;
    fast : integer ;
END ;

VAR AzMove      : byte ;      { Antenna Movement Controls }
    ElMove      : byte ;
    MoveCmd     : byte ;      { MoveCmd = AzMove + ElMove }
    MoveFast    : Boolean ;   { Antenna Speed Setting }
    AzStopped   : Boolean ;
    ElStopped   : Boolean ;
    AzOffset    : real ;
    ElOffset    : real ;

    PntFile : TEXT ;

    Az        : integer ;
    El        : integer ;
    Sector    : byte ;
    Num       : byte ;

    fcn       : integer ;

PROCEDURE CmdAntenna ;

BEGIN
    MoveCmd := AzMove + ElMove ;
    PORT[portb] := MoveCmd ;
END ;

PROCEDURE MoveCCW ;

BEGIN
    If MoveFast Then AzMove := $04 Else AzMove := $02 ;
    gotoxy(11,4) ;
    write('CCW ') ;
    AzStopped := false ;
END ;

```

```
PROCEDURE MoveCW ;  
  
BEGIN  
  If MoveFast Then AzMove := $03 Else AzMove := $01 ;  
  gotoxy(11,4) ;  
  write('CW ') ;  
  AzStopped := false ;  
END ;
```

```
PROCEDURE MoveUP ;  
  
BEGIN  
  If MoveFast Then ElMove := $40 Else ElMove := $20 ;  
  gotoxy(19,4) ;  
  write('UP ') ;  
  ElStopped := false ;  
  CmdAntenna ;  
END ;
```

```
PROCEDURE MoveDown ;  
  
BEGIN  
  If MoveFast Then ElMove := $30 Else ElMove := $10 ;  
  gotoxy(19,4) ;  
  write('DOWN') ;  
  ElStopped := false ;  
  CmdAntenna ;  
END ;
```

```
PROCEDURE azim(var az : integer) ;  
  
  Var hi,lo : byte ;  
  
BEGIN  
  PORT[portc] := $10 ;  
  hi := PORT[porta] ;  
  lo := PORT[portc] ;  
  lo := lo and $0F ;  
  az := 16*hi + lo ;  
  PORT[portc] := $0 ;  
END ;
```

```

PROCEDURE elev(var el : integer) ;

  Var hi,lo : byte ;

BEGIN
  PORT[portc] := $20 ;
  hi := PORT[porta] ;
  lo := PORT[portc] ;
  lo := lo and $0F ;
  el := 16*hi + lo ;
  PORT[portc] := $0 ;
END ;

PROCEDURE StopAZ ;

BEGIN
  AzMove := 0 ;
  CmdAntenna ;
  gotoxy(11,4) ;
  write('STOP')
  AzStopped := true ;
END ;

PROCEDURE StopEL ;

BEGIN
  ElMove := 0 ;
  CmdAntenna ;
  gotoxy(19,4) ;
  write('STOP')
  ElStopped := true ;
END ;

PROCEDURE PutCmd(cmd : Byte) ;

  Var s : Byte ;

BEGIN
  repeat
    s := PORT[StatusReg] ;
    until (s and $04) <> 0 ;
    PORT[CmdReg] := cmd ;
END ;

```

```
PROCEDURE PutData(d : Byte) ;  
  
  Var s : Byte ;  
  
BEGIN  
  repeat  
    s := PORT[StatusReg] ;  
  until (s and $02) = 0 ;  
  PORT[DataReg] := d ;  
END ;
```

```
PROCEDURE GetData(Var d : Byte) ;  
  
  Var s : byte ;  
  
BEGIN  
  repeat  
    s := PORT[StatusReg] ;  
  until (s and $01) <> 0 ;  
  d := PORT[DataReg] ;  
END ;
```

```
FUNCTION AvgPwr : Integer ;  
  
  Const Gain      = 0 ;  
        Channel = 0 ;  
  
  Var hi,lo : byte ;  
  
BEGIN  
  PutCmd(ReadAnalog) ;  
  PutData(Gain) ;  
  PutData(Channel) ;  
  GetData(lo) ;  
  GetData(hi) ;  
  AvgPwr := hi*256 +lo ;  
END ;
```

```

PROCEDURE InitialDAS ;
  Var junk : byte ;

BEGIN
  PORT[CmdReg] := StopCmd ;
  junk := PORT[DataReg] ;
  PutCmd(ClearErrCmd) ;
  PutCmd(SetOutCmd) ;
  PutData(0) ;
  PutCmd(SetInCmd) ;
  PutData(1) ;
  PutCmd(ReadCmd) ;
  PutData(0) ;
  PutData($FF) ;
END ;

```

```

(*DAS OUTPUT BYTE FORMAT *)  

{  

{ ----- }  

{ | Rx ACK | Latch Stb | Hi/Low Nib | ??? | Data Nib | }  

{ ----- }  

(*    7          6          5          4          3          0  *)  

{  


```

```

PROCEDURE OutToDAS(b : Byte) ;

  Var hi,lo : Byte ;
    s : byte ;

BEGIN
  hi := b div 16 ;
  lo := b and $0F ;

{ Wait For Port To Be Ready }
{ DAS ready for next Byte }

repeat
  PutCmd(ReadCmd) ;
  PutData(1) ;
  GetData(s) ;
until ((s and $40) <> 0) ;

```

```

{ Set Hi/Low Nibble Select To Low Nibble }

PutCmd(WriteCmd) ;
PutData(0) ;
PutData($DF) ;

{ OutPut Low Nibble with Latch Signal Low }

PutCmd(WriteCmd) ;
PutData(0) ;
PutData(lo or $90) ;

{ Return Latch Hi while maintaining Low Nibble data and H/L }

PutCmd(WriteCmd) ;
PutData(0) ;
PutData(lo or $D0) ;

{ Set Hi/Low Select to Hi and the HI Nibble }

PutCmd(WriteCmd) ;
PutData(0) ;
PutData(hi or $F0) ;

{ Output Hi Nibble and Hi Select while Latch Signal goes Low }

PutCmd(WriteCmd) ;
PutData(0) ;
PutData(hi or $B0) ;

{ Maintain Hi Nibble and Hi Select While Latch goes HI }

PutCmd(WriteCmd) ;
PutData(0) ;
PutData(hi or $F0) ;

END ;

PROCEDURE InFromDAS(Var d : Byte) ;

Var hi,lo : Byte ;
      s      : Byte ;

BEGIN

```

```

( Wait for Data Byte from DAS )

repeat
    PutCmd(ReadCmd) ;
    PutData(1) ;
    GetData(s) ;
until (s and $80) <> 0 ;

( Set H/L Select to HI Nibble )

PutCmd(WriteCmd) ;
PutData(0) ;
PutData($FF) ;

( Input Hi Nibble )

PutCmd(ReadCmd) ;
PutData(1) ;
GetData(hi) ;
hi := (hi and $OF) * 16 ;

( Set H/L Select to Low Nibble )

PutCmd(WriteCmd) ;
PutData(0) ;
PutData($DF) ;

( Input Low Nibble )

PutCmd(ReadCmd) ;
PutData(1) ;
GetData(lo) ;
lo := lo and $OF ;

( Signal DAS Data Received With the Acknowledge line )

PutCmd(WriteCmd) ;
PutData(0) ;
PutData($7F) ;
PutCmd(WriteCmd) ;
PutCmd(0) ;
PutCmd(Writata($FF) ;

d := hi or lo ;

END ;

```

```

PROCEDURE SignalDAS(AvgPwr,Az,E1 : integer ;
                     Sector,Num : byte) ;

Var s : byte ;

BEGIN
  InFromDAS(s) ;
  gotoxy(1,10) ;
  write('AvgPwr = ',AvgPwr:6) ;
  OutToDAS(HI(AvgPwr)) ;
  OutToDAS(LO(AvgPwr)) ;
  write(' Az = ',az:6) ;
  OutToDAS(HI(Az)) ;
  OutToDAS(LO(Az)) ;
  write(' EL = ',el:6) ;
  OutToDAS(HI(E1)) ;
  OutToDAS(LO(E1)) ;
  write(' Sector = ',sector:2,Num:5) ;
  OutToDAS(Sector) ;
  OutToDAS(Num) ;
END ;

```

```

PROCEDURE Point(AzP : integer ; ElP : integer) ;

VAR daz : integer ;
    del : integer ;
    dly : Boolean ;

BEGIN
  If AzP > 4095 Then AzP := AzP - 4096
  Else If AzP < 0 Then AzP := AzP + 4096 ;
  If ElP > 2096 Then ElP := 2096
  Else If ElP < 1188 Then ElP := 1188 ;

  gotoxy(26,4) ;
  case Sector of
    0: write(' DIV ') ;
    1: write(' RHI2') ;
    2: write('SCAN ') ;
    3: write('PATH ') ;
    4: write(' RHI1') ;
    5: write('OTHER') ;
    6: write('PTRN ') ;
  end ;

```

```

write(Num:3) ;
if (Sector = 2) or (Sector = 3) then dly:= true else dly:= false;

gotoxy(2,4) ;
if MoveFast
then begin
    write('FAST') ;
end else begin
    write('SLOW') ;
end ;

azim(az) ;
daz := az-azp ;
If daz < 0 Then MoveCW Else MoveCCW ;
If abs(daz) < 3 Then StopAz ;

elev(el) ;
del := el-elp ;
IF del < 0 Then MoveDown Else MoveUp ;
If abs(del) < 3 Then StopEl ;

CmdAntenna ;

repeat
    azim(az) ;
    gotoxy(40,4) ;
    write(az:5) ;
    daz := az - azp ;
    If abs(daz) < 43 Then StopAz ;
    If daz < 0 Then MoveCW Else MoveCCW ;
    If abs(daz) < 4 Then StopAz ;

    elev(el) ;
    gotoxy(48,4) ;
    write(el:5) ;
    del := el - elp ;
    If (abs(del) < 53) and (not MoveFast) then StopEl ;
    If (dly) and (not (Num = 0)) and (not (el > 2015)) then delay(59) ;
    If del < 0 Then MoveDown Else MoveUp ;
    If abs(del) < 4 then StopEl ;
    If (abs(del) < 40) and (abs(daz) < 40) then MoveFast := false ;
    CmdAntenna ;
until AzStopped and ElStopped ;
azim(az) ;
elev(el) ;
END ;

```

```

PROCEDURE Location ;
BEGIN
  Sector := 5 ;
  Num := 0 ;
  gotoxy(26,4) ;
  write('OTHER') ;

  repeat
    Azim(Az) ;
    Elev(El) ;
    gotoxy(40,4) ;
    write(az:5,' ',el:5) ;
    SignalDAS(AvgPwr,Az,El,Sector,Num) ;
  until false ;
END ;

PROCEDURE SCAN ;
VAR azp,elp : integer ;
  sc : integer ;
  np : integer ;

  c : char ;
  k,l : integer ;

  tbl : ARRAY[0..255] of PointRec ;
  tr : integer ;

  azdir,eldir : integer ;

  hi,lo : byte ;

BEGIN
  gotoxy(1,20) ;
  write('Reading Antenna Scan Table') ;

  tr := 0 ;

  while not eof(pntfile) do begin
    with tbl[tr] do begin
      read(pntfile,c) ;
      if c='*' then readln(pntfile) ;

```

```

        readln(pntfile,azdeg,eldeg,sector,num,fast) ;
        azc := round((azdeg + AzOffSet) * dtc) ;
        elc := round((ElOffset - eldeg) * dtc) ;
        gotoxy(28,20) ;
        write(sector:2,num:3) ;
    end ;
    tr := tr + 1 ;
end ;
tr := tr - 1 ;
gotoxy(1,20) ;
ClrEol ;

k := tr ;

REPEAT
    k:= k + 1 ;
    if k > tr then k := 0 ;
    azp := tbl[k].azc ;
    elp := tbl[k].elc ;
    Sector := tbl[k].Sector ;
    Num := tbl[k].Num ;
    IF tbl[k].fast=1 THEN MoveFast := true ELSE MoveFast := false ;
    Point(azp,elp) ;
    SignalDAS(AvgPwr,Az,El,Sector,Num) ;
UNTIL false ;
END ;

```

```

PROCEDURE FixedPoint ;

Var azp,elp : integer ;
      azc,elc : real ;

BEGIN
    gotoxy(1,20) ;
    ClrEol ;
    write('Azimuth? ') ;
    read(azc) ;
    write(' Elevation? ');
    read(elc) ;
    azp := round((azc + AzOffset) * dtc) ;
    elp := round((ElOffset - elc) * dtc) ;
    gotoxy(1,21) ;
    ClrEol ;

```

```

        write('Az count: ',azp:4,'    El count: ',elp:4) ;
        Sector := 5 ;
        Num := 0 ;
        MoveFast := false ;
        Point(azp,elp) ;
        Location ;
END ;

PROCEDURE ManualPoint ;
Var azp,elp : integer ;
      azc,elc : real ;

BEGIN
  REPEAT
    gotoxy(1,20) ;
    ClrEol ;
    write('Azimuth? ') ;
    read(azc) ;
    write(' Elevation? ');
    read(elc) ;
    azp := round((azc + AzOffset) * dtc) ;
    elp := round((ElOffset - elc) * dtc) ;
    gotoxy(1,21) ;
    ClrEol ;
    write('Az count: ',azp:4,'    El count: ',elp:4) ;
    Sector := 5 ;
    Num := 0 ;
    MoveFast := false ;
    Point(azp,elp) ;
  UNTIL false ;
END ;

PROCEDURE Pattern ;
Var azp,elp : integer ;
      azc,elc : real ;

BEGIN
  elp := round((ElOffset - elc) * dtc) ;
  Sector := 6 ;
  Num := 0 ;
  MoveFast := False ;

```

```

azc := 0.0 ;
REPEAT
    elc := -2.5 * cos((azc - 90.5)*3.141593/180.0) ;
    elp := round((ElOffset - elc) * dtc) ;
    azp := round((azc + AzOffSet) * dtc) ;
    gotoxy(1,20) ;
    write('Azimuth: ',azc:6:1,' Elevation: ',elc:6:1) ;
    azc := azc + 1.0 ;
    Point(azp,elp) ;
    SignalDAS(AvgPwr,Az,El,Sector,Num) ;
    IF Num < 255 Then Num := Num + 1 Else Num := 0 ;
UNTIL azc >= 360.0 ;
END ;

```

Procedure BeamShape ;

```

var azd,eld : real ;
    azc,elc : integer ;

BEGIN
    Sector := 6 ;
    Num := 0 ;
    eld := -3.0 ;
    WHILE eld <= 3.0 DO BEGIN
        azd := 85.0 ;
        WHILE azd <= 95.0 DO BEGIN
            azc := round((azd + AzOffSet) * dtc) ;
            elc := round((ElOffset - eld) * dtc) ;
            point(azc,elc) ;
            SignalDAS(AvgPwr,Az,El,Sector,Num) ;
            azd := azd + 0.5 ;
        END ;
        eld := eld + 0.5 ;
    END ;
END ;

```

PROCEDURE TESTSignalDAS ;

```

Var s : byte ;
    k : integer ;
    avgpwr,az,el,sector,num : integer ;

```

```

BEGIN
avgpwr := 165 ;
az := 170 ;
el := 55 ;
sector := 12 ;
num := 3 ;
repeat
(   InFromDAS(s) ;
    OutToDAS(HI(AvgPwr)) ;
    OutToDAS(LO(AvgPwr)) ;
    OutToDAS(HI(Az)) ;
    OutToDAS(LO(Az)) ;
    OutToDAS(HI(El)) ;
    OutToDAS(LO(El)) ;
    OutToDAS(Sector) ;
    OutToDAS(Num) ; )
    for k := 0 to 255 do begin
        if (k mod 8) = 0 then InFromDAS(s) ;
        OutToDAS(k) ;
    end ;
    write('.');
until false ;
END ;

```

```

BEGIN

assign(pntfile,'antenna.dat') ;
reset(pntfile) ;
readln(pntfile,AzOffSet,ElOffSet) ;
readln(pntfile) ;

REPEAT
    InitialDAS ;
    PORT[portd] := $91 ;
    StopAz ;
    StopEl ;
    ClrScr ;

    writeln('Antenna Control, PC-TO-DAS Commuication Program') ;
    writeln('Select Program Mode') ;
    writeln
    writeln('1 - Run Antenna Scan Program') ;
    writeln('2 - Monitor Antenna Location') ;
    writeln('3 - Fixed Point the Antenna ') ;
    writeln('4 - Manual Antenna, No DAS ') ;

```

```
writeln('5 - PPI Antenna Pattern Scan') ;
writeln('6 - Beam Shape Pattern Scan ') ;
writeln ;
write('Enter Selection (1-6)? ') ;
readln(fcn) ;

ClrScr ;
writeln('           COMMAND                      LOCATION') ;
writeln(' SPEED    AZIMUTH   ELEV     SECTOR    AZIMUTH   ELEV') ;
writeln(' -----  -----  -----  -----  ---  -----  -----') ;

CASE fcn OF
  1: SCAN ;
  2: LOCATION ;
  3: FixedPoint ;
  4: ManualPoint ;
  5: Pattern ;
  6: BeamShape ;
  7: TestSignalDAS ;
END ;
UNTIL false ;
```

APPENDIX 5

RADAR CROSS SECTION PROGRAM: RCS

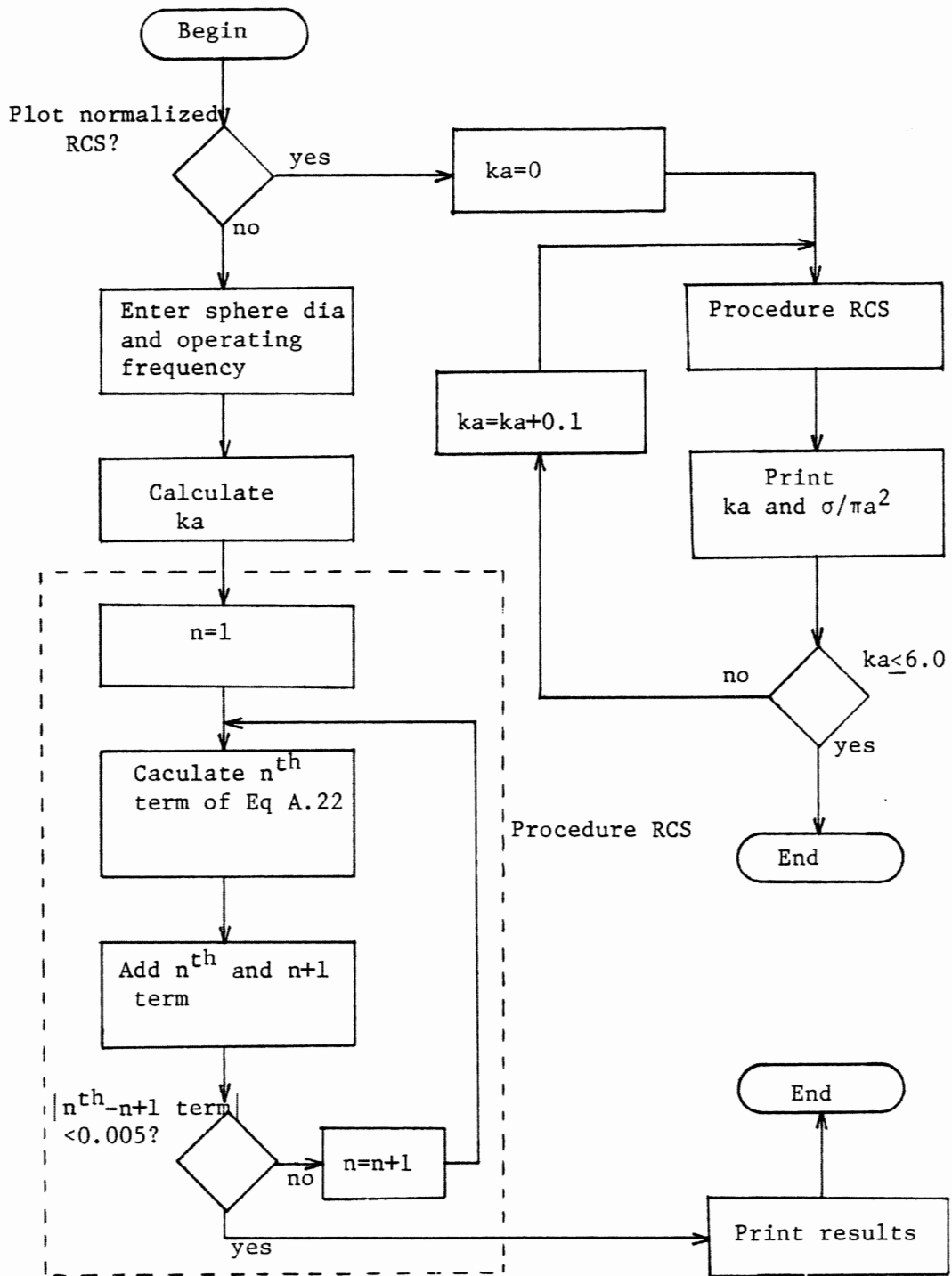


Figure A.5.1 Flow Diagram for Program RCS

```

(*$U++)
(*$A-*)
PROGRAM      RCS;

*****  

RCS calculates the Radar Cross Section
of a metal sphere  

DATE: May 1986  

PROGRAMMER: Dennis Sweeney  

LANGUAGE: Turbo Pascal 3.0 for
Z-80 CP/M machine
*****)

```

Type

```

Complex = record
  re, im : real ;
end ;

Var        K,M,N      : integer ;
          P,Q      : integer ;
          C, C1, z : real    ;
          Dia, Freq : real    ;

FUNCTION J(N : integer; z : real) : real ;

(*FUNCTION J(N) calculates a Bessel function of fractional
order*)

Begin
  If N = 0 then J := sin(z)/z
  else
    If N = 1 then J := sin(z)/(z*z) - cos(z)/z
    else
      If N = 2 then J := J(1,z)*3.0/z - J(0,z)
      else
        If N = 3 then J := J(2,z)*5.0/z - J(1,z)
        else
          If N = 4 then J := J(3,z)*7.0/z - J(2,z)
          else

```

```

If N = 5 then J := J(4,z)*9.0/z - J(3,z)
else
If N = 6 then J := J(5,z)*11.0/z - J(4,z)
else
If N = 7 then J := J(6,z)*13.0/z - J(5,z)
else
If N = 8 then J := J(7,z)*15.0/z - J(6,z)
else
If N = 9 then J := J(8,z)*17.0/z - J(7,z)
else
If N = 10 then J := J(9,z)*19.0/z - J(8,z)
else
If N = 11 then J := J(10,z)*21.0/z - J(9,z)
else
J := J(11,z)*23.0/z - J(10,z) ;
End ;
FUNCTION Y( N : integer; z : real ) : real ;

(*FUNCTION Y(N) calculates the Neumann function of
fractional order*)

Begin
If N = 0 then Y := -cos(z)/z
else
If N = 1 then Y := Y(0,z)/z - sin(z)/z
else
If N = 2 then Y := Y(1,z)*3.0/z - Y(0,z)
else
If N = 3 then Y := Y(2,z)*5.0/z - Y(1,z)
else
If N = 4 then Y := Y(3,z)*7.0/z - Y(2,z)
else
If N = 5 then Y := Y(4,z)*9.0/z - Y(3,z)
else
If N = 6 then Y := Y(5,z)*11.0/z - Y(4,z)
else
If N = 7 then Y := Y(6,z)*13.0/z - Y(5,z)
else
If N = 8 then Y := Y(7,z)*15.0/z - Y(6,z)
else
If N = 9 then Y := Y(8,z)*17.0/z - J(7,z)
else
If N = 10 then Y := Y(9,z)*19.0/z - J(8,z)
else
If N = 11 then Y := Y(10,z)*21.0/z - Y(9,z)
else

```

```

        Y := Y(11,z)*23.0/z - Y(10,z) ;
End ;

FUNCTION Jprime(N : integer; z : real ) :real ;
(*FUNCTION Jprime(N) calculates the derivative of the
Bessel function*)

Begin
    Jprime := J(N-1,z) - J(N,z)*(N+1)/z ;
End;

FUNCTION Yprime(N : integer; z : real ) :real ;
(*FUNCTION Yprime(N) calculates the derivative of the
Neumann function*)

Begin
    Yprime := Y(N-1,z) - Y(N,z)*(N+1)/z ;
End ;

FUNCTION Sign(N : integer) :integer ;
(*FUNCTION Sign(N) determines the sign of the Nth term of
the RCS summation*)
Var
    I : integer ;
    R : integer ;

Begin
    R := 1 ;
    For I := 1 to N do
        R := -1*R ;
    Sign := R ;
End ;

FUNCTION RCS(z :real) :real ;
(*FUNCTION RCS(Z) calculates the radar cross section of z*)

Var      A, B      : complex ;
        C, C1, Mag : real ;
        H, Hprime : complex ;
        N          : integer ;

```

```

Begin
B.re := 0.0 ;
B.im := 0.0 ;
N := 0 ;
REPEAT
  N := N+1 ;
  C :=C1 ;
  H.re := z*J(N,z) ;
  H.im := z*Y(N,z) ;
  Hprime.re := J(N,z) + z*Jprime(N,z) ;
  Hprime.im := Y(N,z) + z*Yprime(N,z) ;

  A.re := H.re*Hprime.re - H.im*Hprime.im ;
  A.im := H.im*Hprime.re + H.re*Hprime.im ;

  Mag := Sign(N)*(2.0*N+1)/(Sqr(A.re)+Sqr(A.im)) ;

  B.re := Mag*A.re + B.re ;
  B.im := Mag*(-A.im) + B.im ;
  C1 := (Sqr(B.re)+Sqr(B.im))/Sqr(z) ;
  WriteLN(N,' ',z:4:2,' ',C1:12:10) ;
UNTIL Abs((C-C1)/C1)< 0.0005 ;

(* Summation terminated when the difference between two
subsequent terms differ by less than 0.05%*)

RCS := C1 ;
End ;

PROCEDURE PLOT ;

  (PROCEDURE PLOT produces a plot of normalized
    RCS (sigma/pi*a*a)
    versus ka*)

Begin
Write(lst,' ') ;
For P :=1 to 18 do begin
  C :=P/5.0 ;
  Write(lst,' ',C:3:1) ;
End ;
WriteLn(lst) ;

```

```

For K := 1 to 19 do Write(lst,' *') ;
WriteLn(lst) ;
Write(lst,' ') ;
For K := 1 to 77 do Write(lst,'*') ;
WriteLn(lst) ;
For K := 1 to 63 do
Begin
  z :=0.1*K ;
  C1 := RCS(z) ;
  P := Trunc(C1*20) ;
  Write(lst,z:3:1,'*') ;
  If P <> 0 Then begin
    For Q :=1 to P-1 do Write(lst,' ') ;
    Write(lst,'*') ;
  End ;
  For Q :=P to 71 do write(lst,' ') ;
  WriteLn(lst,C1:4:2) ;
End ;

End ;

BEGIN (*Main Program*)

WriteLn('Radar Cross Section Plot (1)') ;
WriteLn('RCS of given sphere (2)') ;
Write('Enter choice number ') ;
ReadLn(N) ;

IF N = 1 Then PLOT
Else
begin
  Write('Enter sphere diameter in INs ') ;
  ReadLn(Dia) ;
  Dia := Dia * 2.54;
  Write('Enter operating frequency in MHz ') ;
  ReadLn(Freq) ;
  z := PI * Freq * Dia / 30000 ;
  C1 := RCS(z) ;
  C := C1 * PI * Sqr(Dia/100) ;
  WriteLn ;
  WriteLn('ka= ',z:6:4,' Sigma/PI*a*a = ',C1:6:4,' RCS =
    ',C:6:4,' meters') ;
End ;
END.

```

The vita has been removed
from the scanned document